ANALYSIS OF THERMALLY INDUCED DAMAGE IN COMPOSITE SPACE STRUCTURES

by

Cecelia Hyun Seon Park

S.B., Massachusetts Institute of Technology

(1992)

Submitted to the Department of Aeronautics and Astronautics

in Partial Fulfillment of

the Requirements for the Degree of

Master of Science

in Aeronautics and Astronautics

at the

Massachusetts Institute of Technology

January 1994

Signature of Author _____

Department of Aeronautics and Astronautics
January, 1994

Certified by _____

Professor Hugh L. McManus
Thesis Supervisor

Accepted by _____

Professor Harold Y. Wachman
Chairman, Departmental Graduate Committee

ANALYSIS OF THERMALLY INDUCED DAMAGE IN COMPOSITE SPACE STRUCTURES

by

Cecelia H. Park

Submitted to the Department of Aeronautics and Astronautics on January, 1994 in partial fulfillment of the requirements for the Degree of Master of Science.

Abstract

Unprotected structure in space is subjected to severe temperature extremes. Microcracks in the plies of composite structures have been observed to form under these conditions. Verified, general design tools are necessary to predict, avoid, and/or live with transverse cracking in composite space structures. A shear lag solution of the stresses in the vicinity of the crack, combined with a simple energy criteria, was used to predict matrix cracking. Thermal cycling fatigue was accounted for by assuming that cyclic loading decreases the material's resistance to cracking. These methods were combined to predict crack densities and degraded laminate properties as functions of temperature and thermal cycles. A general analysis, valid for all plies of any laminate configuration, including interactions between cracks in various plies, was developed. The method includes effects such as material softening and temperature dependent material properties. The analysis was incorporated in a computer program. Experiments were performed to measure crack densities to verify the analytical predictions. A variety of laminates were cooled to progressively lower temperatures. The measured crack densities were correlated to the analytical predictions and were found to be dependent on ply thickness. The predicted behavior of thick plies correlated with experimental observations reasonably well, but experimental observation of thin plies showed a variety of unpredicted behaviors. The validity of the assumptions used in current matrix cracking analyses were examined experimentally by X-radiography, edge inspections, and inspections of the configuration of cracks throughout the volume of samples carried out by sanding. Complex behavior of the matrix cracking as functions of ply thickness, ply angle, and closeness to free edges, not previously reported, was observed. These results were interpreted to help explain deviations from the analytical predictions in thin plies. Analytically, a 3D free edge stress analysis was used to understand observed cracking behavior near the edges. The results raise serious questions about current practices in both experimental determination of cracking damage through observation of sample edges and analytical prediction of these cracks.

Thesis Supervisor: Hugh L. McManus

Title: Assistant Professor, Department of Aeronautics and Astronautics, Massachusetts Institute of Technology.

ACKNOWLEDGEMENTS

i'd like to thank prof. mcmanus for all the knowledge he has shared and everything he has taught me (or tried). it was definitely an educational and rewarding experience to work with someone so enthusiastic and intelligent. i really appreciate all the support i received. i would also like to thank everyone at nasa langely for their support. special thanks to dr. tompkins, dr. bowles, james shen and joan funk.

i would not be writing this acknowledgement had it not been for dr. bhat and soon-to-be dr. tsang. they are the most caring and generous people i know who make telac what it is. you guys set a great example for everyone-telac will definitely miss your presence. thanks to rich for the late (very late) night talks, wardle for being a dork and jason and scott for all their help. i really appreciate all the support i've received from everyone at telac. thanks to deb, ping, and liz for letting me bother them!

there are many people i need to thank for putting up with me during my years at mit. special thanks to little park, kat, and rob! i would not have survived mit without them. thanks to lester for all his support during my thesising. i would like to list all the great friends who have helped me out and put up with me, but my thesis is due... i am truly grateful to <u>everyone</u> for making my past 5 years here actually enjoyable.

finally, i would like to thank my family for all their support. obviously i would not have been able to do any of this without them. thanks mom and dad for everything. peter and john for being...my brothers? :) i cannot thank you guys enough!

wow. i am finally done.

thank you God.

FOREWORD

This research was completed at the Technology Laboratory for Advanced Composites at the Massachusetts Institute of Technology. The work was partially funded by a NASA Spacegrant Fellowship and NASA Langely Research Center grant NAG-1-1463.

TABLE OF CONTENTS

ABSTRACT 3
ACKNOWLEDGEMENT 5
FOREWORD 7
LIST OF FIGURES 11
LIST OF TABLES 16
NOMENCLATURE 17
1. INTRODUCTION 21
2. PREVIOUS WORK 26
2.1 OVERVIEW OF ANALYTICAL APPROACHES 26
2.2 MECHANICAL APPLICATIONS 27
2.3 THERMAL APPLICATIONS 29
2.4 ANALYSIS OF THERMALLY LOADED CROSSPLY LAMINATE .. 30
3. PROBLEM STATEMENT 32
4. ANALYTICAL METHODS 33
4.1 APPROACH 33
4.2 DERIVATION OF BASIC ENERGY EQUATIONS 38
4.2.1 Stress Distribution and Displacement Field 38
4.2.2 Strain Energy Release Rate 43
4.2.3 Degradation of Laminate Properties 46
4.3 IMPLEMENTATION FOR THERMAL PROGRESSIVE AND CYCLIC LOADS 47
4.3.1 Crack Density as Function of Temperature 48
4.3.2 Crack Density as Function of Thermal Cycles 48
4.3.3 Solution Algorithm Including Secondary Effects 50
4.3.4 Derivation of Stiffness Constant 52
4.4 FREE EDGE STRESS ANALYSIS 55
4.5 COMPUTER PROGRAMS 55
5. EXPERIMENTAL METHODS 58
5.1 PREPARATION OF SPECIMENS 58
5.2 MICROCRACK EXAMINATION 60
5.3 THERMAL PROGRESSIVE TESTING 62
5.4 CRACK CONFIGURATION STUDY 63

5.4.1 X-Radiography 66
5.4.2 Examination of Microcrack Distribution Throughout Volume of Laminate 66
5.4.3 Control Tests 69
6. RESULTS 71
6.1 THERMAL PROGRESSIVE COOLING 71
6.1.1 Crack Density vs. Decreasing Temperature 71
6.1.2 Laminate Properties vs. Decreasing Temperature 82
6.1.3 Parametric Studies 89
6.2 CRACK CONFIGURATION STUDY 91
6.2.1 X-Radiography 91
6.2.2 Edge Comparison 91
6.2.3 Sanding Edges 94
6.3 FREE EDGE STRESS ANALYSIS 100
7. DISCUSSION 105
7.1 PLY THICKNESS EFFECTS 105
7.2 PLY ORIENTATION EFFECTS 107
7.3 EDGE EFFECTS 108
8. CONCLUSIONS 110
8.1 SUMMARY 110
8.2 RECOMMENDATIONS 110
REFERENCES 112
APPENDIX A: COMPUTER CODE MANUAL AND DOCUMENTATION. 119
APPENDIX B: PROGRESSIVE THERMAL LOADING ANALYTICAL AND EXPERIMENTAL RESULTS 129
APPENDIX C: RESULTS OF FREE EDGE STRESS ANALYSIS 158

LIST OF FIGURES

Figure 1.1	Examples of microcracks on edges of laminates. Photomicrographs of crossply [02/902]s specimen under 50x magnification and quasi-isotropic laminate [0/45/90/-45]s under 200x magnification (0° ply is not visible)	22
Figure 1.2	Thermally loaded unconstrained plies and constrained laminate. CTE mismatch causes microcracks to appear.	24
Figure 4.1	Crack formation in an arbitrary ply. Cracks grow to span the ply thickness instantaneously.	34
Figure 4.2	Crack formation in laminate. We assume cracks form suddenly through the width of the laminate as shown in the process (a) to (b).	35
Figure 4.3	Graph of the change in strain energy as a function of crack length.	37
Figure 4.4	Laminate showing two cracks, 2h apart, in a cracking ply group embedded in the rest of a smeared laminate.	39
Figure 4.5	Free body diagram of small section of laminate.	41
Figure 4.6	(a) A laminate with two cracks, A and B, spaced 2h apart. (b) Same laminate with the appearance of an additional crack C.	45
Figure 4.7	Laminate with crack spacing of h subjected to thermal loads.	49
Figure 4.8	Flow chart of algorithm used in analysis.	51
Figure 4.9	Top view of laminate with equally spaced cracks in 45° and 90° plies. Illustrates difference in crack density from geometric effect.	57
Figure 5.1	Different damage types on free edges of laminates.	61
Figure 5.2	Thermal profile of progressive testing procedure.	64
Figure 5.3	(a) Edge view of laminate sanded off with x increment (b) Top view of laminate with example q ply crack. Illustration of difference in edge inspection after sanding.	67
Figure 6.1	Analytical and experimental correlation of crack density vs. decreasing temperature. 30 ply of [02/±30]s laminate.	73

Figure 6.2 Analytical and experimental correlation of crack density vs. decreasing temperature. -30 ply of [02/±30]s laminate. 74
Figure 6.3 Analytical and experimental correlation of crack density vs. decreasing temperature. 45 ply of [0/45/90/-45]s laminate. . 76
Figure 6.4 Analytical and experimental correlation of crack density vs. decreasing temperature. 45 ply of [0/45/90/-45]s laminate. . 77
Figure 6.5 Analytical and experimental correlation of crack density vs. decreasing temperature. -452 ply of [0/45/90/-45]s laminate. 78
Figure 6.6 Analytical and experimental correlation of crack density vs. decreasing temperature. 452 ply of [02/452/902/-452]s laminate. 79
Figure 6.7 Analytical and experimental correlation of crack density vs. decreasing temperature. 902 ply of [02/452/902/-452]s laminate. 80
Figure 6.8 Analytical and experimental correlation of crack density vs. decreasing temperature. -454 ply of [02/452/902/-452]s laminate. 81
Figure 6.9 Analytical stiffness prediction vs. temperature for [0/45/90/-45]s laminate. Laminate longitudinal stiffness normalized by undamaged value. 83
Figure 6.10 Analytical stiffness prediction vs. temperature for [02/452/902/-452]s laminate. Laminate longitudinal stiffness normalized by undamaged value. 84
Figure 6.11 Analytical stiffness prediction vs. temperature for [0/90/0/90]s laminate. Laminate longitudinal stiffness normalized by undamaged value. 85
Figure 6.12 Analytical CTE prediction vs. temperature for [0/45/90/-45]s laminate. 86
Figure 6.13 Analytical CTE prediction vs. temperature for [02/452/902/-452]s laminate. 87
Figure 6.14 Analytical CTE prediction vs. temperature for [0/90/0/90]s laminate. 88
Figure 6.15 Parametric studies using temperature dependent material properties and material softening effects. 90

Figure 6.16 X-ray photographs of microcracks in [0/45/90/-45]s and [02/902]s specimens. 92
Figure 6.17 Sanding results for [02/±30]s specimen showing crack configuration through width. 95
Figure 6.18 Sanding results for [0/45/90/-45]s specimen showing crack configuration through width in 90 plies. 97
Figure 6.19 Sanding results for [0/+45/90/-45]s specimen showing crack configuration through width in +45 and -452 plies. 98
Figure 6.20 Sanding results for [0/+45/90/-45]s specimen showing crack configuration through width. 99
Figure 6.21 Sanding results for [02/+452/902/-452]s specimen showing crack configuration through width. 101
Figure 6.22 Sanding results for [0/+45/90/-45]s specimen showing crack configuration through width. 102
Figure 6.23 Transverse in-plane stress distribution near the free edge of a [0/45/90/-45]s laminate. 103
Figure B.1 Analytical and experimental correlation of crack density vs. decreasing temperature. 45 ply of [0/45/90/-45]s laminate. . 130
Figure B.2 Analytical and experimental correlation of crack density vs. decreasing temperature. 90 ply of [0/45/90/-45]s laminate. . 131
Figure B.3 Analytical and experimental correlation of crack density vs. decreasing temperature. -452 ply of [0/45/90/-45]s laminate. 132
Figure B.4 Analytical CTE prediction vs. temperature for [0/45/90/-45]s laminate. 133
Figure B.5 Analytical stiffness prediction vs. temperature for [0/45/90/-45]s laminate. Laminate longitudinal stiffness normalized by undamaged value. 134
Figure B.6 Analytical and experimental correlation of crack density vs. decreasing temperature. 45 ply of [0/±45/90]s laminate..... 135
Figure B.7 Analytical and experimental correlation of crack density vs. decreasing temperature. -45 ply of [0/±45/90]s laminate. 136
Figure B.8 Analytical and experimental correlation of crack density vs. decreasing temperature. 902 ply of [0/±45/90]s laminate. ... 137
Figure B.9 Analytical CTE prediction vs. temperature for [0/±45/90]s laminate. 138

Figure B.10 Analytical stiffness prediction vs. temperature for [0/±45/90]s laminate. Laminate longitudinal stiffness normalized by undamaged value. 139
Figure B.11 Analytical and experimental correlation of crack density vs. decreasing temperature. 90 ply of [0/90/±45]s laminate..... 140
Figure B.12 Analytical and experimental correlation of crack density vs. decreasing temperature. 45 ply of [0/90/±45]s laminate..... 141
Figure B.13 Analytical and experimental correlation of crack density vs. decreasing temperature. -452 ply of [0/90/±45]s laminate. .. 142
Figure B.14 Analytical CTE prediction vs. temperature for [0/90/±45]s laminate. 143
Figure B.15 Analytical stiffness prediction vs. temperature for [0/90/±45]s laminate. Laminate longitudinal stiffness normalized by undamaged value. 144
Figure B.16 Analytical and experimental correlation of crack density vs. decreasing temperature. 452 ply of [02/452/902/-452]s laminate. 145
Figure B.17 Analytical and experimental correlation of crack density vs. decreasing temperature. 902 ply of [02/452/902/-452]s laminate. 146
Figure B.18 Analytical and experimental correlation of crack density vs. decreasing temperature. -454 ply of [02/452/902/-452]s laminate. 147
Figure B.19 Analytical CTE prediction vs. temperature for [02/452/902/-452]s laminate..... 148
Figure B.20 Analytical stiffness prediction vs. temperature for [02/452/902/-452]s laminate. Laminate longitudinal stiffness normalized by undamaged value. 149
Figure B.21 Analytical and experimental correlation of crack density vs. decreasing temperature. 90 ply of [0/90/0/90]s laminate..... 150
Figure B.22 Analytical and experimental correlation of crack density vs. decreasing temperature. 902 ply of [0/90/0/90]s laminate.... 151
Figure B.23 Analytical CTE prediction vs. temperature for [0/90/0/90]s laminate. 152

Figure B.24 Analytical stiffness prediction vs. temperature for [0/90/0/90]s laminate. Laminate longitudinal stiffness normalized by undamaged value. 153
Figure B.25 Analytical and experimental correlation of crack density vs. decreasing temperature. 30 ply of [02/±30]s laminate..... 154
Figure B.26 Analytical and experimental correlation of crack density vs. decreasing temperature. -302 ply of [02/±30]s laminate. 155
Figure B.27 Analytical CTE prediction vs. temperature for [02/±30]s laminate. 156
Figure B.28 Analytical stiffness prediction vs. temperature for [02/±30]s laminate. Laminate longitudinal stiffness normalized by undamaged value. 157
Figure C.1 Transverse in-plane stress distribution near free edge of [0/45/90/-45]s laminate. 159
Figure C.2 Transverse in-plane stress distribution near free edge of [0/±45/90]s laminate. 160
Figure C.3 Transverse in-plane stress distribution near free edge of [0/90/±45]s laminate. 161
Figure C.4 Transverse in-plane stress distribution near free edge of [02/452/902/-452]s laminate. 162
Figure C.5 Transverse in-plane stress distribution near free edge of [0/90/0/90]s laminate. 163
Figure C.6 Transverse in-plane stress distribution near free edge of [02/±30]s laminate. 164

LIST OF TABLES

Table 5.1 Specimen information. 59

Table 5.2 Test matrix 65

Table 6.1 Material Properties 72

Table 6.2 Results of edge comparison of side A and side B 93

NOMENCLATURE

a_o	Total thickness of laminate
a_1	Thickness of rest of laminate
a_2	Thickness of laminate outside cracking ply group
$[A]$	Laminate stiffness matrix
A_{11}	Component of laminate stiffness matrix
E_1	Equivalent axial stiffness of laminate outside cracking ply group
E_2	Equivalent axial stiffness of cracking ply group
E_o	Equivalent axial stiffness of entire laminate
E^{eff}	Effective laminate stiffness
E_{li}	Longitudinal modulus
E_{ti}	Transverse modulus
G	Strain energy release rate
G_c	Critical strain energy release rate
G_i	Shear modulus
h	Crack spacing
k	Proportionality constant in shear lag analysis
l	Crack length
l_c	Critical crack length
n	Number of plies in laminate
N	Thermal cycles
q	Shear stress
$[Q_i]$	Ply stiffness matrix of i^{th} ply
$Q_{11(i)}$	Component of ply stiffness matrix of i^{th} ply
$Q_{12(i)}$	Component of ply stiffness matrix of i^{th} ply

$Q_{22(i)}$	Component of ply stiffness matrix of i^{th} ply
$Q_{66(i)}$	Component of ply stiffness matrix of i^{th} ply
t_c	Thickness of cracking ply group
t_i	Thickness of i^{th} ply
T	Temperature
T_{sf}	Stress free temperature
$[T_i]$	Transformation matrix of i^{th} ply
u_1	Displacement in rest of laminate in axial direction
u_2	Displacement in cracking ply group in axial direction
U	Strain energy of body
W	Work done by an external load
x	Coordinate system axis
y	Coordinate system axis
α_1	Average coefficient of thermal expansion in the laminate outside the cracking ply group
α_2	Coefficient of thermal expansion in cracking ply group
α^{eff}	Effective laminate longitudinal coefficient of thermal expansion
α_{li}	Longitudinal coefficient of thermal expansion
α_{ti}	Transverse coefficient of thermal expansion
$[\alpha]^e$	Effective coefficient of thermal expansion vector
ΔT	Change in temperature relative to stress free temperature
ΔU	Change in internal energy
ΔW	Change in external work
ε_1	Longitudinal strain in the laminate outside the cracking ply group
ε_2	Longitudinal strain in the cracking ply group
ε_e	Average strain

ϕ_c	Rotation factor for cracking ply c
κ_i	Knockdown factor of i^{th} ply
ν_i	Major Poisson's ratio
θ_c	Ply angle of cracking ply group
θ_i	Ply angle of i^{th} ply
θ_i'	Ply angle of ith ply after rotation
ρ	Crack density
σ_1	Average longitudinal stress of the laminate outside the cracking ply group
σ_2	Longitudinal stress of the cracking ply group
σ_a	Average stress due to externally applied mechanical load
σ_e	Equivalent applied thermal stress
σ_{fc}	First ply failure stress
ξ	Shear lag parameter

CHAPTER 1

INTRODUCTION

Advanced composite materials are widely used in space applications because of their attractive structural properties. Their high specific strength, light weight, low coefficient of thermal expansion, and high stiffness are especially advantageous in dimensionally critical structures such as solar reflectors, space science instruments, communication satellites, antennae, and their support structures because deformations can be held to a minimum.

A concern in utilizing composite materials in these applications is damage caused by the space environment. Thermal cycling, which induces thermal stresses in space structures, is one of these concerns. During orbit, spacecraft travel in and out of the earth's shadow, going through cycles of high and low temperatures. The exact thermal history depends on orbital parameters, surface coating, and structural size, but in general, exposed space structures are subjected to approximate temperature extremes of ±150°F in low earth orbit (LEO) and ±250°F in geosynchronous earth orbit (GEO). In a typical vehicle with a service time of 10 years, approximately 5000 thermal cycles could occur in GEO or 10,000 cycles in LEO. More specifically, the Space Station Freedom, with a 30 year projected lifetime, could experience 175,000 thermal cycles (one every 90 minutes in LEO), with temperatures ranging from +150°F to -150°F.

The first observed damage from the thermal environment is matrix dominated cracks induced by thermal stresses in individual plies of composite laminates. We refer to this type of damage as a microcrack or matrix crack. Examples are illustrated in Figure 1.1. Photomicrographs show microcracks visible at the edges of crossply $[0_2/90_2]_S$ and quasi-isotropic $[0/45/90/-45]_S$

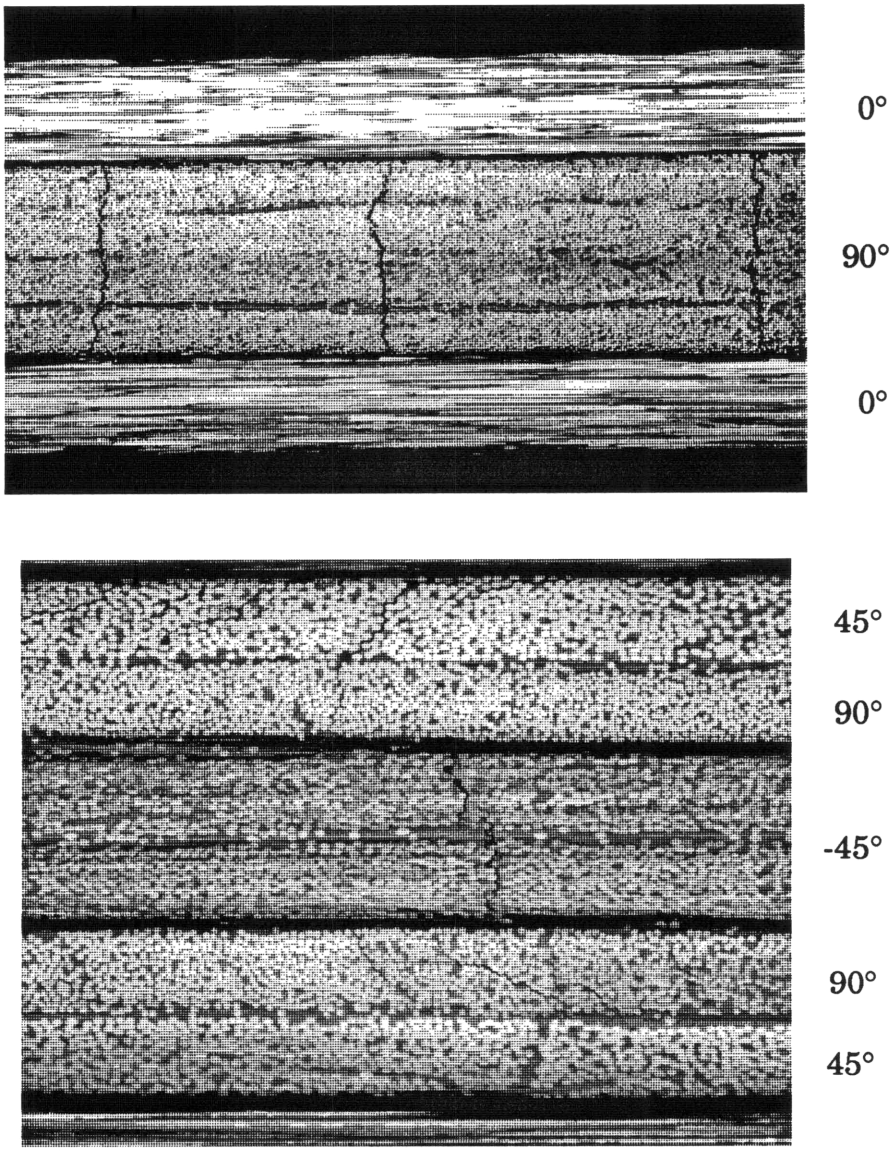

Figure 1.1 Examples of microcracks on edges of laminates. Photomicrographs of crossply $[0_2/90_2]_S$ specimen under 50x magnification and quasi-isotropic laminate $[0/45/90/-45]_S$ under 200x magnification (0° ply is not visible).

laminates. Microcracking is a phenomenon which can effect the thermal and mechanical properties of composite materials. This can significantly effect structural integrity and degrade performance in space applications. In later stages, extensive microcracking could cause premature failure. More importantly, this type of damage can cause degradation of laminate properties, which is an important issue where dimensional stability is critical. When composite structures are designed with specific material properties (i.e. low CTE, high stiffness) in mind, results may be disastrous if these properties deviate from design values.

Microcracking damage is basically caused by coefficient of thermal expansion (CTE) property mismatch. Figure 1.2 illustrates the basis of the thermal microcracking problem. The plies of a composite laminate have different CTE values because of their various orientations. If the plies were independent and unconstrained, they would be able to freely expand or contract according to their individual CTE's when subjected to thermal loading. In actuality they are laminated together and therefore constrain each other, creating high stresses and microcracks.

Engineers and researchers have realized that microcracking is an important issue in structural reliability and durability. There has been much testing on the cracking of laminates and the resulting property degradation. From experimentation, effects important to the damage state, such as different material types, laminate geometries, and ply thicknesses, have been identified. Rather than conducting time consuming tests for every possible proposed material and laminate, a greater understanding of this damage mechanism is required. We need analytical capabilities to predict crack density and the cracks' effects on laminate properties. This will give us not only the ability to quantify the damage but also a tool to critically analyze the problem.

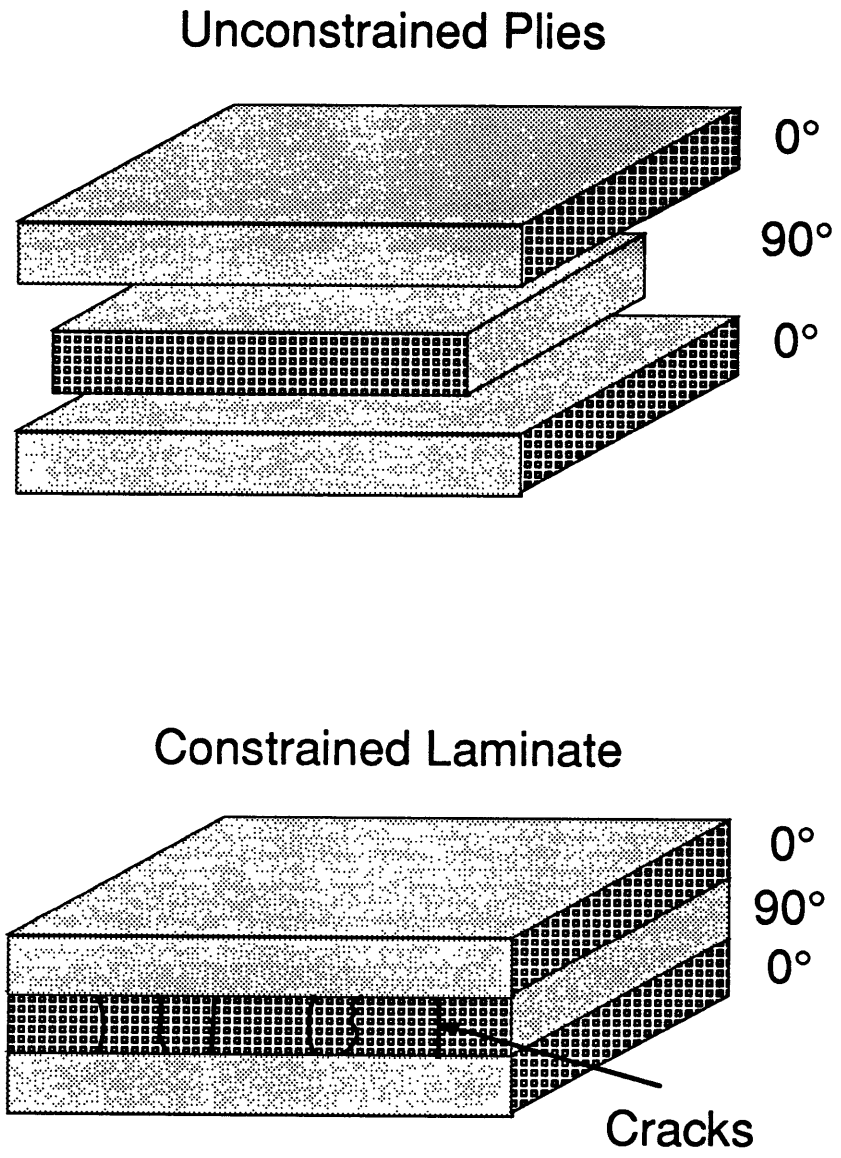

Figure 1.2 Thermally loaded unconstrained plies and constrained laminate. CTE mismatch causes microcracks to appear.

To attain this capability, we first studied the previous work relevant to our problem. This will be reviewed in Chapter 2. Chapter 3 contains the problem statement summarizing the completed research. The analytical methods used will be discussed in Chapter 4. We will present the general model which was formulated and implemented into a computer program to predict damage. A three dimensional stress analysis was also completed to understand effects of free edges on our analysis. Chapter 5 describes the types of experiments conducted. We tested various composite specimens to verify the analytical predictions. Additionally, experiments were performed to confirm the assumptions used in the development of the analysis. Finally, all the analytical and experimental results and correlations will be discussed in Chapter 6. Conclusions and recommendations for further research will be presented in Chapter 7.

CHAPTER 2

PREVIOUS WORK

Few previous studies address thermal cycling damage in composite space structures. No completed work allows for quantitative prediction of crack density and laminate property degradation due to the thermal environment. However, research has been performed in the general area of microcracking damage from mechanical loading. Many studies in the progressive (monotonically increasing) loading and fatigue loading of composite laminates have been reported. However, only a small subset is applicable to our problem. Only relevant studies, those which contribute to our predictive work in thermal applications, will be addressed here. Most of this work has been concentrated on the specific topic of progressive loading of crossply laminates. In thermal applications, some analytical work has been conducted, but quantitative, predictive capabilities are minimal. Much of the research in thermal applications has been devoted to gathering experimental data and results.

In this chapter, analytical approaches will be briefly reviewed for background. Then studies relating to mechanical applications that are relevant to our thermal problem will be discussed. The discussions are divided into progressive loading and fatigue loading applications. Lastly, the research on thermal cycling is reviewed with an emphasis on the limited predictive work.

2.1 OVERVIEW OF ANALYTICAL APPROACHES

Many different types of analytical approaches exist. The various methods use either a fracture mechanics or strength of materials failure criterion to predict damage. Both require knowledge of the stress state, which can be

obtained by a variety of methods. These methods are either analytical (e.g. shear lag analysis, classical laminated plate theory, variational method) or numerical (finite element method).

Once the stress field is derived, the fracture mechanics techniques use the stress state to determine energy change during crack formation. The calculated energy is typically compared with the critical strain energy release rate, which is a material property. If the released energy is greater than the critical strain energy release rate, the energy criteria for crack appearance is satisfied. In contrast to usual fracture mechanics techniques, the growth of cracks is not predicted. Instead, it is presumed that if cracks are energetically feasible they will form. This is equivalent to assuming that critical flaws exist throughout the material. The strength based approaches use the derived stress state to compare with the material failure property. In the simplest example, cracks form when the maximum predicted ply stress exceeds the ply failure strength, a material property.

Within the two basic approaches, studies diverge into different areas. For instance, research is conducted at different scales. Studies are sometimes performed to study mechanics at the ply and laminate level. On the other hand, microstructural studies analyze the response of the fiber and matrix and their interactions. Statistical methods can also be incorporated to all of these approaches. In fracture mechanics methods a probabilistic starting crack location is used whereas in strength approaches a probabilistic strength distribution is assumed.

2.2 MECHANICAL APPLICATIONS

Many analytical models have been proposed to address cracking and its effects on laminate properties under mechanical progressive loading. Classical

Laminated Plate Theory (CLPT) combined with the strength of materials method has been applied to attempt crack initiation prediction. An *in situ* transverse strength property is used in the failure criterion [1, 2]. This method does not seem to be adequate in general cases. Flaggs and Kural [1] found that the *in situ* strength is not a ply property but is dependent on ply thickness and laminate geometry.

Lee and Daniel [3] also used the strength criterion to predict cracking but developed the stress field using a shear lag analysis. Some statistical work has been reported by Peters [4-6]. He used a shear lag solution for stresses and a strength based failure criterion with a probabilistic strength distribution.

Much work has been done using the fracture mechanics approach. A shear lag analysis to approximate stresses near a crack and an energy criterion to predict the appearance of a crack is used in this technique [7-15]. Laws and Dvorak [8] also incorporated a probabilistic model for crack distributions.

There has been similar work using the fracture mechanics and energy method but using an analysis other than shear lag to predict stresses. A variational approach has been used by Nairn [16] and Varna and Berglund [17]. They use principles of minimum complementary potential energy to derive approximate stress and strain fields. Tan and Nusimer [18] used 2D elasticity to derive their analysis. Lim and Hong used a finite element analysis to correlate crack density to reduced laminate properties [10].

Additionally, research has been done using continuum damage mechanics (CDM) models [19, 20] These are thermodynamics based models which represents damage (cracking) as a set of internal state variables. This approach is fracture mechanics driven. The damage is considered as a energy dissipative mechanism so that cracking can be predicted.

A great amount of literature on various aspects of the fatigue of composites exists [21-27]. These reports, concerned with the characterization and prediction of fatigue damage, have extensive descriptions and measurements of this phenomena. However, the problem we are concerned with, the problem of matrix cracks, is not the central issue of most of these studies. More often it is used as an indication or metric of damage. A limited number of reports refer to the analysis of crack density and property degradation caused by mechanical fatigue loading. Most of these studies transferred progressive loading analysis techniques to fatigue [19, 28-30]. For example, CDM work was incorporated into fatigue applications by Paas et al. [19]. Petitpas et al. [30] developed a shear lag based stress model and used a maximum strength criteria for crack prediction. They then empirically formulated a relation between effective failure strength and number of cycles to predict crack density during fatigue loading.

Most of the quantitative analyses for mechanical loading are restricted to monotonically increasing loading of crossply laminates. There have been some who derived their analysis incorporating general angle laminates [7, 11, 31] but in general, these reports have not fully proven these capabilities.

2.3 THERMAL APPLICATIONS

Many of the analytical studies presented for mechanical loading applications incorporated a residual thermal stress. However, this thermal input was incorporated only as a fixed factor in the analyses.

A limited amount of analytical work has been done to directly address the cracking of thermally loaded composites. Classical Laminated Plate Theory (CLPT) was initially attempted to study microcracking [32-34]. Adams [33] used CLPT and *in situ* transverse strength to predict the onset of microcracking.

Additionally, the ply discount method was used by Bowles [34] to predict reduction of properties with little success. These analyses have emphasized the damage mechanics at the ply level.

Micromechanics methods approach the problem at a different scale to study fiber and matrix interactions [32, 34-38]. This approach allows studies of various microstructural parameters and their effects on microdamage development. Bowles derived thermally induced stresses using finite element analysis. Then he predicted fiber matrix debonding initiation and location by comparing the maximum radial stress at the interface to the interfacial bond strength.

Most of the research dedicated to the thermal loading problem has been in experimental testing and observation of thermal cycling damage and its effects on laminate properties [39-47]. Knouff [41] tested to see if fiber type and properties had an effect on microcracking under thermal cycling. He fit a hyperbolic function to experimental data of crack density versus thermal cycles and found the rate of crack density increase to be dependent on fiber type. Numerous other experiments were conducted by Tompkins et al. [44-47] to measure properties such as CTE, stiffness, strain and crack density after thermal cycling. Manders and Maas [42] tried testing thin plies (i.e. 0.001 inches compared to the usual 0.005 inches) to see if cracking and property degradation was minimized. Bowles and Shen [39] tested fabric for the same purposes.

2.4 ANALYSIS OF THERMALLY LOADED CROSSPLY LAMINATES

McManus et al. [48] conducted an analytical predictive study of thermally loaded crossplies. They used the fracture mechanics approach with a shear lag

approximation of stresses near a crack. Crack density in one 90° ply group and reduced laminate properties were derived as a functions of monotonically decreasing temperature. The effects of thermal cycling were included in the analysis using a material degradation fatigue model. In addition, they completed statistical work on the distribution of cracks. A Monte Carlo simulation was used to predict crack locations along with the crack density.

A computer program was written to incorporate all these aspects of the analysis. The code gives crack density and reduced laminate properties as functions of monotonically decreasing temperature or number of thermal cycles.

Experimental work was also completed to correlate with the analytical predictions. They monotonically cooled crossply specimens and inspected the edges for microcracks, tracking crack density and distribution under an optical microscope. Thermal cycling tests were also performed. Specimens were progressively cool and cycled in a thermal environmental chamber

The final results of the analysis were shown to correlate well with the progressive cooling and thermal cycling experiments. The model was also used to conduct parametric studies to understand various factors in the damage mechanism. One important result is that laminates with thinner ply groups were predicted to crack at lower temperatures or number of thermal cycles, but eventually crack more. However, cracks in thinner plies do not effect predicted laminate properties as much as they do in thicker plies. Overall, the analytical model proved to be an accurate and reliable approach with the crossply laminates.

CHAPTER 3

PROBLEM STATEMENT

Our goal is to gain a better understanding of matrix cracking in composite space structures. This goal is pursued by 1) developing a generalized analytical technique, 2) correlating the analysis with experiments, and 3) studying the validity of the assumptions underlying the analytical method.

The analytical technique is a generalization of a fracture mechanics model which uses a shear lag derivation of the stress state. All plies in an arbitrary layup are analyzed under progressive and fatigue thermal loading. The interaction of cracks forming in one layer with existing cracks in other layers is included. Additionally, material softening effects and temperature dependence of material properties are modelled. The result is an analytical model with predictive capabilities. Given laminate geometry, layup, material property information and thermal loading history, the analysis calculates crack density and degraded laminate properties as functions of thermal loading.

Experiments are conducted on a variety of composite laminates to correlate with the analytical predictions. A thermal environmental chamber is set up to monotonically cool composite specimens. Afterwards, the edges of the laminates are inspected under an optical microscope to determine the number of cracks and their spatial distribution.

The validity of the assumptions and ideas used in our analysis is also investigated. X-ray photography and a series of edge inspections is used to examine the three dimensional crack configuration throughout the volume of the specimen. Analytically, a three dimensional free edge stress analysis is used to investigate the significance of edge effects to cracking.

CHAPTER 4

ANALYTICAL METHODS

The analytical methods presented in this chapter are used to model damage in composite laminates due to thermal loading. An energy method is used to predict crack density and laminate property variations. This approach uses a shear lag stress solution and a fracture mechanics failure criteria. The matrix microcracking behavior and the assumptions used in the model will first be explained. Then the basic energy equations for crack appearance will be derived. An algorithm to apply this method to the progressive cooling and thermal cycling problems for any type of laminate will then be described. It includes effects such as material softening and temperature dependent material properties. Additionally, a three dimensional interlaminar stress analysis will be discussed to investigate edge effects not addressed in the general model.

4.1 APPROACH

An understanding of microcrack formation is necessary to model the damage development. Figure 4.1 shows a series of edge views of a laminate with matrix cracks illustrated in one arbitrary ply. We assume that cracks grow up and down, spanning the ply thickness. They also propagate parallel to the fibers, through the width of the composite laminate as shown in Figure 4.2a. Cracks are shown in all plies of a $[45/90]_S$ layup. The analysis assumes that the appearance of a new crack shown in Figure 4.2b is an instantaneous process. Microcracks form through the thickness and straight across the width of the laminate as a single mechanism. Our study is concentrated on modelling the process illustrated in Figure 4.2.

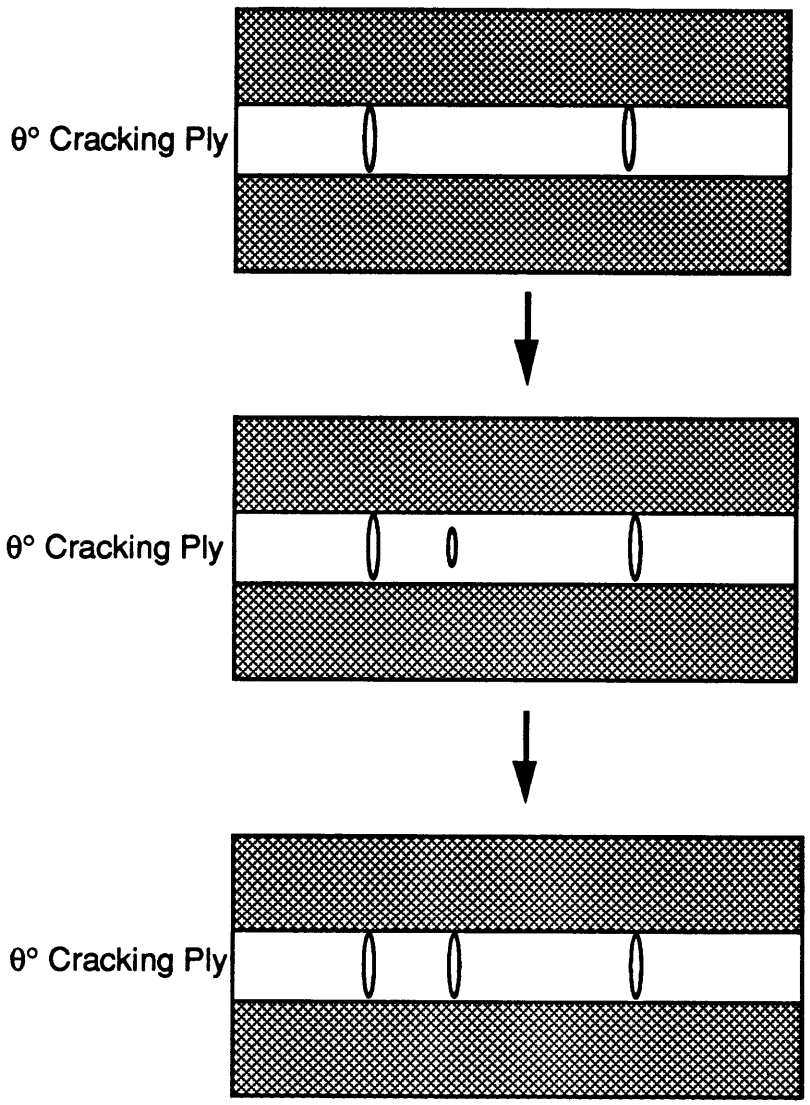

Figure 4.1 Crack formation in an arbitrary ply. Cracks grow to span the ply thickness instantaneously.

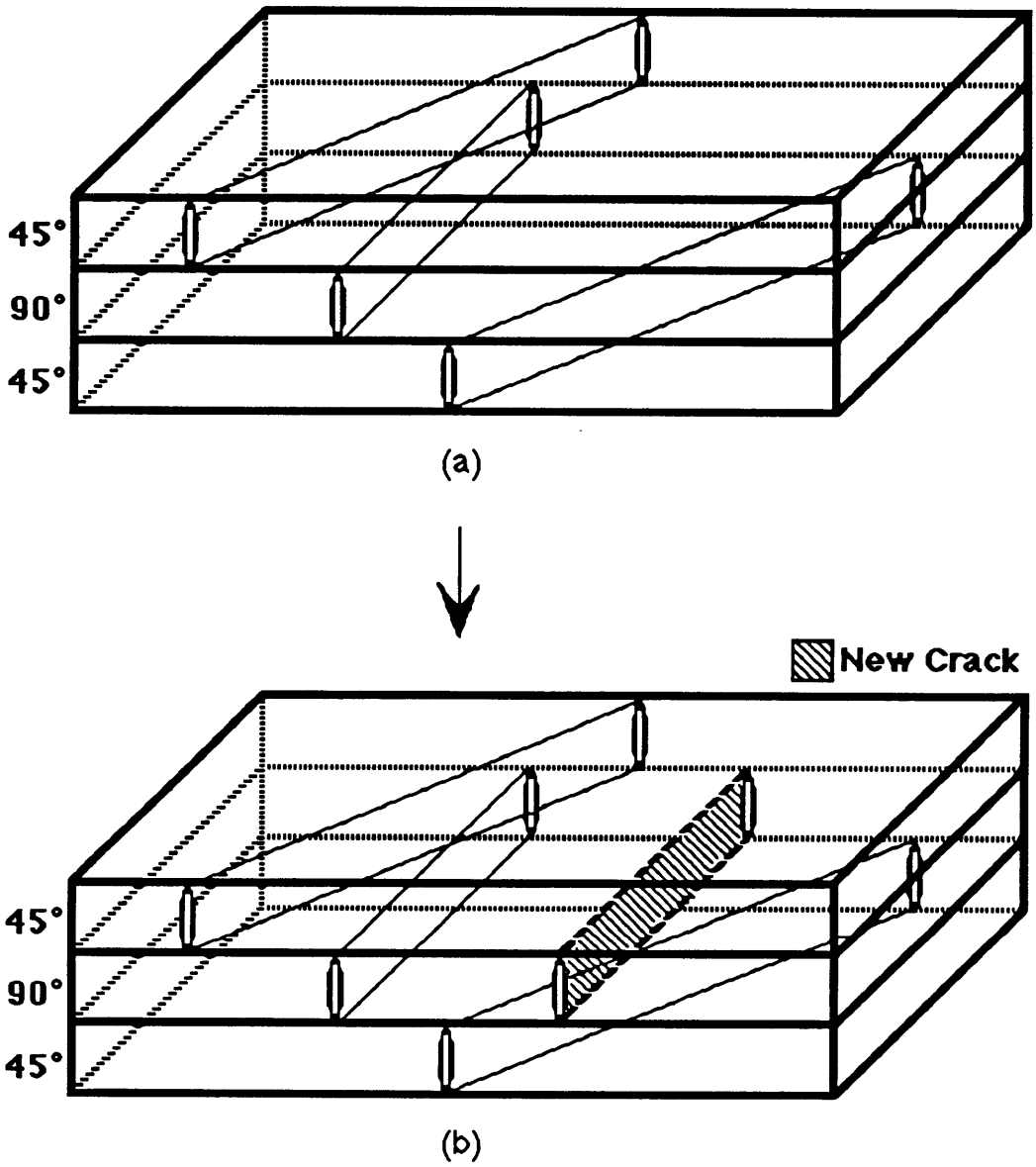

Figure 4.2 Crack formation in laminate. We assume cracks form suddenly through the width of the laminate as shown in the process (a) to (b).

The fracture mechanics approach has two criteria for crack formation. The first is an energy criteria; a crack will grow when energetically favorable. That is, a crack grows when the strain energy release rate, G, generated from crack growth, reaches some critical value G_c

$$G \geq G_c \tag{4.1}$$

where

$$G = \frac{1}{a_2}\frac{d}{dl}(W-U) \tag{4.2}$$

W is the work done by any external load, U is the strain energy of the body, l is the crack length, and a_2 is the thickness of the cracking body. The critical strain energy release rate, G_c, is considered a material property and is a measure of the fracture toughness. This property is usually referred to as the interlaminar fracture toughness.

The second requirement for crack formation is that it is mechanistically possible. A basic assumption in our model is that there are an abundant number of starter cracks of critical size, l_c. The graph in Figure 4.3 illustrates that, for a ply crack of the type described in Figure 4.2, the strain energy release rate is not dependent on crack size once a critical crack size is reached. This is due to the fact that a cracking ply is restrained by other plies. The energy criterion for crack formation in this case is only a function of the loading or strain energy.

When composites store energy from loading, some of the energy is released by the appearance of a crack. The change in energy of this process is computed to compare with G_c

$$\Delta W - \Delta U \geq a_2 G_c \tag{4.3}$$

where ΔW and ΔU are the change in external work and internal energy from the state of Figure 4.2a to that of Figure 4.2b. This is a criterion for the appearance

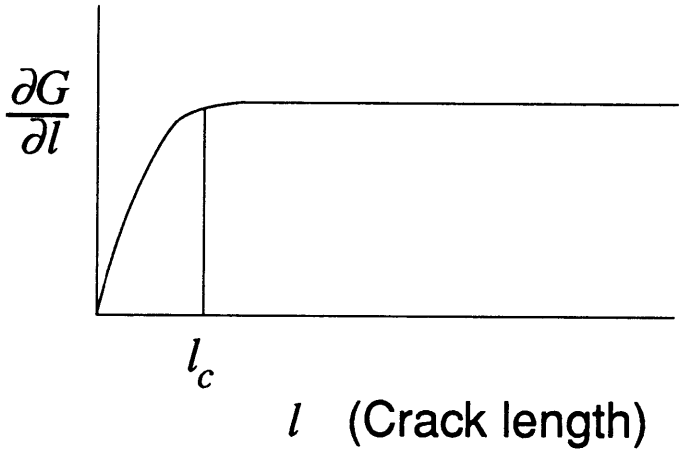

Figure 4.3 Graph of the change in strain energy as a function of crack length.

of cracks rather than their growth. As mentioned earlier, critical starter cracks exist and the energy release is constant with crack length, so fully formed cracks appear instantaneously once the energy criteria is satisfied.

4.2 DERIVATION OF BASIC ENERGY EQUATIONS

To calculate the strain energy release rate used in the fracture mechanics technique, the stress state in a body with and without a crack must be known. The stress distribution around a crack is derived using a shear lag approximation. Using these solutions, the equations for crack appearance and resulting laminate property reduction are derived.

4.2.1 Stress Distribution and Displacement Field

In our shear lag analysis, we consider a laminate as in Figure 4.4. The stress state is derived between any two cracks, $2h$ apart. We are modelling the laminate as made up of two components: a cracking ply group, and the rest of the laminate which is smeared together to make up the other group. The coordinates are selected so that the y-axis is parallel to the fiber direction in the cracking ply group. All stresses, strains, displacements, and properties are in reference to the axial direction (the x-axis). They are also per unit width in the y direction, which is into the page in Figure 4.4. A '0' subscript denotes properties of the entire combined laminate. Similarly, the subscripts '2' and '1' represent properties of the cracking ply group and the rest of the laminate, respectively. Thus, α_2 is the coefficient of thermal expansion (CTE) of the cracking ply group in the axial direction and α_1 is the CTE of the rest of the laminate in the x direction. E_2 is the uncracked axial stiffness of the cracking ply group, E_1 is the axial stiffness of the remainder of the laminate and E_0 is the axial stiffness of the entire laminate

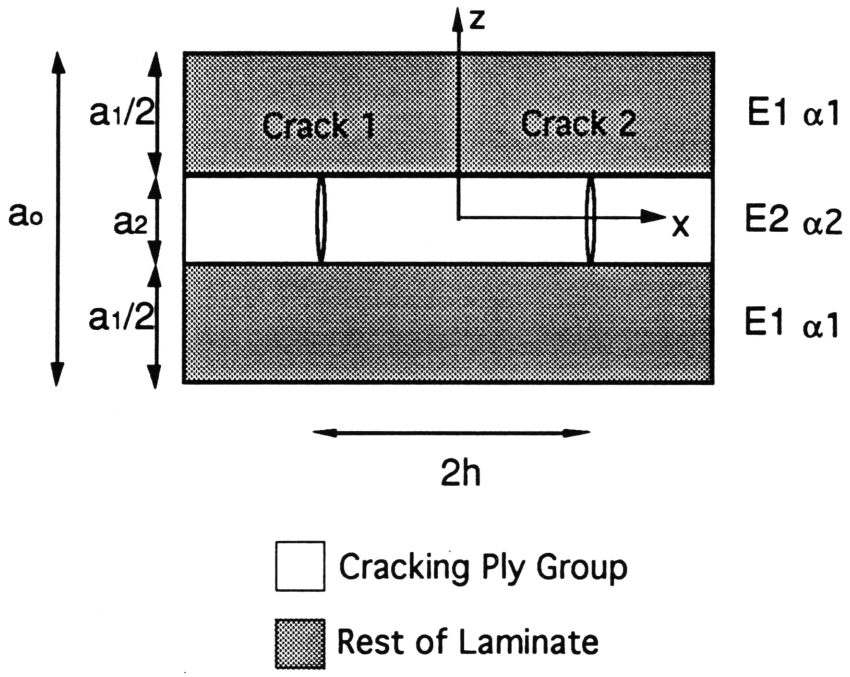

Figure 4.4 Laminate showing two cracks, 2h apart, in a cracking ply group embedded in the rest of a smeared laminate.

$$E_o = \frac{E_1 a_1 + E_2 a_2}{a_1 + a_2} \tag{4.4}$$

where a_2 is the thickness of the cracking ply group and a_1 is the thickness of the rest of the laminate. The equivalent stiffnesses, E_1 and E_2, will be evaluated in Section 4.3.3 which details classical laminated plate theory (CLPT) calculations used in the analysis.

Equilibrium of the laminate illustrated in Figure 4.5 requires

$$a_1\sigma_1 + a_2\sigma_2 = \sigma_a(a_1 + a_2) \tag{4.5}$$

with σ_1 and σ_2 representing the axial stresses in the different ply groupings and σ_a is the average stress due to externally applied mechanical load. These stresses are related to the strains:

$$\sigma_1 = E_1(\varepsilon_1 - \alpha_1 \Delta T) \qquad \sigma_2 = E_2(\varepsilon_2 - \alpha_2 \Delta T) \tag{4.6}$$

where ΔT is the change in temperature relative to the stress free temperature. The cure temperature of the material system is usually considered to be the stress free temperature T_{sf}, and $\Delta T = T - T_{sf}$. The strain/displacement relations are

$$\varepsilon_1 = \frac{du_1}{dx} \qquad \varepsilon_2 = \frac{du_2}{dx} \tag{4.7}$$

where ε_2 and u_2 are the strain and displacement in the axial direction of the cracking ply group, and ε_1 and u_1 represent the same variables in the rest of the laminate. Combining the stress/strain (Eq. 4.6) and strain/displacement (Eq. 4.7) equations gives us

$$\frac{\sigma_1}{E_1} = \frac{du_1}{dx} - \alpha_1 \Delta T \qquad \frac{\sigma_2}{E_2} = \frac{du_2}{dx} - \alpha_2 \Delta T \tag{4.8}$$

Equilibrium of each ply grouping in Figure 4.5 can be written as

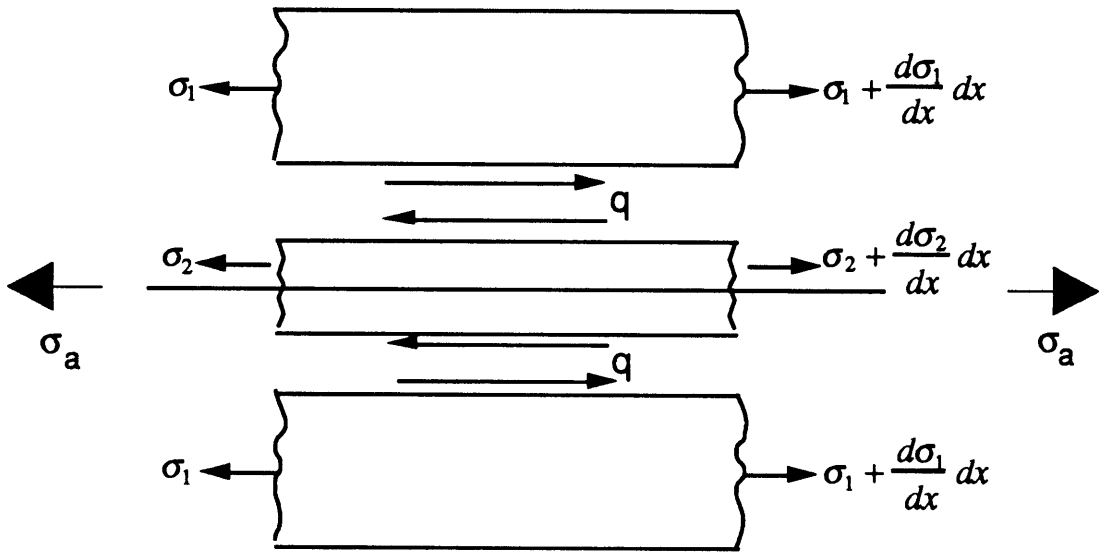

Figure 4.5 Free body diagram of small section of laminate.

$$q = -\left(\frac{a_1}{2}\right)\frac{d\sigma_1}{dx} \qquad q = \left(\frac{a_2}{2}\right)\frac{d\sigma_2}{dx} \tag{4.9}$$

where q is the shear stress which is assumed to be proportional to the relative displacement:

$$q = k(u_2 - u_1) \tag{4.10}$$

The variable k is a proportionality constant analogous to the shear modulus. This constant represents a complex combination of the shear moduli of the different ply groups and the interlaminar layer between them. In this development, it will be treated as a fitting parameter in the shear lag solution. Equating the x derivatives of Eqs. 4.9 and 4.10 and making appropriate substitutions using Eq. 4.8 gives us:

$$\left(\frac{a_2}{2}\right)\frac{d^2\sigma_2}{dx^2} = k\left(\frac{du_2}{dx} - \frac{du_1}{dx}\right) \tag{4.11}$$

$$\frac{d^2\sigma_2}{dx^2} = \frac{2k}{a_2}\left(\frac{\sigma_2}{E_2} - \frac{\sigma_1}{E_1} + (\alpha_2 - \alpha_1)\Delta T\right) \tag{4.12}$$

Substituting for σ_1 from Eq. 4.5 results in a second order differential equation which is a function of the stress in only the cracking ply group.

$$\frac{d^2\sigma_2}{dx^2} - 2k\left(\frac{E_1a_1 + E_2a_2}{a_1a_2E_1E_2}\right)\sigma_2 = \frac{2k}{a_2}\left[-\frac{\sigma_a(a_1+a_2)}{a_1E_1} + (\alpha_2 - \alpha_1)\Delta T\right] \tag{4.13}$$

The differential equation can be simplified by substituting E_o in Eq. 4.4 and rearranging:

$$\frac{d^2\sigma_2}{dx^2} - \frac{4\xi^2}{a_2^2}\sigma_2 = -\lambda \tag{4.14}$$

where ξ is the shear lag parameter:

$$\xi = \sqrt{\frac{k(E_1a_1 + E_2a_2)a_2}{2a_1E_1E_2}} \tag{4.15}$$

and

$$\lambda = \frac{2k(E_1a_1 + E_2a_2)}{a_1a_2E_1E_o}\sigma_a - \frac{2k}{a_2}(\alpha_2 - \alpha_1)\Delta T \tag{4.16}$$

The general form of the solution to differential equation (4.14) is:

$$\sigma_2 = \frac{\lambda a_2^2}{4\xi^2} + A\sinh\left(\frac{2\xi}{a_2}x\right) + B\cosh\left(\frac{2\xi}{a_2}x\right) \tag{4.17}$$

Using the boundary conditions that the stress at the two crack locations is zero (σ_2=0 at $\pm h$) we can solve for the coefficients.

$$A = 0 \tag{4.18}$$

$$B = -\frac{\lambda a_2^2}{4\xi^2\cosh\left(\frac{2\xi}{a_2}h\right)} \tag{4.19}$$

Substituting the coefficients gives the final expressions for stress distribution in the cracking ply group:

$$\sigma_2 = \frac{\lambda a_2^2}{4\xi^2}\left[1 - \frac{\cosh\left(\frac{2\xi}{a_2}x\right)}{\cosh\left(\frac{2\xi}{a_2}h\right)}\right] \tag{4.20}$$

$$\sigma_2 = \frac{a_2k}{2\xi^2}\left[\frac{(E_1a_1 + E_2a_2)\sigma_a}{a_1E_1E_2} - (\alpha_2 - \alpha_1)\Delta T\right]\left[1 - \frac{\cosh\left(\frac{2\xi}{a_2}x\right)}{\cosh\left(\frac{2\xi}{a_2}h\right)}\right] \tag{4.21}$$

4.2.2 Strain Energy Release Rate

With the completed derivation of the stress field between any two cracks, the strain energy released from the appearance of a new crack can be

formulated. For now, we will assume an uniform crack distribution. We derive the change in strain energy between the two states illustrated in Figure 4.6a and 4.6b, which will be referred to as the initial and final states, respectively. We assume that the strain energy release rate per unit width is:

$$\Delta G = \frac{\Delta W - \Delta U}{a_2} \tag{4.22}$$

where ΔW is work done by the load, ΔU is the change in stored elastic strain energy, and a_2 is the thickness of the cracking ply group. Our assumption is that this laminate is under fixed mechanical or thermal loads.

Given the stress fields calculated in the previous section, the strain energy in the laminate between any two cracks separated by distance h can be calculated. The energy released by the appearance of a new crack half way between two existing ones is calculated as follows. The internal energy of the initial configuration (Figure 4.6a) is calculated. The internal energy of the configuration including the new crack (Figure 4.6b) is calculated using the same method. The energy in the two regions from crack A to crack C and crack C to crack B are calculated using separation $h/2$ in place of h in the original calculations. Then the energy in the two regions are summed. The energy released from the appearance of a new crack C is then

$$\Delta U = U(h) - 2U(h/2) \tag{4.23}$$

where $U(x)$ is the energy in the laminate between two cracks distance x apart.

To evaluate ΔU, the energy formulation of Laws and Dvorak [8], with some changes in notation is used. The derivation will not be repeated here. The only modifications are that the applied mechanical load is assumed to be zero, while the thermal loading, reduced to a residual stress term by Laws and Dorak, is the active loading term.

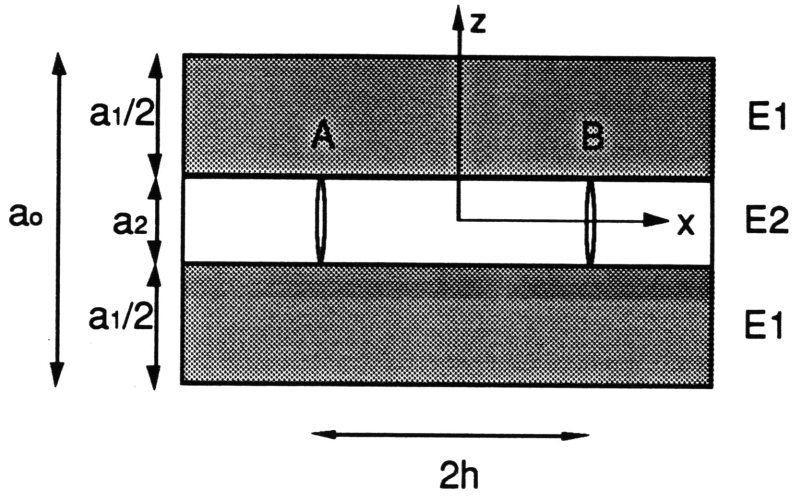

(a)

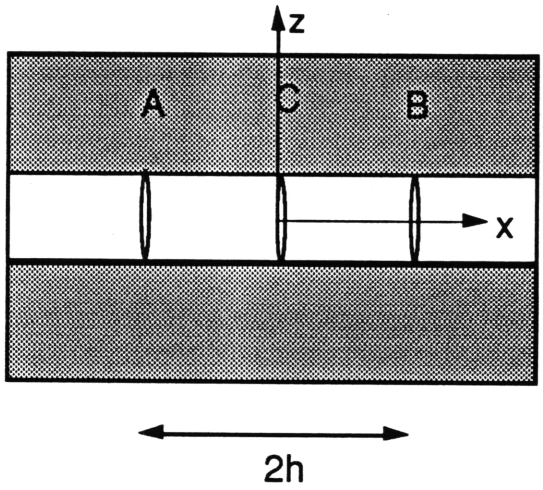

(b)

Figure 4.6 (a) A laminate with two cracks, A and B, spaced 2h apart. (b) Same laminate with the appearance of an additional crack C.

Equation 4.21 has thermal and mechanical components. Note that a change in temperature has the same effect on the stress in the cracking ply as an equivalent mechanical load

$$\sigma_e = \frac{a_1 E_1 E_2 (\alpha_1 - \alpha_2)}{E_1 a_1 + E_2 a_2} \Delta T \qquad (4.24)$$

This equivalent stress is included as a "residual stress", without justification, by Laws and Dvorak. This equivalent stress may be substituted directly into the expression for the strain energy release rate per unit crack length from Laws and Dvorak

$$\Delta G = \frac{\Delta W - \Delta U}{a_2} = \frac{a_2 (a_1 + a_2) E_2}{2\xi a_1 E_1 E_o} \sigma_e^2 \left[2 \tanh\left(\frac{\xi h}{a_2}\right) - \tanh\left(\frac{2\xi h}{a_2}\right) \right] \qquad (4.25)$$

Nairn [16] held some reservations concerning the methods used by previous reseachers, including Laws and Dvorak, for incorporating residual stresses. However, use of alternate energy formulations was found to have only a small effect on crack prediction in cases relevant to this study.

4.2.3 Degradation of Laminate Properties

Expressions for reduced laminate properties resulting from microcracking are now needed. Laws and Dvorak [8] derived the loss of stiffness in a cracked laminate. The average strain of the segment between cracks *A* and *B*, separated by a distance of *2h*, in the uncracked portion of a mechanically loaded laminate can be shown to be

$$\varepsilon_a = \frac{\sigma_a}{E_o} \left[1 + \frac{a_2^2 E_2}{2\xi h a_1 E_1} \tanh\left(\frac{2\xi h}{a_2}\right) \right] \qquad (4.26)$$

This expression can be valid for any two sections *2h* apart. Substituting the expression for crack density:

$$\rho = \frac{1}{h} \tag{4.27}$$

and rearranging gives the effective stress/strain relation for the cracked laminate:

$$\sigma_a = E(\rho)\varepsilon_a \tag{4.28}$$

where

$$E(\rho) = \frac{E_o}{1 + \frac{\rho a_2^2 E_2}{2\xi a_1 E_1} tanh\left(\frac{2\xi}{\rho a_2}\right)} \tag{4.29}$$

is the new laminate stiffness as a function of crack density. McManus et al. [48] went a step further to derive reduction of all laminate properties due to cracking. Considering the reduction in stiffness to be caused entirely by a reduction of stiffness in the cracking ply group, they define a knockdown factor, κ, due to the microcracks

$$E_2(\rho) = \kappa E_2 \tag{4.30}$$

where κ can be calculated as:

$$\kappa = a_1 E_1 \left[1 - \frac{a_2\rho}{2\xi} tanh\left(\frac{2\xi}{a_2\rho}\right)\right]\left[a_1 E_1 + a_2 E_2 \frac{a_2\rho}{2\xi} tanh\left(\frac{2\xi}{a_2\rho}\right)\right]^{-1} \tag{4.31}$$

The knockdown factor is used to recalculate all of the laminate properties. The details of this method are given in Section 4.3.4.

4.3 IMPLEMENTATION FOR THERMAL PROGRESSIVE AND CYCLIC LOADS

The basic formulations for crack appearance and reduced laminate properties are used to derive expressions to predict crack density and degraded

properties due to progressive and cyclic thermal loading. The model is general enough to include all arbitrary laminate configurations, and includes modelling of various secondary effects.

4.3.1 Crack Density as Function of Temperature

The basic energy criteria developed in Eq. 4.25 can be expressed as a function of applied thermal loading, ΔT, for the laminate shown in Figure 4.7. Substituting the expression for the equivalent stress Eq. 4.24, simplifying with Eq. 4.4, and equating ΔG to G_c, the final expression for the energy criteria is:

$$G_c = \frac{a_1 a_2 E_1 E_2 (\alpha_2 - \alpha_1)^2 \Delta T^2}{2\xi(a_1 E_1 + a_2 E_2)} \left[2\tanh\left(\frac{\xi h}{a_2}\right) - \tanh\left(\frac{2\xi h}{a_2}\right) \right] \qquad (4.32)$$

If we assume an existing uniform crack spacing $2h$, then at a thermal load ΔT the criteria above will be satisfied and new cracks will form midway between the existing cracks, resulting in a new crack spacing h. An existing crack spacing just under $2h$ will not satisfy the criteria, and no new cracks will form. In practice, the crack spacing is not uniform, and the true crack spacing will fall somewhere between these extremes. Hence, the crack density, ρ, at temperature change ΔT is:

$$\frac{1}{2h} < \rho \leq \frac{1}{h} \qquad (4.33)$$

where h satisfies Eq. 4.32. Note that Eq. 4.32 can be solved explicitly for ΔT given h, but if we require h (or ρ) for a given ΔT, it must be solved graphically or numerically.

4.3.2 Crack Density as Function of Thermal Cycles

To predict crack density as a function of cyclic thermal loading, a fatigue model was developed by McManus et al. [48]. To account for thermal cycling, we

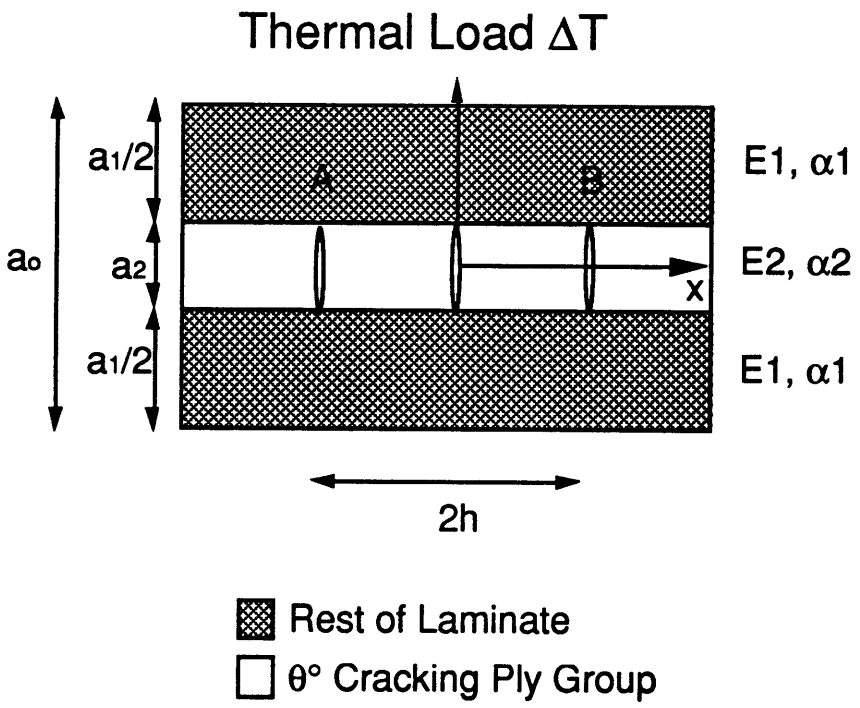

Figure 4.7 Laminate with crack spacing of h subjected to thermal loads.

assume that fatigue loading decreases a material's resistance to cracking. A decrease in the first ply failure stress due to cyclic loading has been observed. Given the experimentally determined first ply failure stress, σ_{fc}, as a function of loading cycles, N, and the original critical strain energy release rate for the desired material system, $G_c(0)$, the critical strain energy release rate can be expressed as a function of N:

$$G_c = G_c(0)\left[\sigma_{fc}(N)/\sigma_{fc}(0)\right]^2 \tag{4.34}$$

This fatigue model will be incorporated to solve for crack density as a function of thermal cycles in Eq. 4.32.

4.3.3 Solution Algorithm Including Secondary Effects

This analysis calculates crack density for every ply of any general laminate, and the resulting degraded laminate properties. The algorithm includes effects such as material softening and temperature dependent material properties. "Material softening" refers to the fact that existing cracks will effect the behavior of the entire laminate, changing its response to further loading. This allows cracking in one ply to realistically affect the cracking behavior of the other plies in the laminate. We incorporate the effects of cracking in all plies such that the reduced properties at each temperature or cyclic load increment reflect the damage incurred in all plies at all previous loads. Material properties are also known to be dependent on temperature. We use temperature dependent material properties, linearly interpolating between temperatures at which data is available.

Figure 4.8 shows a flow chart describing the basic algorithm. It will be described for the case of progressive thermal loading. The analysis starts at the

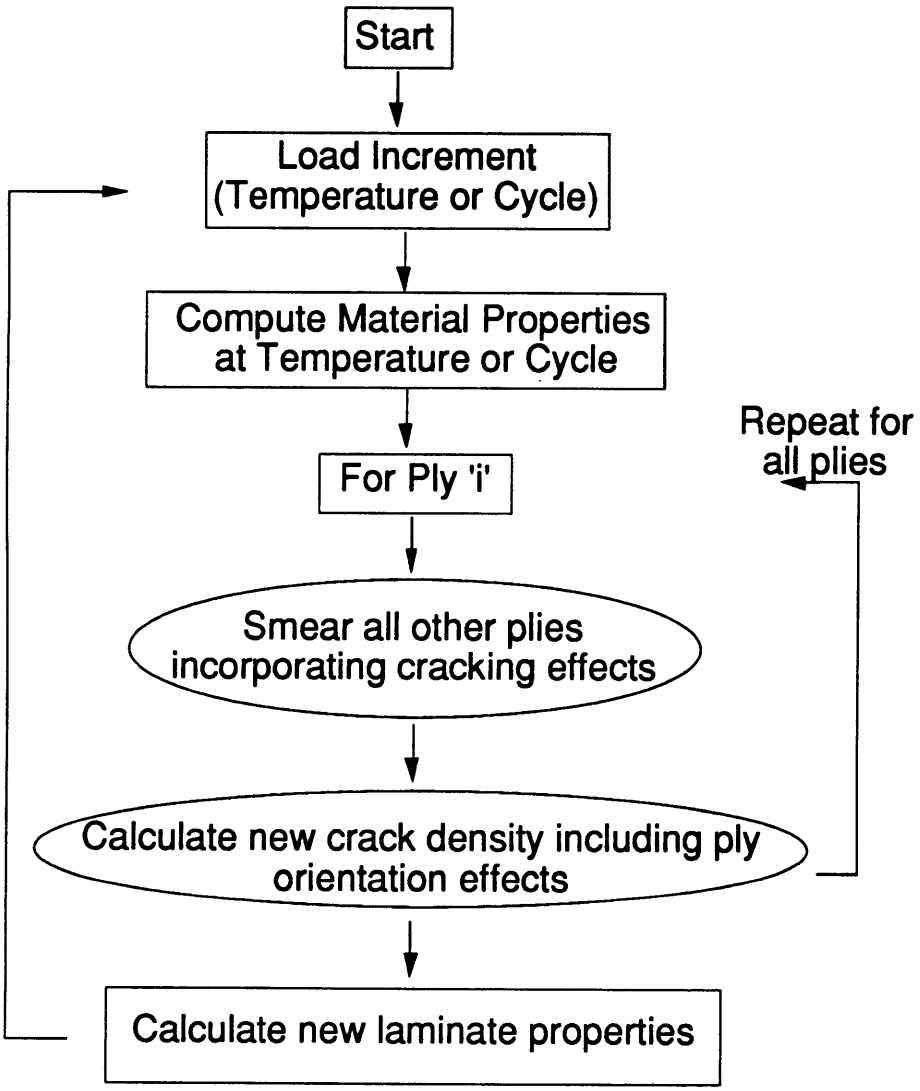

Figure 4.8 Flow chart of algorithm used in analysis.

stress free temperature and increments to a user specified minimum temperature. At each new temperature, the material properties are computed. The ply 'i' is designated as the cracking ply group. A coordinate system is selected so that its x-axis corresponds to the fiber direction of this ply group. Properties of the rest of laminate are smeared together. The effects of existing cracks in the rest of the laminate are included at this stage. The crack density in ply i at this temperature is then calculated. Equation 4.32 is solved for h using a bisection iteration numerical method and crack density ρ follows from Eq. 4.27. This procedure is repeated for every ply at this temperature. After computing the crack density for every ply, the overall laminate properties are calculated to reflect all the damage at this temperature. These steps are iterated to calculate crack density and laminate properties at progressively lower temperatures.

4.3.4 Derivation of Stiffness Constant

Laminate theory (CLPT) [49] is used to derive the stiffness constants used in the above analysis. The equivalent stiffnesses, E_o, E_1, and E_2 are necessary to solve for crack spacing in Eq. (4.32). The effective laminate properties are also required to complete the analysis. First, appropriate material properties are obtained as functions of temperature or cycle number. For each ply i, we have material properties E_{li} (longitudinal stiffness), E_{ti} (transverse stiffness), ν_i (major Poisson's ratio), G_i (shear stiffness) α_{li} (longitudinal CTE) and α_{ti} (transverse CTE). Ply i has a thickness of t_i. The fibers of each ply are aligned at an angle θ_i to the x-axis of a global coordinate system. The cracking ply group, c, is treated as a single layer with orientation θ_c. The crack formation analysis is carried out in an alternate coordinate system defined such that the fibers of the cracking ply group are aligned parallel to its y-axis. In this coordinate system, the ply angles are defined:

$$\theta_i' = \theta_i + \varphi_c \tag{4.35}$$

where,

$$\varphi_c = 90° - \theta_c \tag{4.36}$$

The necessary laminate properties for computing crack density and property degradation can be calculated as follows:

$$[A] = \sum_{i=1}^{n} [\overline{Q_i}]\, t_i \tag{4.37}$$

$$[\overline{Q_i}] = [T_i^{-1}][Q_i][T_i^T] \tag{4.38}$$

$$[Q_i] = \begin{bmatrix} Q_{11(i)} & Q_{12(i)} & 0 \\ Q_{12(i)} & Q_{22(i)} & 0 \\ 0 & 0 & Q_{66(i)} \end{bmatrix} \tag{4.39}$$

$$Q_{11(i)} = \frac{E_{li}}{D_i} \qquad Q_{12(i)} = \frac{\nu_i E_{ti}}{D_i}$$

$$Q_{22(i)} = \frac{E_{ti}}{D_i} \qquad Q_{66(i)} = \frac{G_i}{D_i} \tag{4.40a-e}$$

$$D_i = 1 - \nu_i^2 \frac{E_{ti}}{E_{li}}$$

$$[T_i] = \begin{bmatrix} \cos^2\theta_i' & \sin^2\theta_i' & 2\sin\theta_i'\cos\theta_i' \\ \sin^2\theta_i' & \cos^2\theta_i' & -2\sin\theta_i'\cos\theta_i' \\ -\sin\theta_i'\cos\theta_i' & \sin\theta_i'\cos\theta_i' & \cos^2\theta_i' - \sin^2\theta_i' \end{bmatrix} \tag{4.41}$$

The equivalent stiffnesses required in Eq. 4.32 are:

$$E_o = \frac{A_{11}}{a_o} \tag{4.42}$$

$$E_2 = Q_{22(c)} \tag{4.43}$$

$$E_1 = \frac{E_o a_o - E_2 a_2}{a_1} \tag{4.44}$$

where a_2 is the thickness of the cracking ply group ($a_2 = t_c$). The total thickness is $2a_o$ and $a_1 = a_o - a_2$. The crack density is now computed for ply c. Once ply c has started cracking, the properties of that ply are 'knocked down' due to the cracking damage. A knockdown factor for ply i is defined by Eq. 4.31. For all subsequent calculations, the components are changed as follows:

$$\begin{aligned} Q^c_{11(i)} &= Q_{11(i)} \\ Q^c_{12(i)} &= \kappa_i Q_{12(i)} \\ Q^c_{22(i)} &= \kappa_i Q_{22(i)} \\ Q^c_{66(i)} &= \kappa_i Q_{66(i)} \end{aligned} \qquad \text{(4.45a-d)}$$

These steps (4.35 to 4.45) are repeated for each ply ($c = 2$ *to* $n-1$) to predict crack densities and changes in properties for each ply.

After all the plies have been analyzed in this manner, the degraded effective laminate properties are calculated at each loading:

$$E^{eff} = \frac{1}{A'_{11} a_o} \qquad (4.46)$$

$$[A'] = [A^{-1}] \qquad (4.47)$$

$$[\alpha]^e = [A'] \sum_{i=1}^{n} [\overline{Q}_i][\overline{\alpha}_i] t_i \qquad (4.48)$$

$$[\overline{\alpha}_i] = [T^T] \begin{Bmatrix} \alpha_{li} \\ \alpha_{ti} \\ 0 \end{Bmatrix} \qquad (4.49)$$

$$\alpha^{eff} = \alpha^e_{11} \qquad (4.50)$$

All these steps are repeated for each thermal loading increment until completion of an entire thermal profile. Each increment incorporates the 'knocked down' properties of all the plies from the previous increment, and

temperature or cycle dependent properties for the conditions of the current increment.

4.4 FREE EDGE STRESS ANALYSIS

The analytical procedure developed predicts stresses in each ply of a laminate using the assumptions of CLPT. Interlaminar stresses are assumed to be zero. However, at the free edge of a laminate,

$$\sigma_{yy} = \sigma_{xy} = \sigma_{yz} = 0 \qquad (4.51)$$

CLPT is no longer valid at these boundaries and out-of-plane, interlaminar stresses become large near the free edge. Given that most of our experimental results involve observation of microcracks at the edges, the free edge stress state is clearly important to our problem.

To analytically explore the three dimensional free edge stress state, the analysis of Bhat [50] was used. The analysis calculates the three dimensional stress distribution near the free edge of a laminate at all interfaces. The stresses of interest in our case were not the out-of-plane stresses examined by most researchers. Instead, we examined the behavior of the in-plane stresses near the free edge. These stresses were extracted from the full three dimensional analysis. The computer code by Bhat was modified to compute the in-plane stress distribution in each ply in the ply's coordinate system.

4.5 COMPUTER PROGRAMS

Two computer programs were modified to incorporate the various analyses described above. The computer code CRACKOMATIC takes material properties, laminate geometries, and thermal loading history and predicts crack density and corresponding degraded laminate properties. The two types of calculations are

1) tabulation of crack density and degraded material properties as functions of monotonically decreasing temperature and 2) tabulation of crack density and degraded material properties as functions of thermal cycles. Also included are user options to incorporate material softening effects and temperature dependent material properties. The resulting output is a table with columns listing thermal load (ΔT or N), corresponding crack density of any selected plies, and corresponding reduced laminate properties. These can be used to generate plots of cracking and changing laminate properties as the laminate is thermally cycled or progressively cooled.

The program output reports crack densities as they could be observed on the edge of a specimen. This requires that the calculated results, which are expressed in ply coordinates, be adjusted to account for a geometric effect. Figure 4.9 illustrates this effect. The figure shows a laminate with cracks in the 45° and 90° direction. The crack spacing (h) is the same, but due to the geometry of the laminate, the crack count is higher in the 90° (9 cracks) than in the 45° ply (6 cracks). The reported crack density, ρ_c, is the calculated density, ρ_{co}, multiplied by a geometric factor:

$$\rho_c = \rho_{co} \sin(\theta_i) \tag{4.52}$$

The manual for CRACKOMATIC is in Appendix A. The document describes the program in detail and shows sample sessions. The program source code is available by request from the author or the TELAC laboratory.

The free edge analysis computer program tabulates interlaminar stresses as well as the in-plane stresses from the free edge to a depth of 2mm into the laminate. The program requires material properties, laminate geometry and ply stresses which can be calculated by laminate analysis.

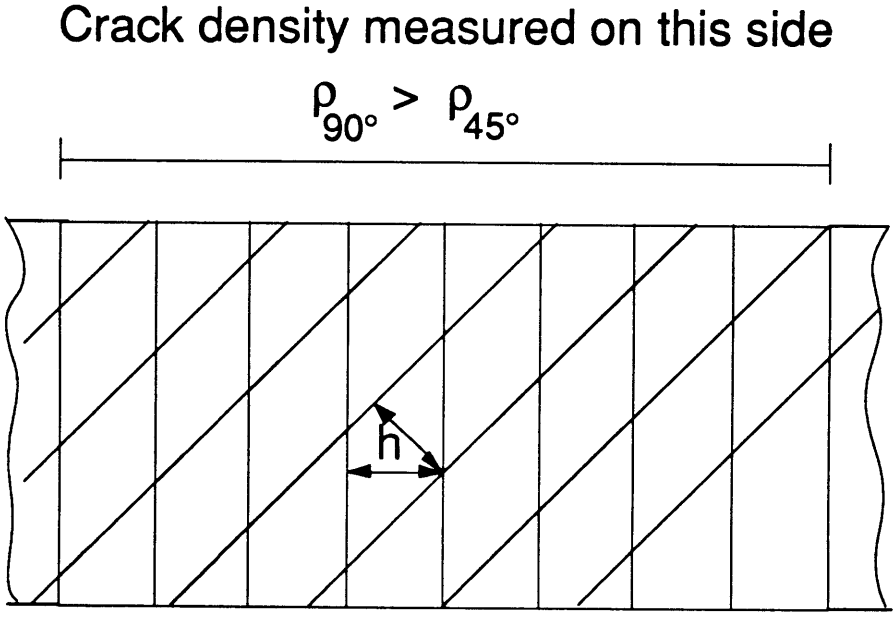

Figure 4.9 Top view of laminate with equally spaced cracks in 45° and 90° plies. Illustrates difference in crack density from geometric effect.

CHAPTER 5

EXPERIMENTAL METHODS

Experimental research was conducted to correlate with the analytical predictions and to check the assumptions incorporated into the cracking analysis. A variety of different laminates were cooled to progressively lower temperatures and the density and locations of the resulting cracks were examined. Crack density and distribution along the specimen edges was determined by edge inspection. Crack configuration throughout the volume of the laminates was determined using X-radiography and edge inspections after sanding.

5.1 PREPARATION OF SPECIMENS

All laminates were fabricated at NASA Langley Research Center (LaRC) according to the manufacturer's recommended procedure. The laminates were made as 12" by 12" panels, using 0.005 inch (0.127mm) plies. These panels were cut into 3" by 0.5" inch (75 by 12.5 mm) specimens. The laminate types and number of specimens used are listed in Table 5.1. The specimens were polished along one of their long edges. This polished edge is referred to as Side A. The opposite edge, which was not polished, is referred to as Side B. Specimens made from the P75/934 graphite epoxy material system were cut and polished at NASA LaRC using their standard procedures. Specimens made from the P75/ERL 1962 material system were prepared at MIT Technology Laboratory for Advanced Composites (TELAC). We used a water cooled diamond blade for cutting and 0.7 micron grit powder for polishing, using a standard TELAC procedure [51].

Table 5.1 Specimen information.

Laminate Layup	Material	Total Specimens
$[0_2/90_2]_s$	P75/934	3
$[0/90/0/90]_s$	P75/934	4
$[0_2/\pm30]_s$	P75/934	3
$[0/45/90/-45]_s$	P75/934	6
$[0/90/\pm45]_s$	P75/934	4
$[0/\pm45/90]_s$	P75/934	4
$[0_2/45_2/90_2/-45_2]_s$	P75/ERL 1962	3

* All specimens are 3.0 by 0.5 inches

All the specimens were dried to a constant weight. The $[0_2/90_2]_s$, [0/45/90/-45]$_s$, and $[0_2/\pm30]_s$ laminates were dried and stored in a vacuum oven at 75°F for more than six months at NASA LaRC where they were then tested. The panels of [0/90/±45]s, [0/±45/90]s, and [0/90/0/90]s laminates were stored at ambient conditions at NASA LaRC. They were cut into specimens at NASA LaRC and then dried at 160°F in a regular oven at TELAC. The specimens were left in the oven for approximately 8 hours a day for a month. They were stored at room temperature with dessicant when not in the oven. The $[0_2/45_2/90_2/-45_2]_s$ specimens were cut into specimens immediately after being manufactured. They were then dried in the TELAC oven at 160°F for approximately 8 hours a day for two weeks, and stored with dessicant when not in the oven. The weight of the specimens dried at TELAC were frequently measured to check for weight loss. These specimens were stored with dessicant after drying to eliminate moisture absorption and tested within a week.

5.2 MICROCRACK EXAMINATION

Microcracking damage was observed by optical inspection of a polished edge of a specimen. Several different optical microscopes were used at a magnification of 200x. The central one inch of the edge was marked before the first observation. The same region was checked at each stage of testing to determine crack density in a consistent manner. The number of cracks in this region was equal to the crack density in cracks per inch. A tally counter was used to minimize error in taking crack counts.

Figure 5.1 illustrates the different types of damage that have been observed on the free edge of a laminate. Delaminations are visible on one of the laminates. There are also full cracks spanning the ply thickness and sometimes partial cracks. Smaller damage types like fiber/matrix debonding have also been

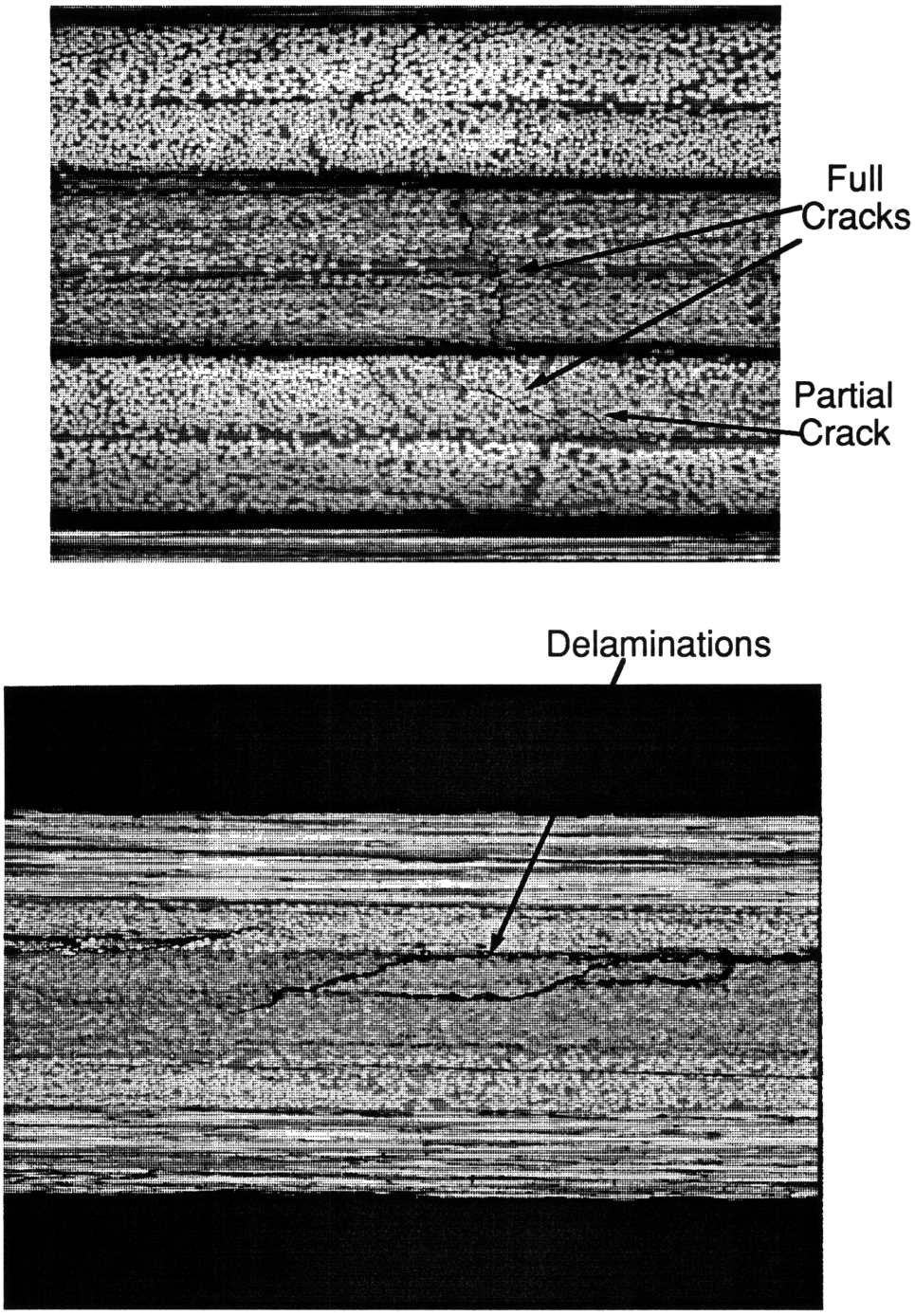

Figure 5.1 Different damage types on free edges of laminates.

observed. In this work, any microcrack extending more than half the thickness of a ply group was counted as a crack. Groups of plies with the same orientation, such as the middle plies of symmetric laminates were considered as one 'thick' ply. We refer to these as 'ply groups'. We also checked a select number of specimens for the distribution of cracks along the edge. We determined where cracks were located spatially, along the inspected one inch span. This was accomplished by one of the following methods: comparing to a ruler with fine gradations placed in the field of view of the microscope, using a micrometer to measure the movement of the microscope platform, or connecting a scaled lens to the microscope to observe crack locations.

5.3 THERMAL PROGRESSIVE TESTING

Specimens were monotonically cooled to progressively lower temperatures. A thermal environmental chamber was put together for this purpose. The internal chamber volume is 4"x4"x12". The chamber uses electrical resistance coils to heat up to 800°F and a liquid nitrogen cooling system to obtain cold temperatures down to -300°F. The specimens are located in a separate shielded compartment within the testing chamber. In this section, the specimens are protected from contact with liquid nitrogen and direct heat radiation so that the specimens are heated and cooled by fan circulated air only. An Omega programmable temperature controller was a part of the system. The controller was calibrated so that the chamber reached or maintained desired temperature points with high accuracy (less than ±3°F offset). We also placed numerous thermocouple sensors within different sections of the chamber to test for temperature gradients. The differences in temperature within the chamber were found to be minimal (e.g. 5°F difference in output of two sensors located 8 inches apart).

A typical example of the thermal loading profile used in monotonically cooling specimens is shown in Figure 5.2. A graph showing time versus temperature illustrates the testing procedure. After inspecting edges for microcracks at room temperature using the procedure in section 5.2, we cooled the specimens to progressively lower temperatures ranging from 75°F to -250°F. Cooling and heating was carried out consistently at about 25° per minute. Once the desired temperature was obtained, the specimens were soaked at that constant temperature for 5 minutes. Then the samples were taken to room temperature and soaked for 5 minutes before examination of damage. The testing was continued in this manner to progressively lower temperatures as shown in the Figure 5.2.

All specimens listed in Table 5.2 were tested as described in the above procedure. Two different temperature profiles were used. The type A progressive testing profile is shown in Figure 5.2. The specimens were cooled to the following temperatures: 0°, -75°, -150°, and -250°F. For type B progressive tests, the specimens were cooled to the following temperatures: 0°, -80° and -200°F. The same ramp rates and soak times were used; only the soak temperatures varied.

5.4 CRACK CONFIGURATION STUDY

In the crack configuration study we attempted to understand cracking behavior within the volume of the entire laminate. The information collected will be referred to as 'crack configuration' data in the report. X-radiography was performed to photograph the cracks within the specimens. We also conducted a series of edge inspections into the width of the laminate by sanding down the edges.

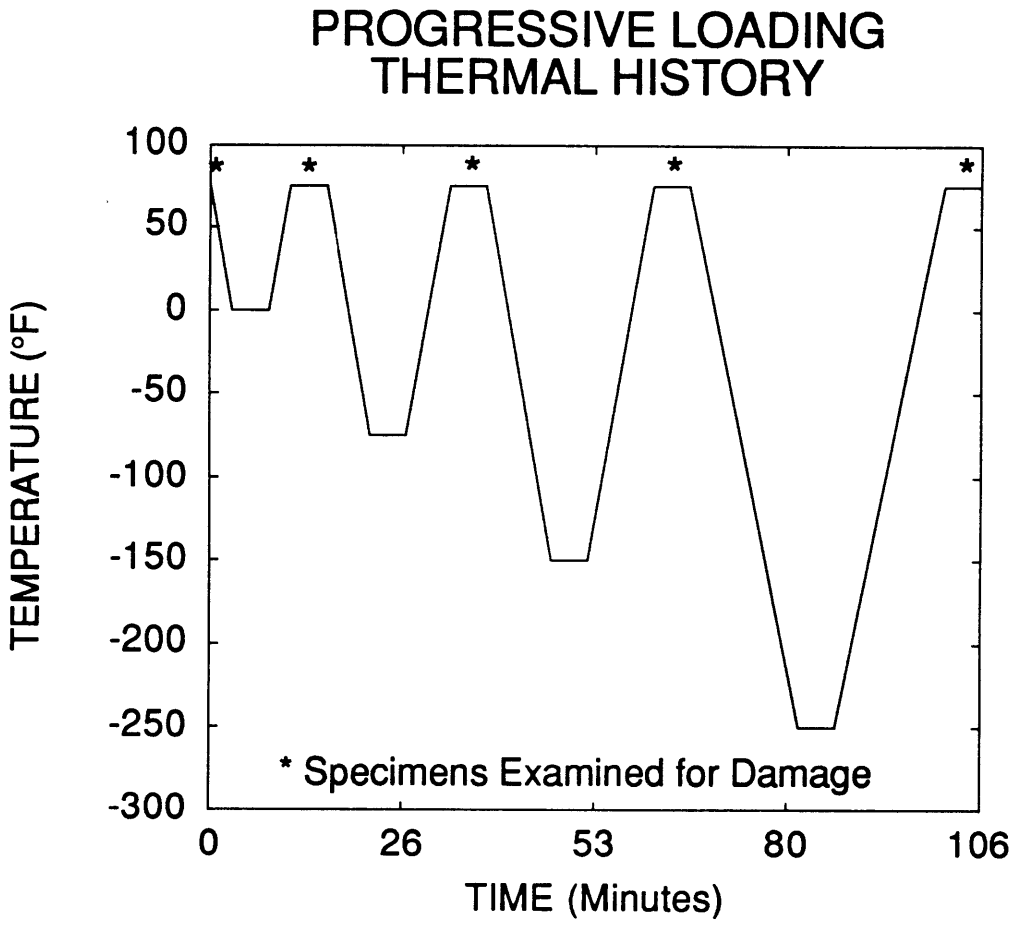

Figure 5.2 Thermal profile of progressive testing procedure.

Table 5.2 Test matrix

	Progressive Test	Crack Configuration Study	
Laminate Layup	Type	X-ray	Sanding
$[0_2/90_2]_S$	*	X	
$[0/90/0/90]_S$	A	X	
$[0_2/\pm30]_S$	B	X	X
$[0/45/90/-45]_S$	B	X	X
$[0/90/\pm45]_S$	A	X	
$[0/\pm45/90]_S$	A	X	
$[0_2/45_2/90_2/-45_2]_S$	A	X	X

* Testing conducted by McManus et al. [48]

5.4.1 X-Radiography

Radiographic examinations were attempted to observe cracks in the specimens. Cracks can be made visible by dye-penetrant enhanced X-ray photography. In this procedure, a special dye-penetrant liquid (di-iodobutane) is applied on the specimens. The dye-penetrant seeps through the cracks and can be seen on X-ray photographs. We used the TELAC X-ray facility to complete this experiment.

The procedure used was to apply dye-penetrant to the edges of the specimen and wait for ten minutes before taking the photograph in the X-ray machine. In an attempt to enhance the visibility of the microcracks, we tried many variations on this method. Variations included longer soaking times, multiple applications, a complete emersion of the entire specimen in the dye-penetrant and cooling specimens before and/or during dye-penetrant applications in an attempt to expand the laminates and open up the cracks.

All specimens listed in Table 5.2 were X-rayed after completion of the progressive cooling tests.

5.4.2 Examination of Microcrack Distribution Throughout Volume of Laminate

The original edge inspection procedure considers only the polished edge, Side A. We also examined the arrangement of cracks throughout the volume of the specimens. First both long edges were polished and inspected. Then material was sanded away from the edges to a desired depth as shown in Figure 5.3a, the edge was polished, and damage was examined again. This procedure was repeated until the entire volume of the specimen had been surveyed.

It was necessary to polish Side B so that the edge could be checked for damage as described in section 5.2. We checked to see if the crack density and

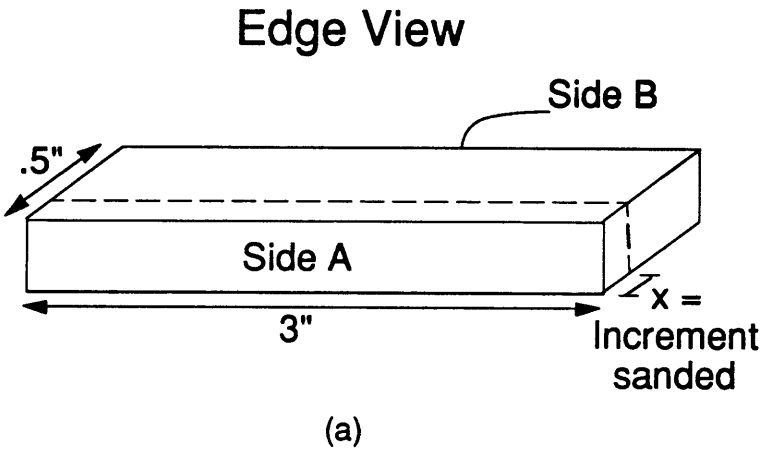

Figure 5.3 (a) Edge view of laminate sanded off with x increment (b) Top view of laminate with example θ ply crack. Illustration of difference in edge inspection after sanding.

locations matched on Side A and Side B. It is relevant to note that Side B was polished after all thermal testing, while Side A was polished beforehand.

To further investigate cracking damage over the entire laminate volume, we sanded down the edges. The basic procedure was to 1) remove a specified increment from the edge using sandpaper, 2) polish and remark the appropriate one inch region where data will be taken and 3) examine under a microscope for crack density and distribution using the procedure in section 5.2. As illustrated in Figure 5.3b, the inspected region must be remarked appropriate to the ply orientation. The figure shows that because the crack is oriented at an angle, the inspected region should be shifted. This process (1-3) was continued until the specimen was examined through the entire internal volume or to the desired depth.

Steps 1-3 above were consistently used but some procedural specifications varied. The standard procedure was to remove increments averaging 1-2mm using dry #180 grit sandpaper. Dry #600 grit sandpaper was then used to remove the last 10% of the increment. The width of the specimen was frequently measured using a vernier caliper to check for even, accurate sanding. Alternative procedures used included using only wet #600 sandpaper, sanding off increments of varying sizes, and examining the specimen through only a partial section of the volume instead of inspecting the entire specimen. Exact procedures will be noted when presenting the results.

The $[0/45/90/-45]_s$, $[0_2/45_2/90_2/-45_2]_s$ and $[0_2/\pm30]_s$ laminates in Table 5.2 were used in these experiments after completion of all thermal loading. One $[0/45/90/-45]_s$ laminate was examined before completion of an entire progressive testing procedure; sanding and edge inspection was performed after cooling to -125°F.

5.4.3 Control Tests

Control tests were performed to establish the sanding procedure. They verified that sanding using proper procedure does not cause additional damage in the specimens. The $[0/45/90/-45]_s$ laminates were used in these experiments. Two types of specimens were used. The first had already been progressively cooled and were significantly microcracked before sanding. The second were new unloaded specimens of the same type. These specimens did not have any cracks in the +45 and -45 plies and a moderate number of cracks in the 90 plies.

In one control experiment we used the specimens that had been thermally loaded and damaged. We sanded one specimen with only the 'rough' #180 sandpaper (dry) and one specimen with the 'fine' #600 sandpaper (with water). The specimens were sanded so that 0.2-0.04 mm of material was removed in each step. This increment (sometimes less than one ply thickness) was small enough that it was felt that the density of pre-existing cracks would not change significantly over the increment and would change gradually over a number of increments. Hence, abrupt changes in crack density could be interpreted as sanding damage. Procedures 1-3 described previously were used.

The results of the specimen tested with fine sandpaper showed no changes in crack density, in the +45 and -45 plies, after sanding a small increment. Changes over a series of longer increments were very gradual. The 90 ply crack density also changed gradually, decreasing as sanding progressed. Evidently, the damage caused by sanding was minimal in this case. The results from the +45 and -45 plies of the specimen tested with the rough sandpaper were similar to the specimen tested with the fine sandpaper. However, the observed crack density of the 90 plies changed drastically. The crack density fluctuated up and down over an extremely small interval. Evidently, these plies were heavily damaged by the rough sandpaper.

The new uncooled specimens were also tested to see if sanding caused additional damage. The +45 and -45 plies did not have any cracks originally and no cracks were created after sanding, using any type of procedure. Use of the rough sandpaper caused much damage to the 90 plies with average crack densities more than doubling. Specimens sanded with just the fine sandpaper showed no additional cracks. Specimens sanded with rough sandpaper followed by the fine sandpaper showed some increase, averaging 25% in the 90 plies.

In conclusion, the control experiments proved that using the fine #600 grit sandpaper was a reliable method for sanding. Using the rough and fine sandpaper combination was also found to be reliable except for a slight increase in the measured 90 ply crack density. In general, the 90 plies are much more susceptible to damage from sanding than the other plies.

CHAPTER 6

RESULTS

Analytical and experimental results are presented in this chapter. The progressive testing results will first be discussed and correlated with analytical predictions. Then the crack configuration study will be reviewed. We will conclude with the results for the three dimensional free edge stress analysis. Thermal cycling results will not be presented. Experimental data is not available to correlate with the analysis.

6.1 THERMAL PROGRESSIVE COOLING

In this section the analytical and experimental results for progressive thermal loading are presented. Crack density as a function of monotonically decreasing temperature will be reviewed, and experimental and analytical results compared. Then analytical predictions for laminate property degradation will also be shown. Last, we will discuss the effects of including material softening and temperature dependent material properties in the analysis. Table 1 shows material properties used in the analysis for the two material systems.

6.1.1 Crack Density vs. Decreasing Temperature

Figure 6.1 shows experimental data and analytical predictions for crack density as functions of decreasing temperature. The results are for the 30 ply of the $[0_2/\pm30]_S$ laminate. The analysis predicts that the ply never starts to crack between 75°F (room temperature) and -250°F. The experiments also show no cracks except some cracks starting at -200°F. Figure 6.2 is a graph of the -30_2

Table 6.1 Material Properties

Material Property	P75/934	P75/ERL 1962
E_l Msi)	34.3	34.3
E_t (Msi)	.90	.96
ν	.29	.29
G (Msi)	.70	.70
Y_t (ksi)	-	3.88
G_{Ic} (J/m^2)	40	104
α_l ($\mu\varepsilon/°F$)	-0.68	-0.53
α_t ($\mu\varepsilon/°F$)	16	22
ξ	.65	.65

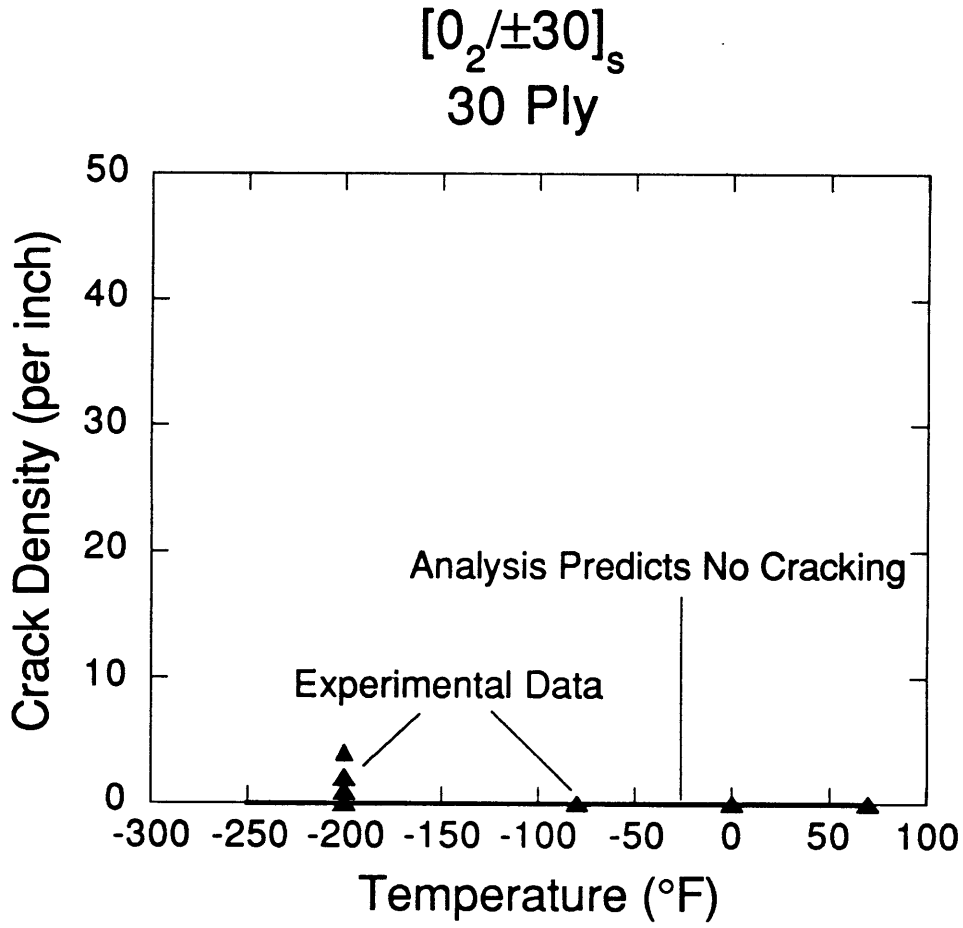

Figure 6.1 Analytical and experimental correlation of crack density vs. decreasing temperature. 30 ply of $[0_2/\pm30]_s$ laminate.

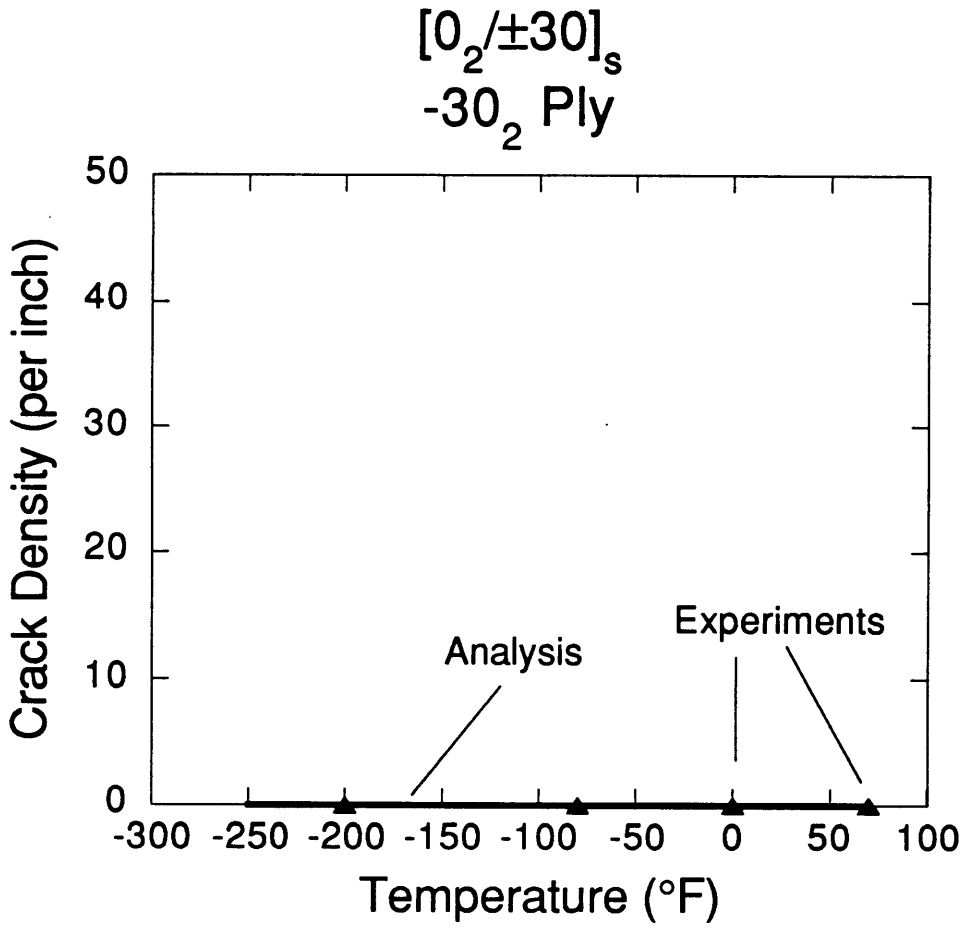

Figure 6.2 Analytical and experimental correlation of crack density vs. decreasing temperature. -30 ply of $[0_2/\pm30]_s$ laminate.

ply group of the same laminate. Experimentally, no cracks ever formed and the analysis correctly predicts this behavior.

The laminate in Figure 6.3 is a quasi-isotropic layup $[0/45/90/-45]_S$. The 45 ply starts to crack at around 75°F and reaches a low crack density of less than ten at -200°F. The general trend of the analytical results do not correlate. We predict cracking to start a little later and to eventually crack to a high density of 30 cracks per inch. The graph for the 90 layer is shown in Figure 6.4. Again, the trends do not match. The data points are very scattered. The analysis correctly predicts the eventual crack density after all loads, but tests show that the cracks initiate at a higher temperature than predicted. The results of the middle -45_2 ply group is illustrated in Figure 6.5. The analytical predictions and test data have similar trends but the model predicts too many cracks in general.

The next figures show results for the $[0_2/45_2/90_2/-45_2]_S$ laminate. Figure 6.6 looks at the 45_2 ply group. The results are similar to the middle -45_2 ply group of the $[0/45/90/-45]_S$ laminate. The trend from the analytical results is similar to the experimental data. However, the crack density is predicted to be higher than what was found from the edge inspections. The analytical and experimental results for the 90_2 ply group, shown in Figure 6.7, follow the same trends. The analysis predicts a slightly smaller crack density than what is observed experimentally. Cracks are observed to initiate at a higher temperature than predicted. In addition, the data is widely scattered. Figure 6.8 is the graph for the middle -45_4 ply group. The cracks develop a little slower than predicted. Otherwise, the analytical results correlate well with the experimental data.

The results for all other specimens and ply groups are similar to the set just discussed. Analytical and experimental results for thermal progressive loading are in Appendix B.

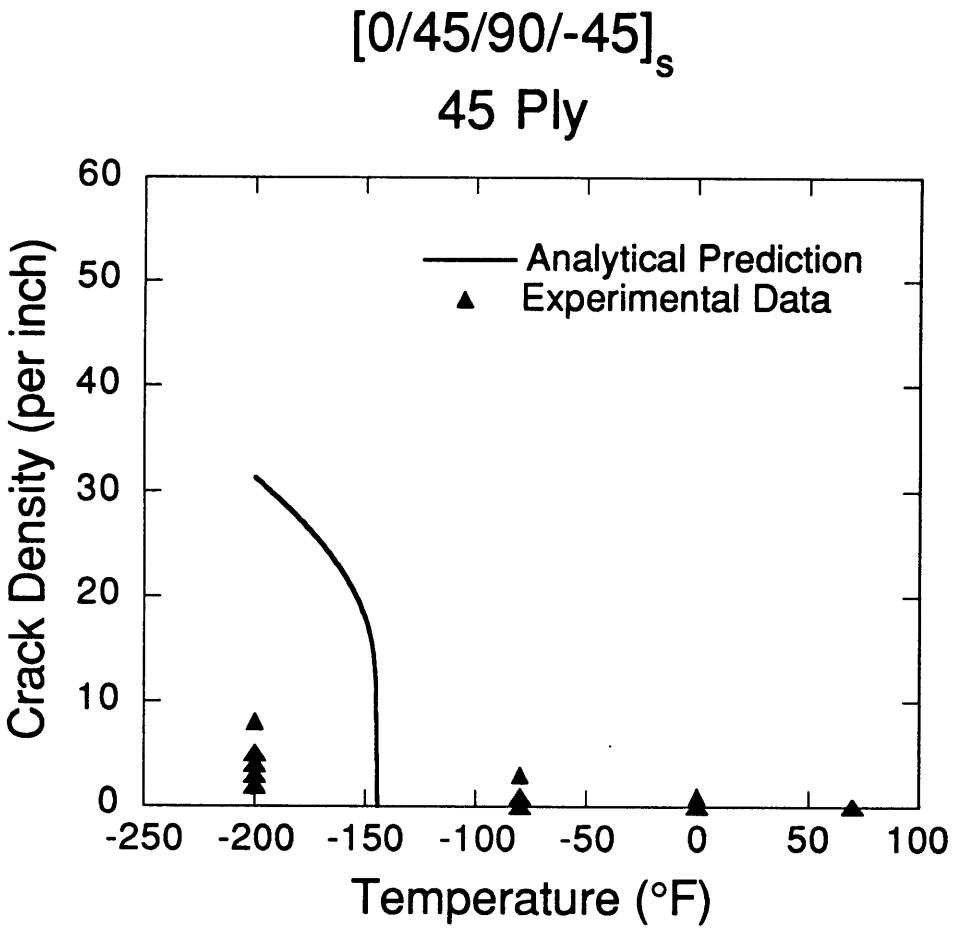

Figure 6.3 Analytical and experimental correlation of crack density vs. decreasing temperature. 45 ply of $[0/45/90/-45]_s$ laminate.

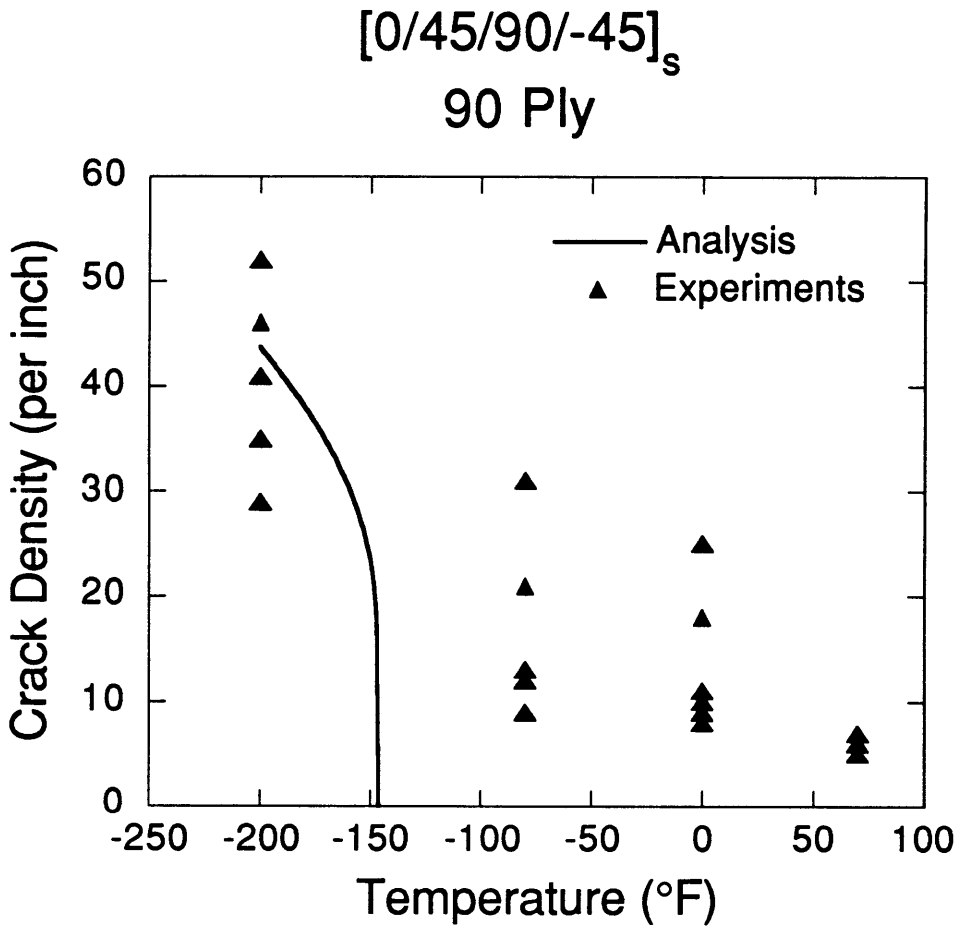

Figure 6.4 Analytical and experimental correlation of crack density vs. decreasing temperature. 45 ply of $[0/45/90/-45]_s$ laminate.

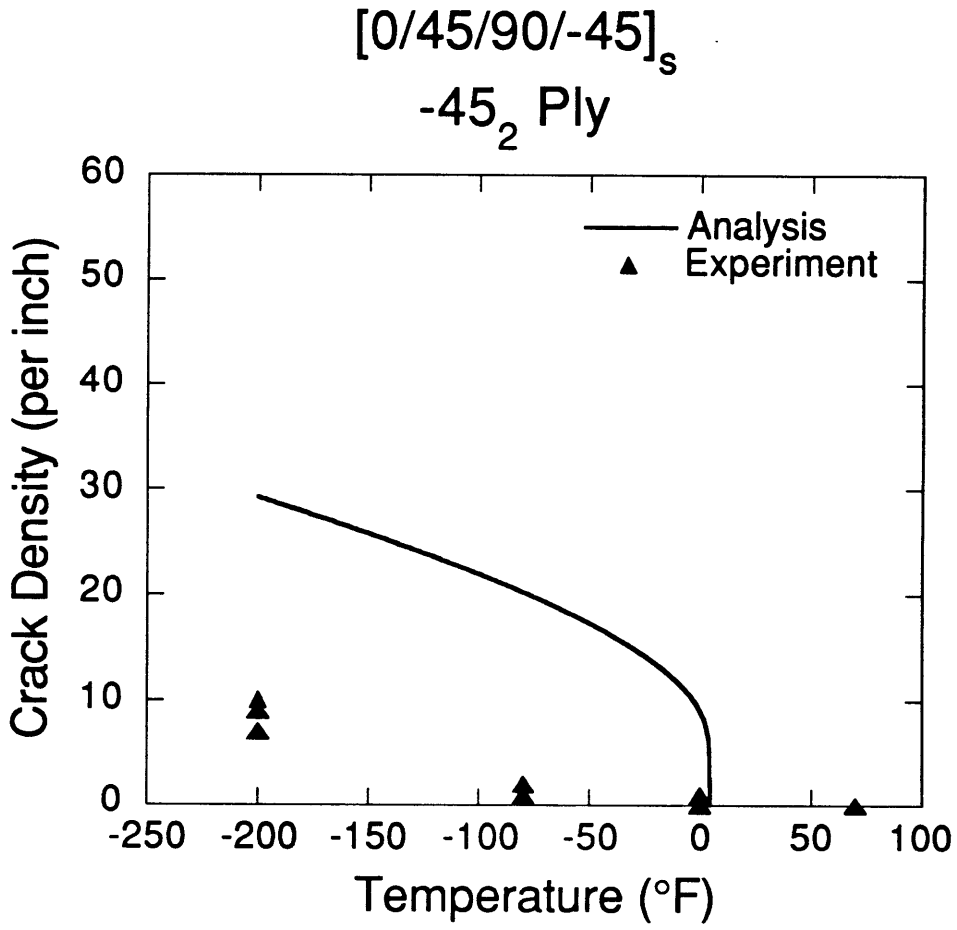

Figure 6.5 Analytical and experimental correlation of crack density vs. decreasing temperature. -45_2 ply of $[0/45/90/-45]_s$ laminate.

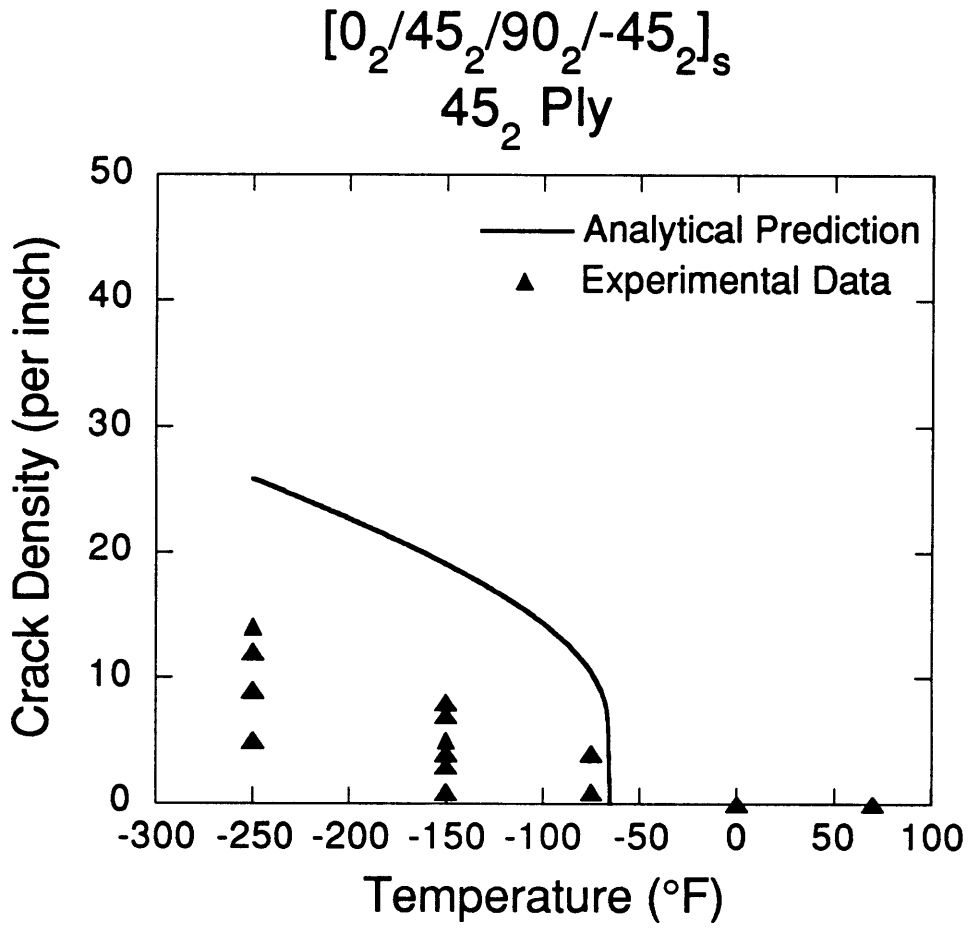

Figure 6.6 Analytical and experimental correlation of crack density vs. decreasing temperature. 45_2 ply of $[0_2/45_2/90_2/-45_2]_s$ laminate.

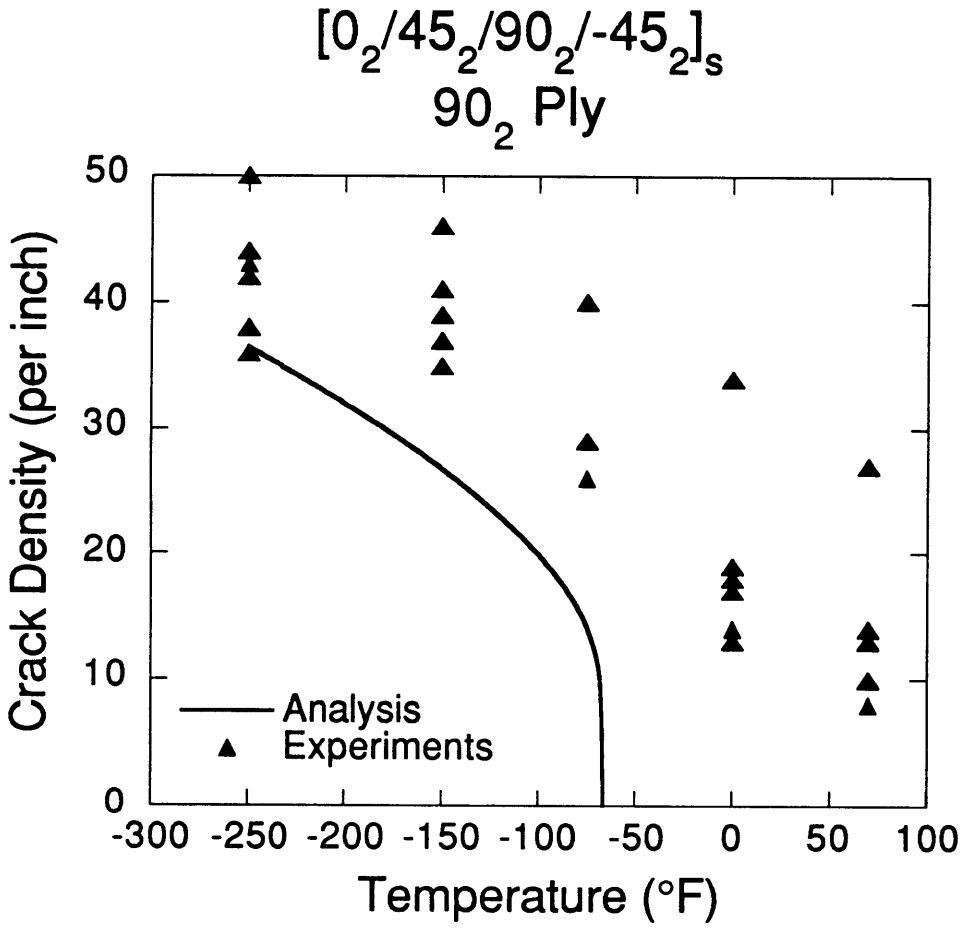

Figure 6.7 Analytical and experimental correlation of crack density vs. decreasing temperature. 90_2 ply of $[0_2/45_2/90_2/-45_2]_s$ laminate.

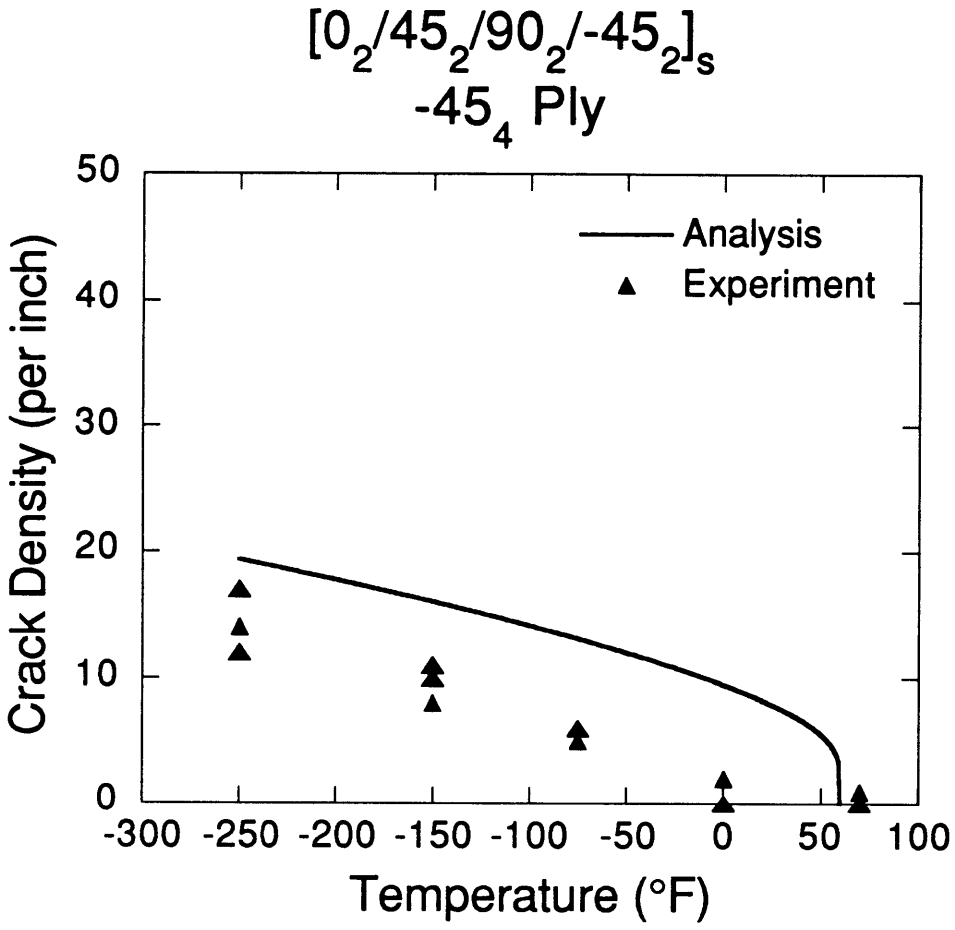

Figure 6.8 Analytical and experimental correlation of crack density vs. decreasing temperature. -45_4 ply of $[0_2/45_2/90_2/-45_2]_s$ laminate.

6.1.2 Laminate Properties vs. Decreasing Temperature

The appearance of microcracks causes degradation of laminate properties. The methods used to predict the resulting changes in properties were reviewed in Section 4.2.3. Analytical results for stiffness and coefficient of thermal expansion (CTE) variations as functions of decreasing temperatures is presented in this section. Effects of temperature dependent material properties were not used; the results reflect property variations exclusively due to cracking damage. Therefore, the changes in properties are permanent. The properties do not return to their original values when the laminate is returned to a higher temperature.

The laminate stiffness degradation from microcracking is shown in Figures 6.9 to 6.11 for the $[0/45/90/-45]_S$, $[0_2/45_2/90_2/-45_2]_S$, and $[0/90/0/90]_S$ specimens respectively. The graphs are normalized laminate longitudinal stiffness versus decreasing temperature and illustrate the change in stiffness from the original value. The stiffness changes were minimal in all of the laminates. A two percent reduction in laminate stiffness property was found in the quasi-isotropic laminates of Figures 6.9 and 6.10. The changes were even smaller in the $[0/90/0/90]_S$ crossply laminate in Figure 6.11.

The changes in coefficient of thermal expansion are illustrated in Figures 6.12 to 6.14. Figure 6.12 shows the laminate CTE versus decreasing temperature for the $[0/45/90/-45]_S$ laminate. The CTE property is greatly affected by thermal loading and cracking. The values change about 300% in the 75°F to -250°F temperature range. The predictions for the $[0_2/45_2/90_2/-45_2]_S$ and $[0/90/0/90]_S$ specimens in Figure 6.13 and 6.14 are similar. The laminate CTE in the $[0_2/45_2/90_2/-45_2]_S$ case even changes sign.

The laminate property changes for all specimens are in Appendix B.

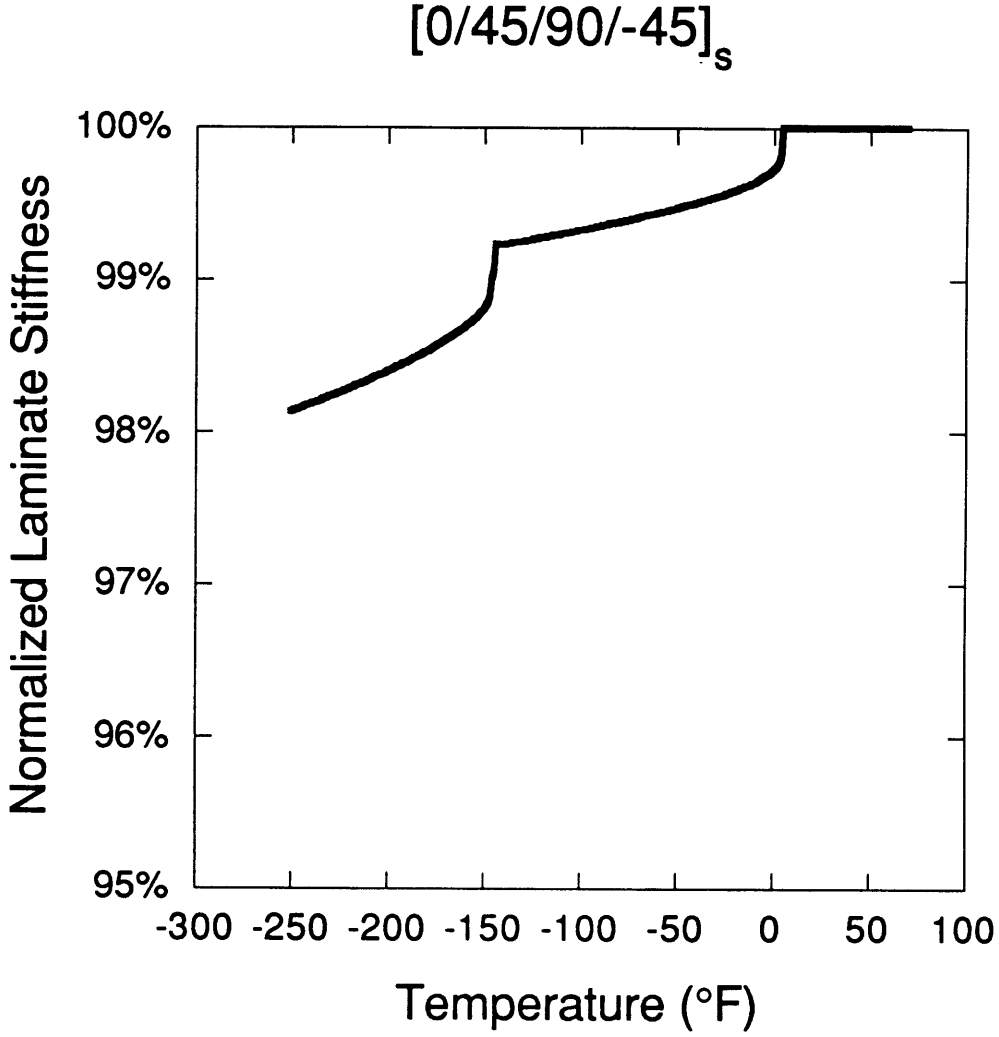

Figure 6.9 Analytical stiffness prediction vs. temperature for $[0/45/90/-45]_s$ laminate. Laminate longitudinal stiffness normalized by undamaged value.

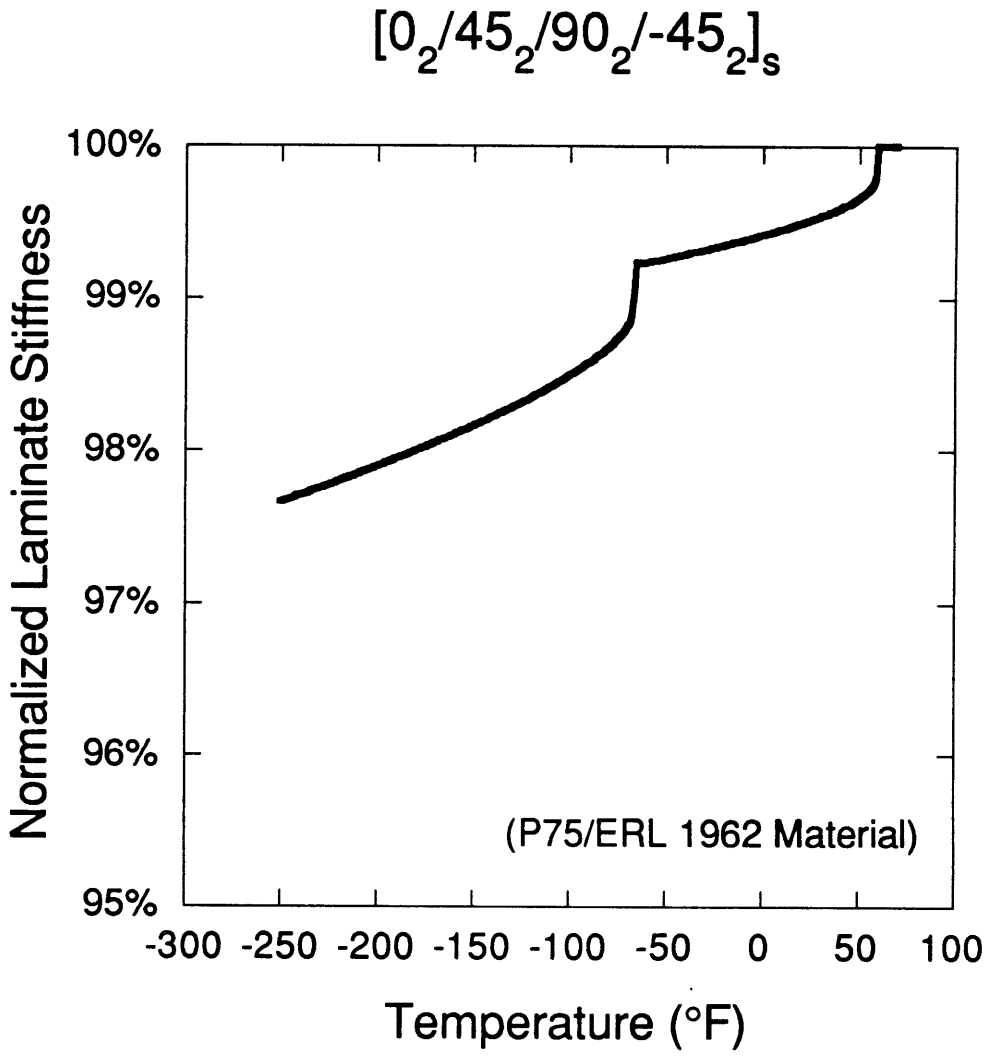

Figure 6.10 Analytical stiffness prediction vs. temperature for $[0_2/45_2/90_2/-45_2]_s$ laminate. Laminate longitudinal stiffness normalized by undamaged value.

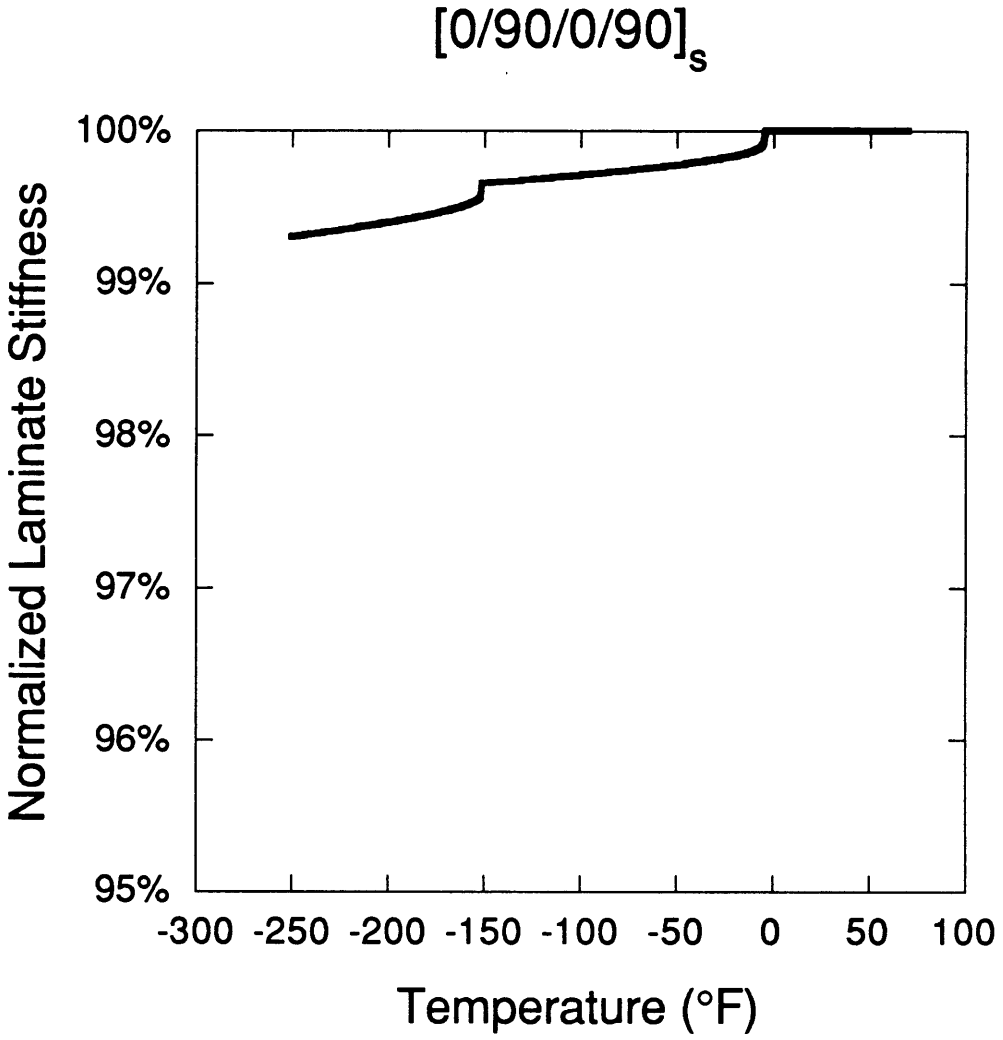

Figure 6.11 Analytical stiffness prediction vs. temperature for $[0/90/0/90]_s$ laminate. Laminate longitudinal stiffness normalized by undamaged value.

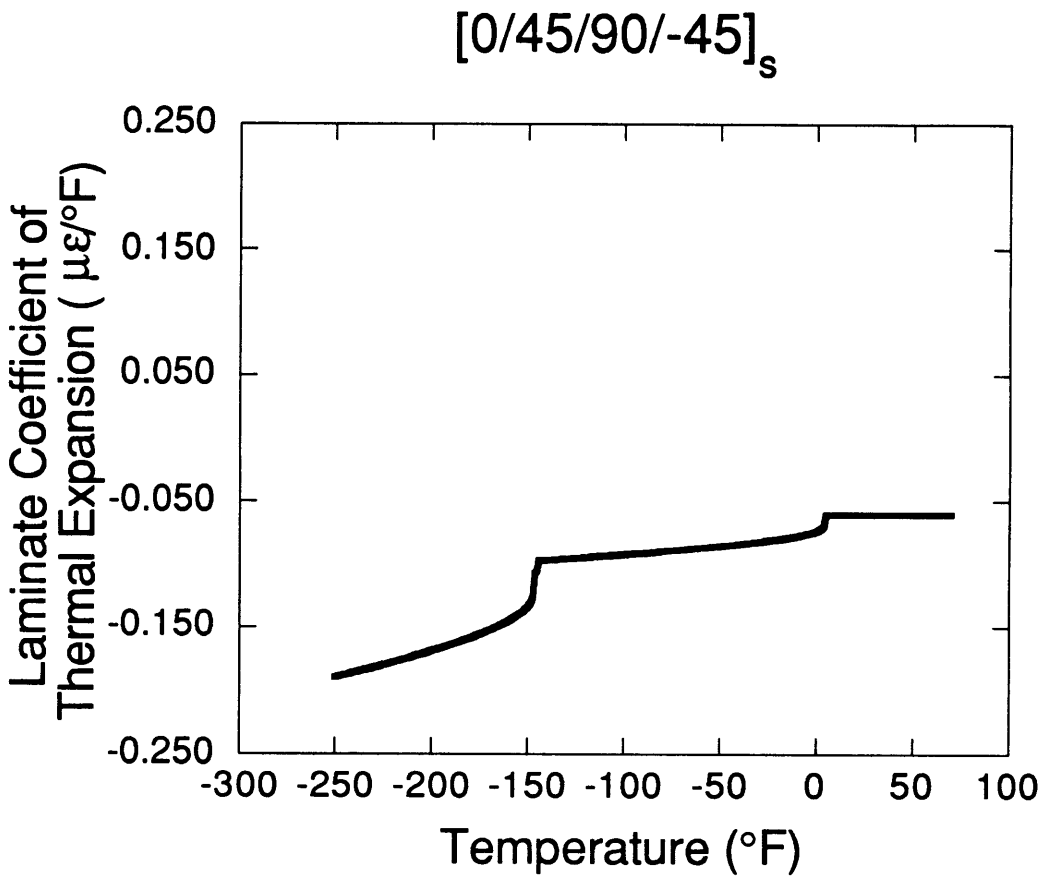

Figure 6.12 Analytical CTE prediction vs. temperature for $[0/45/90/-45]_s$ laminate.

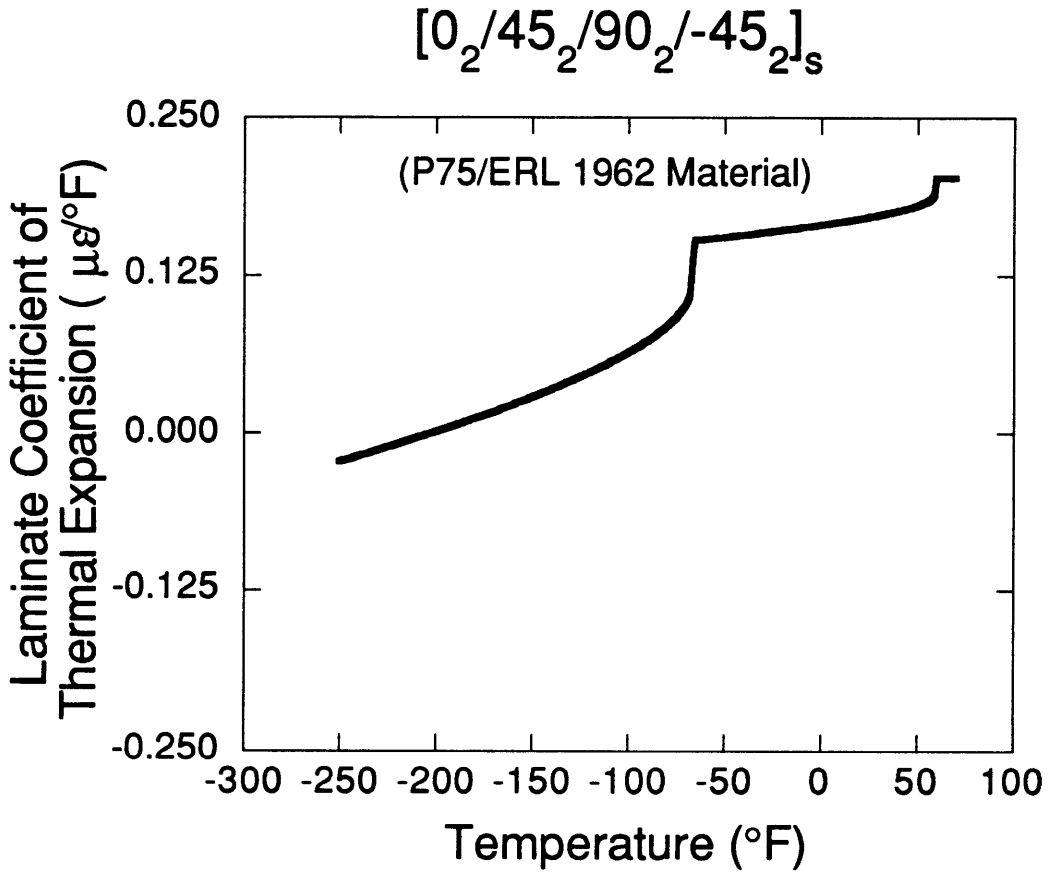

Figure 6.13 Analytical CTE prediction vs. temperature for $[0_2/45_2/90_2/-45_2]_s$ laminate.

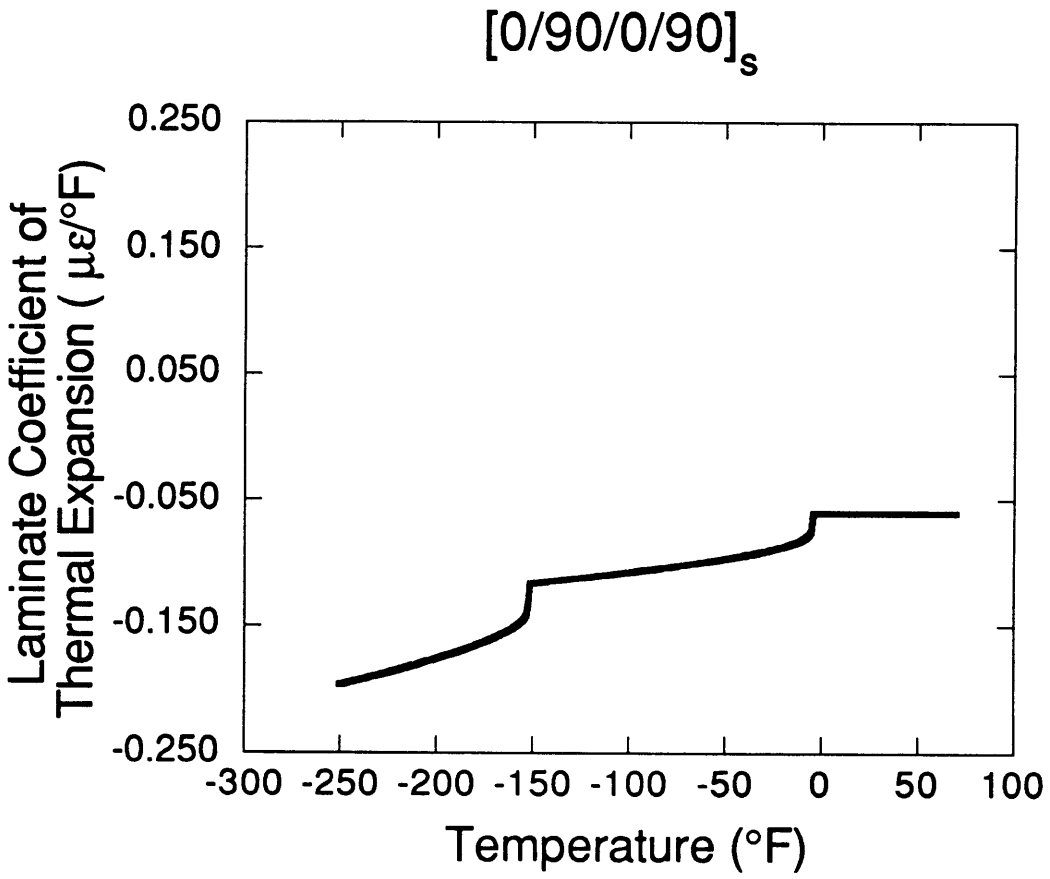

Figure 6.14 Analytical CTE prediction vs. temperature for $[0/90/0/90]_s$ laminate.

6.1.3 Parametric Studies

The general analysis developed in Chapter 4 models effects such as material softening and temperature dependent material properties. We analyzed laminates with and without these effects included in the analysis to gain a better understanding of their importance.

Incorporating material softening in the analysis did not significantly affect the results for crack density and laminate property degradation. This was true for all laminates analyzed. The crack initiation temperature changed by less than 5°F and the crack density changed by less than 3 cracks per inch.

Incorporating temperature dependent material properties into the analysis proved important. We used temperature dependent property data from NASA LaRC for the P75/934 material system [52]. Figure 6.15 illustrates the differences in the analytical results due to modelling temperature dependent material properties and material softening effects. The effects seen are due almost solely to the inclusion of temperature dependent properties. The graphs show analytical predictions for progressive cooling damage in the 90 and 45 plies of a $[0/45/90/-45]_S$ laminate. Using temperature dependent properties causes the analysis to predict earlier crack initiation and more cracking. The trends are, however, similar to the predictions with no effects included.

Interpretation of the effects of temperature dependent material properties is complicated by the small amount of data available. The temperature dependent data used did not precisely match the temperature independent data at any single temperature. The results therefore reflect both the temperature dependence of the properties and their variability from test to test.

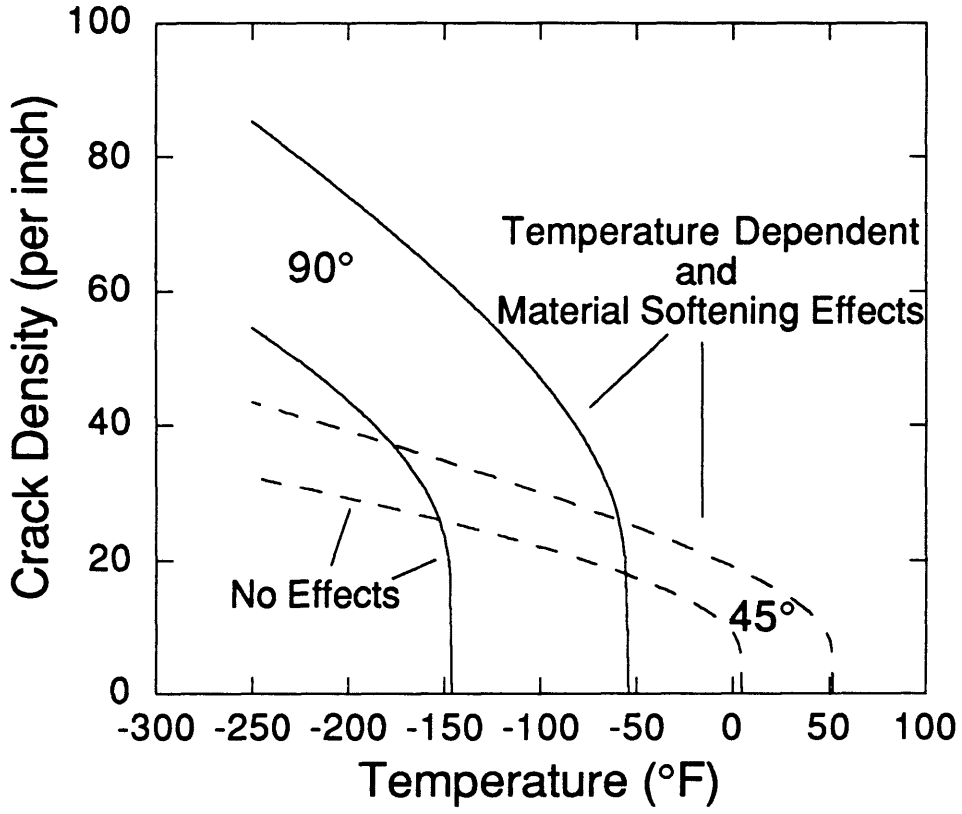

Figure 6.15 Parametric studies using temperature dependent material properties and material softening effects.

6.2 CRACK CONFIGURATION STUDY

The crack configuration study was completed to experimentally explore the assumptions used in the model. More specifically, our goal was to check if the microcracks extend through the width of a laminate as described in Section 4.1. We also want a better interpretation and understanding of the experimental data taken during edge examinations. The X-ray results will first be presented. Then we will compare the edge inspection results for Side A and Side B. Finally, the data from the sanding project will be presented.

6.2.1 X-Radiography

All specimens were X-rayed. However, only cracks in the middle two ply and four ply groups of the specimens were visible on the X-ray photographs. These cracks extended through the width of the laminates, behaving the way we assumed in our analysis. The middle four ply groups of the $[0_2/90_2]_S$ and $[0_2/45_2/90_2/-45_2]_S$ specimens could be seen very clearly on the X-ray photographs. These are shown in Figure 6.16. The cracks in the surface 0 ply group are also visible in both laminates.

The off-center ply groups of the specimens were not so readily visible on the photographs. After attempting many different procedural variations, we saw some evidence of cracks in these ply groups. The results were not of high enough quality to determine if all the cracks went all the way across the laminate, however.

6.2.2 Edge Comparison

Both Side A and Side B were inspected on the $[0_2/90_2]_S$, $[0/45/90/-45]_S$, and $[0_2/\pm30]_S$ laminates. Table 6.2 summarizes the comparisons of the edge examinations. Crack density and distribution data are compared for each

$[0/45/90/-45]_s$

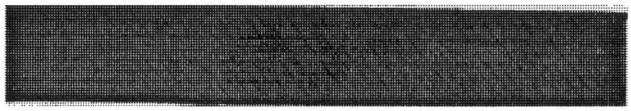

$[0_2/90_2]_s$

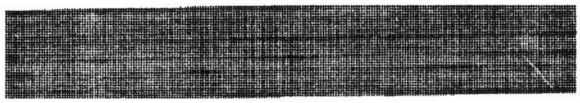

Figure 6.16 X-ray photographs of microcracks in $[0/45/90/-45]_s$ and $[0_2/90_2]_s$ specimens.

Table 6.2 Results of edge comparison of side A and side B

Specimen	Ply	Crack Density	Distribution
[02/902]s	90°	Matched	Matched
[0/+45/90/-45]s	-45°	Matched	Matched
	+45°	Similar	No Match
[02/±30]s	90°	No Match!!	NA
	-30°	NA	NA
	+30°	Similar	No Match

laminate. Side A and Side B results should match if the cracks actually extend through the entire laminate width. The crack density and distribution data for the center 90_4 ply group of the $[0_2/90_2]_S$ specimens matched perfectly. The center -45_2 ply group of the $[0/45/90/-45]_S$ had similar results; data from the Side A and B matched. This confirms what we found from the X-ray photographs.

The crack densities on Side A and B of the thin +45 plies were similar; however, the crack distributions did not match. The thin 90 ply crack density seen on Side B was sometimes two or three times the crack density of Side A. The thin +30 ply of the $[0_2/\pm30]_S$ laminate had similar crack densities in Side A and Side B but the distributions did not match. These results indicate that some (or all) cracks in these single ply groups do not extend through the laminate width.

6.2.3 Sanding Edges

The cracking behavior was checked throughout the volume of the laminate. We performed a series of sandings and edge inspections on three specimens: $[0_2/\pm30]_S$, $[0/45/90/-45]_S$, and $[0_2/45_2/90_2/-45_2]_S$.

Figure 6.17 shows the sanding results for the $[0_2/\pm30]_S$ laminate. A combination of the rough then fine sandpaper was used for these experiments. The graph shows the crack densities at different points through the width of the laminate. The 0mm point is Side A and the 12mm point is Side B. The experimental data points represent the locations where sanding was concluded and edges inspected. The vertical line on the graph differentiates sanding techniques. To the left of the line, all sanding was performed from Side A and to the right of the line, sanding was performed from Side B. One of the +30 plies in the $[0_2/\pm30]_S$ laminate had a small number cracks on the original Side A. When we performed an edge inspection after sanding down 1.7mm, no cracks were

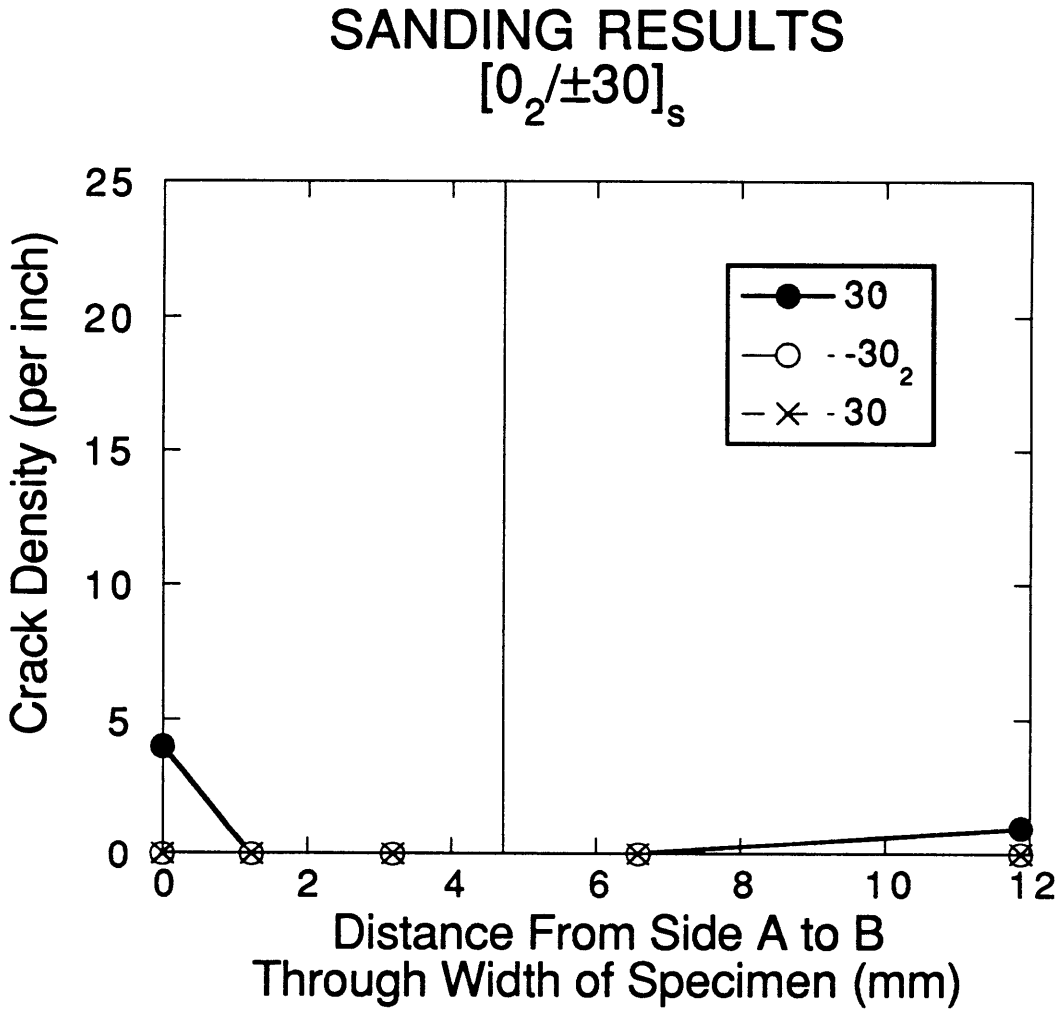

Figure 6.17 Sanding results for $[0_2/\pm30]_s$ specimen showing crack configuration through width.

found. Evidently, the cracks observed were present only near the edge. Continuation of the sanding procedure further into the specimen showed no evidence of other cracks.

Figure 6.18 is the same type of graph for the $[0/45/90/-45]_S$ laminate. The rough and fine sandpapers were used. This figure shows the crack density of the two thin 90° plies through the width. The crack density seems to vary randomly within a band. The damage appears to increase near Side B. The crack location (distribution) data was analyzed to trace individual cracks. We found the cracks to be broken up through the width. We could not track individual cracks; they started and stopped randomly.

Figure 6.19 shows the results for the +45 and -45 plies of the same laminate. The crack density of the middle -45_2 ply group is level through the width. The crack distribution also matched at all data points indicating that the same cracks extend through the laminate. These results match the findings of the previous X-ray and edge comparison experiments.

The sanding results for the +45 plies were extremely surprising. The crack density on Side A and B was less than 10 cracks per inch. However, within the volume of the specimen, we found the crack count to rise to an average of 50 cracks per inch. The crack density fluctuated up and down apparently randomly. The crack distribution data was similar to the distribution results for the 90 ply. Cracks could not be traced through any significant increment of the width.

Figure 6.20 shows all ply groups of a specimen of the same layup. This specimen was sanded a total width of 1.6mm using small increments ranging 0.02-0.4mm. The fine sandpaper was used for sanding. The cracking in the -45_2 ply group is again steady through the examined width. The crack density changes very gradually for the other plies. The damage behavior shown through

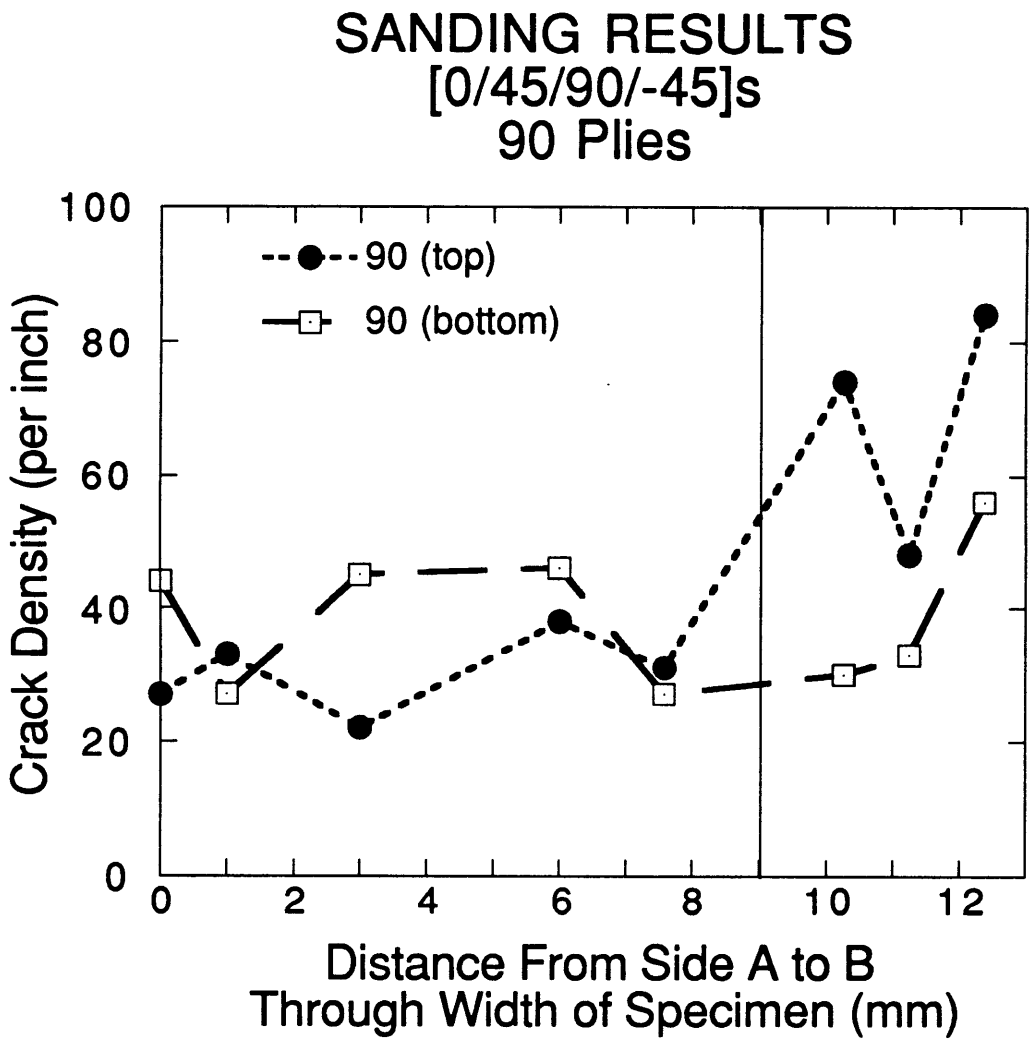

Figure 6.18 Sanding results for $[0/45/90/-45]_s$ specimen showing crack configuration through width in 90 plies.

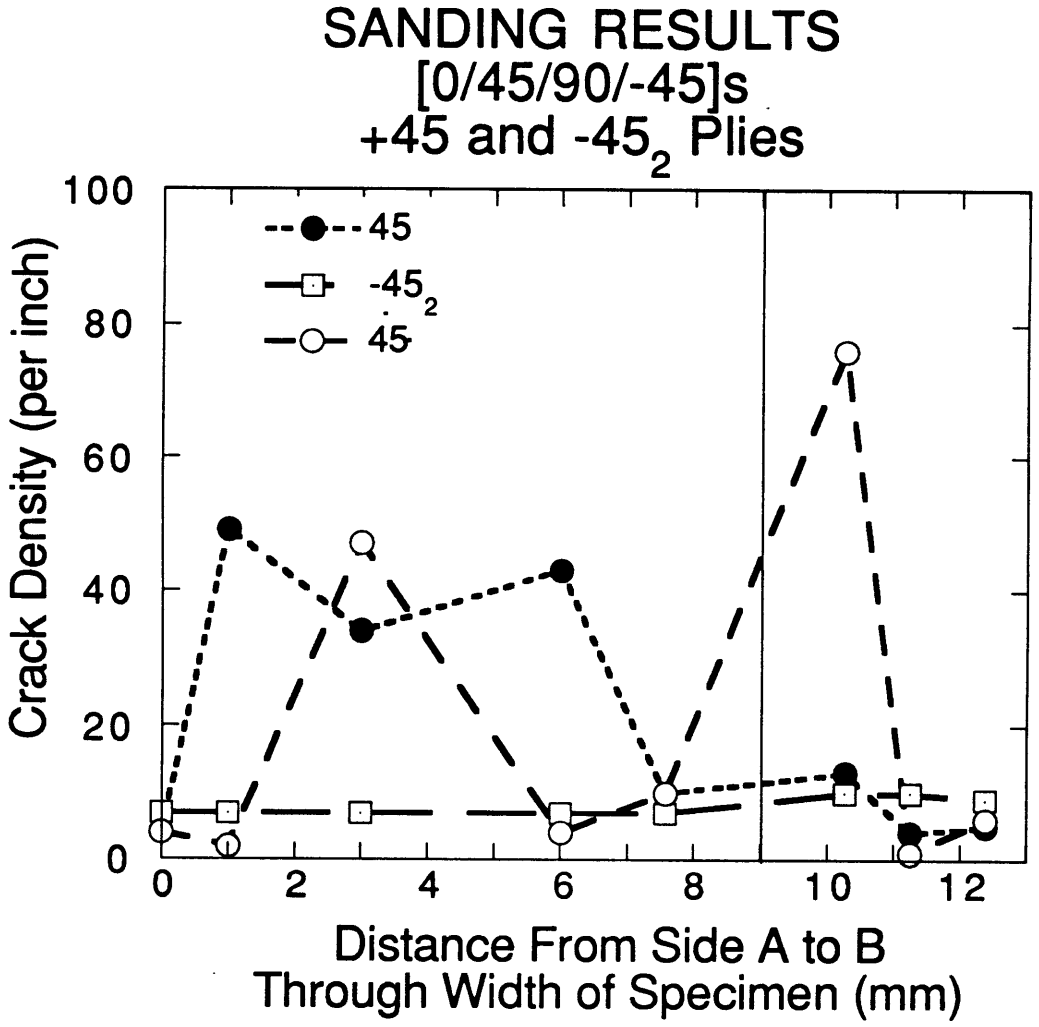

Figure 6.19 Sanding results for [0/+45/90/-45]$_s$ specimen showing crack configuration through width in +45 and -45$_2$ plies.

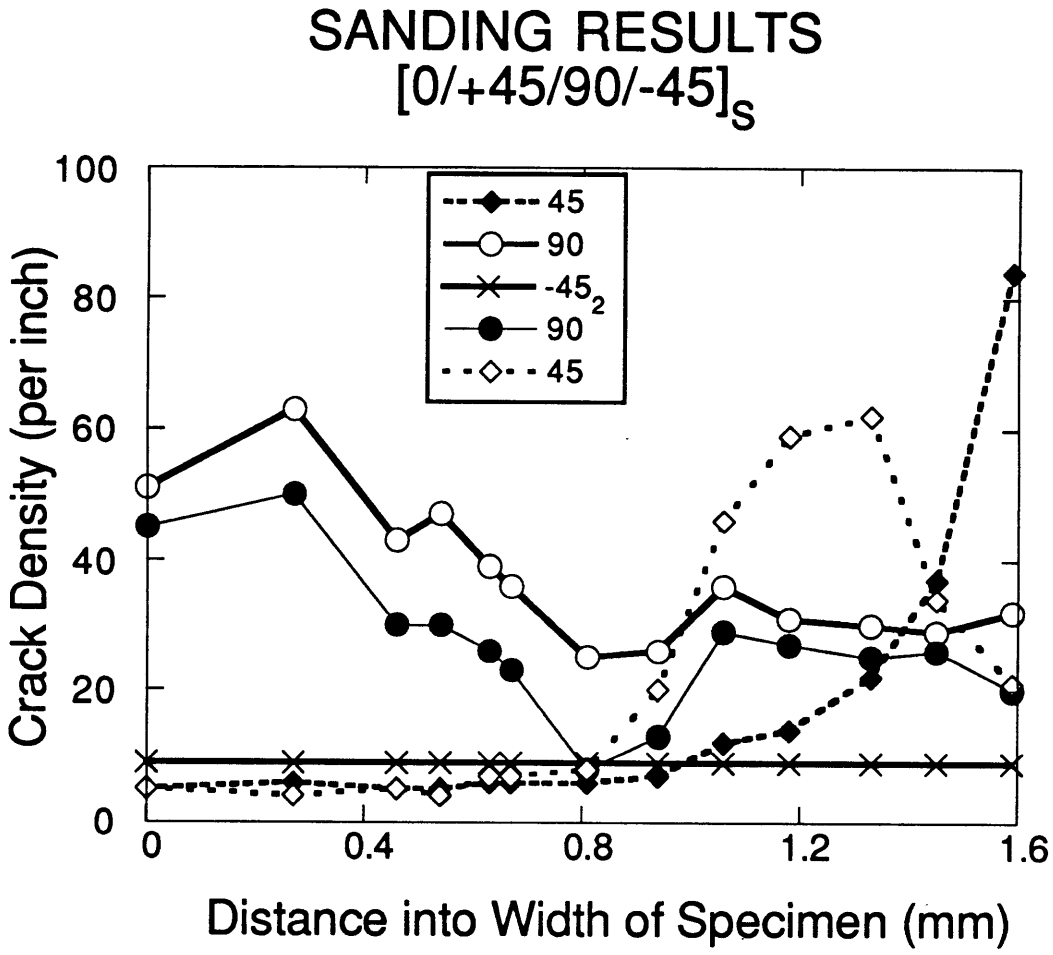

Figure 6.20 Sanding results for $[0/+45/90/-45]_s$ specimen showing crack configuration through width.

the first 1.6mm on Figure 6.20 matches the observed crack development through the first 2mm in Figure 6.18 and Figure 6.19.

Figure 6.21 shows the results for all ply groups of the $[0_2/45_2/90_2/-45_2]_S$ laminate. Fine sandpaper was used. Note that the 0mm point is Side A and the sandings were concluded at 2.5mm in from Side A. The crack density and distribution data show that cracks in the -45_4 ply group are continuous throughout the volume examined. The crack density of one $+45_2$ ply group more than doubles 1.5mm from the original free edge. The crack density of the other $+45_2$ ply and the 90_2 plies changes slightly through the first 2.5mm from Side A.

All the sanding results presented thus far were from specimens after they were cooled to either -200°F or -250°F, at the conclusion of progressive testing. The sanding performed (using fine sandpaper) for the specimen in Figure 6.22 was done after cooling to only -125°F. We wanted to see if the crack configurations were similar at this intermediate stage of thermal loading. Figure 6.22 shows crack density from the original free edge to 4 mm into the width. The trends found in the results are similar to those for the laminate in Figures 18 and 19 which was cooled to -200°F. The crack densities are generally lower in Figure 6.22 because of the less severe cooling.

6.3 FREE EDGE STRESS ANALYSIS

A three dimensional interlaminar stress analysis was completed to study free edge effects. We solved for the in-plane stresses transverse to the fiber direction in each ply. The free edge stress solution is shown in Figure 6.23 for the $[0/45/90/-45]_S$ laminate. The graph shows the stress distribution through the first 2mm from the free edge. The transverse in-plane stress for the 90 ply is virtually level, increasing very slightly at the edge. The transverse stress in the +45 ply is virtually zero at the free edge, and rises to expected values (CLPT) by

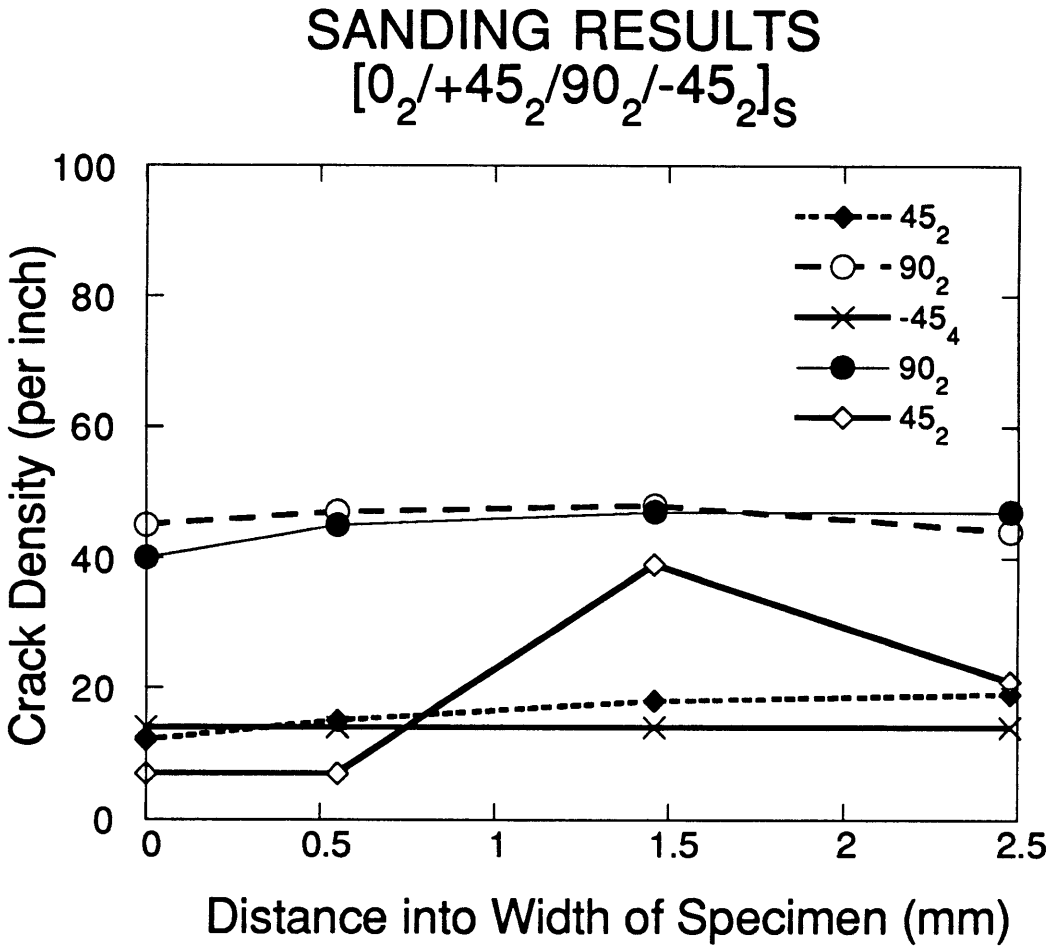

Figure 6.21 Sanding results for $[0_2/+45_2/90_2/-45_2]_s$ specimen showing crack configuration through width.

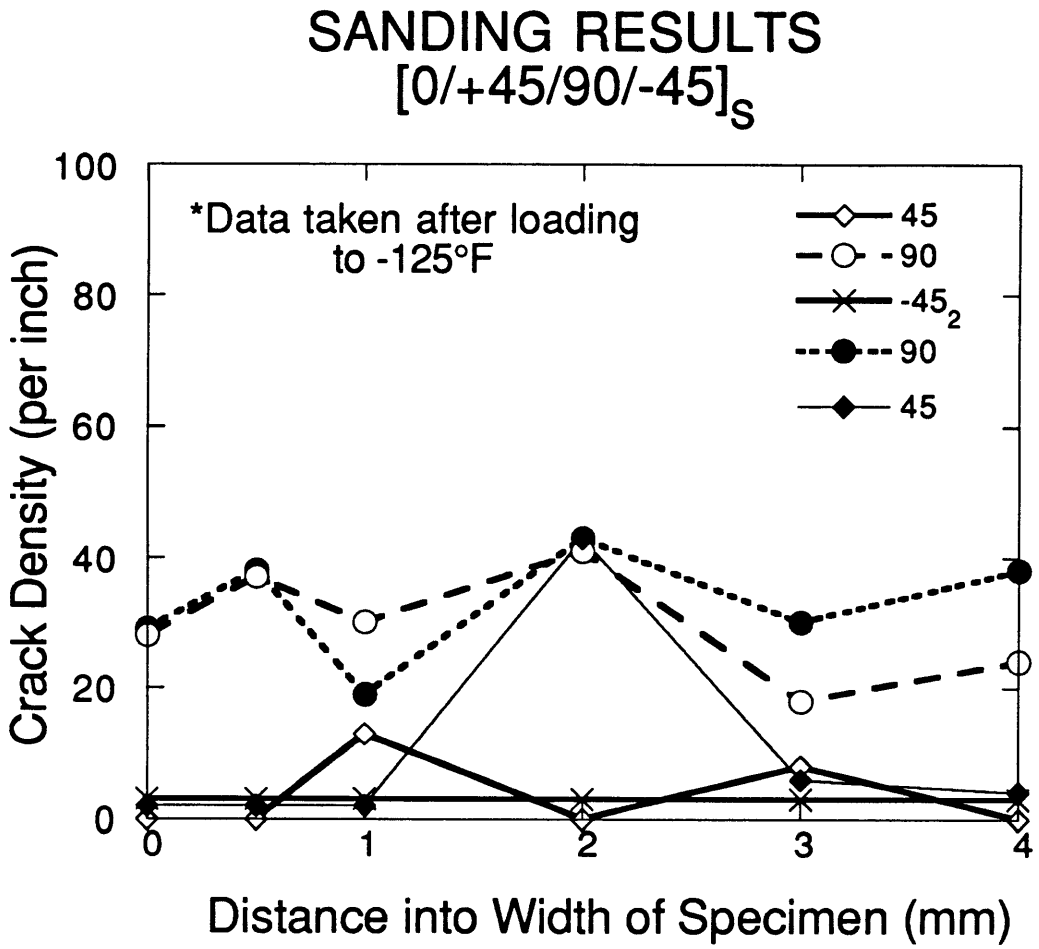

Figure 6.22 Sanding results for $[0/+45/90/-45]_s$ specimen showing crack configuration through width.

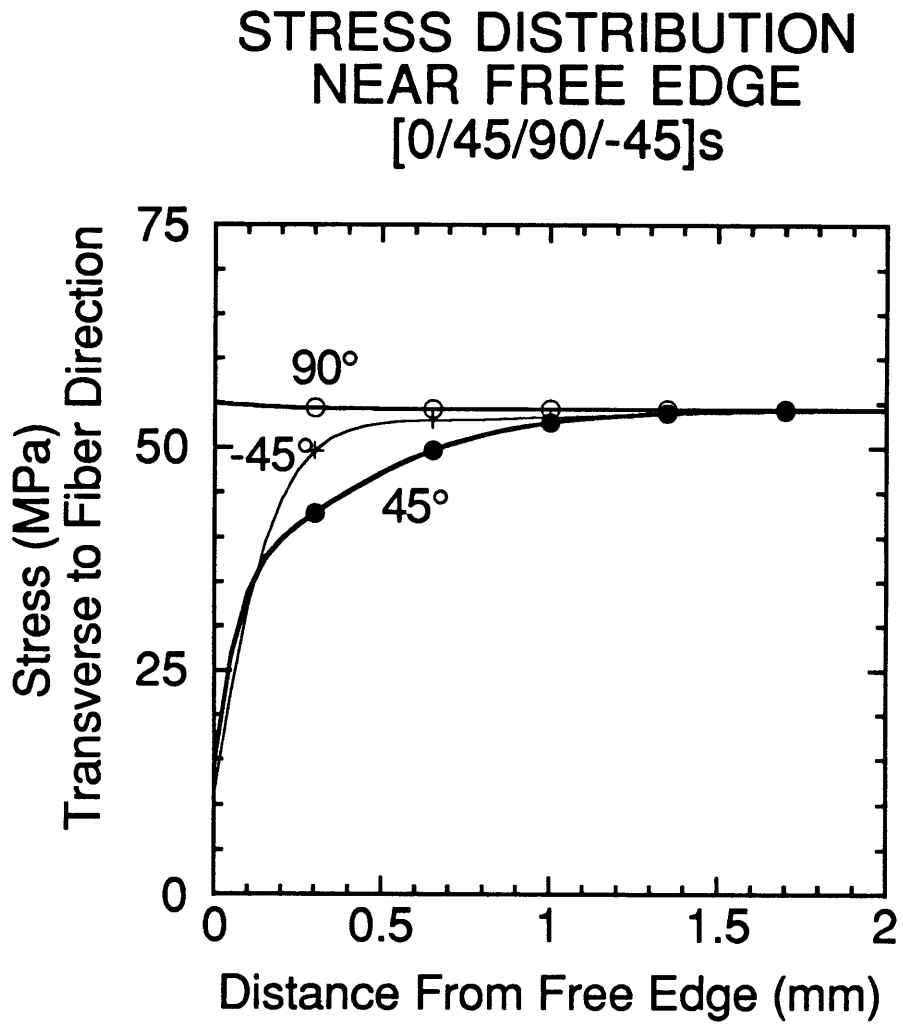

Figure 6.23 Transverse in-plane stress distribution near the free edge of a $[0/45/90/-45]_s$ laminate.

1mm into the laminate. The stress in the -45_2 ply group also starts near zero, but rises to CLPT values quickly. The low stress zone in this ply group is more narrow than that in the +45° ply.

A complete set of the free edge stress results for all the specimens are presented in Appendix C.

CHAPTER 7

DISCUSSION

In this chapter, the results of our research presented in Chapter 6 will be discussed. The analytical and experimental results, and the correlations between them, will be reviewed. The effects of ply thickness, ply angle, and the specimen free edge on the microcracking behavior will be explored.

7.1 PLY THICKNESS EFFECTS

The results of this study show that the thickness of the cracking ply group has a profound effect on the cracking behavior. It is known from previous studies that the ply group thickness has a strong effect on crack density. This study shows that ply group thickness changes not only the number of cracks but their nature and behavior as well.

The thickest ply groups examined, consisting of four plies with a total thickness of 0.020" (0.508mm), behaved according to the assumptions incorporated in our model (and those of many previous authors). Cracks continued through the entire width of the specimens. They were easily visible in X-ray photographs. The results of the sanding experiments were also consistent with the X-rays. The crack density was very well predicted by our analytical technique. McManus et al. also found good correlations in the similar 90_4 groups of $[0_2/90_2]_s$ laminates [48].

The two layer ply groups behaved 'ideally' in most cases, cracking all the way through the specimen width. This was proven through X-rays and sanding experiments for those groups that were located at the center of symmetric laminates. The $[0_2/45_2/90_2/-45_2]_S$ specimen has off center two layer ply groups.

These were difficult to view with X-rays, but the cracks could be traced in sanding studies (Figure 6.21). The 90_2 groups behaved well but the off center $+45_2$ ply group did not appear to behave ideally. In one instance the crack density varied drastically over a short distance through the width. However, it is difficult to make any conclusions from this one data point.

The analytical correlations of crack density for these thick ply groups were moderately successful. Results of the analysis showed similar trends to those of the experimental data. All ply groups with +45 or -45 orientation cracked less than predicted. The 90 two layer groups reached the predicted level of cracking, but cracked at higher temperatures than predicted.

Single plies behaved in a manner inconsistent with the idealized assumptions of the analysis. Wide, apparently random fluctuations in crack density were observed. This implies that the cracks do not extend through the specimen width. The plies appear instead to be shattered or permeated with many small unconnected cracks. The 45 plies consistently show much lower crack densities near free edges, and the 90 plies consistently show higher densities at Side B which was unpolished during testing. This behavior is inconsistent with the analytical assumptions.

Surprisingly, analytical predictions of the actual crack density in the single 90 plies are reasonably good at the final temperature point, although the plies crack at higher temperatures than predicted. The analysis tends to overpredict crack densities when compared to edge counts of cracks in the single 45 plies (Figure 6.3) but are also surprisingly accurate when compared to crack densities in 45 degree plies in the interior of specimens (Figures 6.19 and 21).

7.2 PLY ORIENTATION EFFECTS

The only ply angle dependent effect that the current analysis predicts in a quasi-isotropic layup is the geometric effect described in Figure 4.9. In practice, the observed behavior of plies was highly dependent on their orientation relative to the edge at which cracks were observed.

Most previous studies dealt with the 90 ply groups in crossply laminates. We found that the actual number of cracks correlated well with our analysis in these groups, especially for final crack density (Figures 6.4 and 6.7). On the other hand, the data showed wide scatter, and cracks were observed at higher temperatures than predicted. These effects were doubtlessly related to the vulnerability of these ply groups to damage as was demonstrated in the sanding control test described in Section 5.4.3. They also proved very sensitive to the condition of the edges as shown in Table 6.2. The crack count in Side B was nearly double the count in Side A. This can be accounted for by the fact that Side B was polished after all cooling tests, whereas Side A was polished beforehand. Therefore, Side B had a rough surface where more flaws could initiate cracking. This phenomenon was also observed through a series of experiments by Kitano et al. [53].

The 45 groups all showed much less cracking at free surfaces than expected (Figure 6.3, 6.5, 6.6, and 6.8). However, this data was measured at the free edge. Sanding revealed that in the interior of specimens, the crack density of the +45 ply group reached expected levels, although with a great deal of noise (Figure 6.21). Thicker -45 groups, which behaved more ideally in the sense that the cracks continued through the width, showed fewer cracks than expected everywhere.

The 30 plies showed no cracks except near the free edges, where a few small cracks were noted. Analysis showed that this was not so much a ply angle

effect as a laminate one. The $[0_2/\pm30]_s$ laminate does not develop sufficient thermal stress to cause cracks.

7.3 EDGE EFFECTS

The previously omitted effects of free edges on cracking behavior proved to be very significant. A three dimensional free edge stress analysis explained the reasons for this very clearly.

The analytical results for transverse stress in the 45 ply groups (Figure 6.23) showed that near free edges, for distances equivalent to several thicknesses of the cracking ply groups (see also Figure C.4), this stress is reduced dramatically. This causes fewer cracks to appear in this area. In thin plies, this results in reduced edge crack counts but has little effect on crack densities in the interior. It is interesting to note that the distance to reach the higher CLPT stress values in Figure 6.3 in the 45 ply matches the distance to higher crack density in the sanding results of Figure 6.20. In thicker ply groups, this effect appears to lower overall crack density. We assume that the narrow low stress zone does not impede thick, ideally behaved, through cracks from extending across the laminate. However, the low edge stress may suppress crack initiation at the edge and result in lower crack density. This behavior is not seen in 90 ply groups, which have virtually unchanged in-plane stress near the free edges as seen in Figure 6.23. This is consistent with the results of the sanding experiments where the crack densities at the edges were at approximately the same level as those in the specimen interiors.

These results have disturbing implications for the common practice of measuring damage by edge crack counting. Most work in the literature considers crossply laminates, which do not suffer from this effect. However,

attempts to transfer techniques (either analytical or experimental) developed for crossply laminates to general laminates will be complicated by the effect.

CHAPTER 8

CONCLUSIONS

8.1 SUMMARY

In this study, we developed a general analytical method to predict crack density and degraded laminate properties. We correlated the analytical prediction with experimental data. The ply group thickness was an important factor in these correlations. The thicker (two or four layer) groups showed better correlations between analysis and experiment. We experimentally verified that the cracks behave in the idealized way assumed in the analysis. Cracks in the thin single plies did not prove to follow the assumptions in the model. A new type of analysis is required for laminates with thin plies. Previous successful analytical work has been applied to thick plies, usually in crossply laminates. Therefore, generalizing these analytical methods may be more difficult than previously assumed.

Edge effects proved to be an extremely important factor in our study. The free edge stress analysis correlated very well with the results we obtained from the sanding experiments. We found that the data collected from free edges may not be indicative of the actual damage within the laminates. The edges are also susceptible to damage, and their behavior can be greatly affected by factors such as edge finish. An alarming conclusion is that the current practice of taking crack density data at the specimen edge is not reliable.

8.2 RECOMMENDATIONS

This study has identified important factors in the analysis of microcracking in composite laminates. The assumptions regarding the cracking

behavior used to develop the model must be reevaluated for thin plies. Discontinuous, randomly distributed cracks must be modelled in these plies. The effects of free edges must also be accounted for. The free edge stress analysis needs to be developed and incorporated into the cracking analysis. Finally, we need to develop a definition of crack density that accounts for the random nature of cracking in thin plies and an experimental procedure that accounts for the unreliability of the crack density at the free edges.

REFERENCES

1. Flaggs, D. and Kural, M., "Experimental Determination of the In Situ Transverse Lamina Strength in Graphite/Epoxy Laminates", Journal of Composite Materials, Vol. 16, No. March, 1982, pp. 103-116.

2. Kistner, M., Whitney, J., and Browning, C., "First-Ply Failure of Graphite/Epoxy Laminates", *Recent Advances in Composites in the U.S. and Japan, ASTM STP*, Vol. 864, 1985, pp. 44-61.

3. Lee, J. and Daniel, I., "Progressive Transverse Cracking of Crossply Composite Laminates", *Journal of Composite Materials*, Vol. 24, No. November, 1990, pp. 1225-1243.

4. Peters, P., "The Strength Distribution of 90° Plies in 0/90/0 Graphite-Epoxy Laminates", *Journal of Composite Materials*, Vol. 18, No. November, 1984, pp. 545-555.

5. Peters, P., "Constrained 90-Deg Ply Cracking in 0/90/0 and ±45/90/45 CFRP Laminates", *Composite Materials: Fatigue and Fracture, ASTM STP 907*, 1986, pp. 84-99.

6. Peters, P., "An Experimental Element Technique for Transverse Fracture in CFRP and GFRP", *International Union of Theoretical and Applied Mechanics (IUTAM)*, Blacksburg, VA, 1991,

7. Flaggs, D., "Prediction of Tensile Matrix Failure in Composite Laminates", *Journal of Composite Materials*, Vol. 19, No. January, 1985, pp. 29-50.

8. Laws, N. and Dvorak, G., "Progressive Transverse Cracking in Composite Laminates", *Journal of Composite Materials*, Vol. 22, No. October, 1988, pp. 900-916.

9. Lim, S. and Hong, S., "Prediction of Transverse Cracking and Stiffness Reduction in Cross-Ply Laminated Composites", *Journal of Composite Materials*, Vol. 23, 1989, pp. 695-713.

10. Lim, S. and Hong, C., "Effect of Transverse Cracks on the Thermomchanical Properties of Cross-Ply Laminated Composites", *Composites Science and Technology*, Vol. 34, 1989, pp. 145-162.

11. Thomas, D. and Wetherhold, R., "Progressive Matrix Crack Modeling in Off-Axis Plies", *Proceedings of the American Society of Composites*, Cleveland, Ohio, 1993, pp. 683-692.

12. McCartney, L., "Analytical Models of Stress Transfer in Unidirectional Composite and Cross-Ply Laminates, and Their Application to the Prediction of Matrix/Transverse Cracking", *International Union of Theoretical and Applied Mechanics (IUTAM)*, Blacksburg, VA, 1991,

13. McCartney, L., "Theory of Stress Transfer in a 0°-90°-0° Cross-Ply Laminate Containing a Parallel Array of Transverse Cracks", *J. Mech. Phys. Solids*, Vol. 40, No. 1, 1992, pp. 27-68.

14. Han, Y. and Hahn, H., "Ply Cracking and Property Degradations of Symmetric Balanced Laminates Under General In-Plane Loading", *Composite Science and Technology*, Vol. 35, 1989, pp. 377-397.

15. Highsmith, A. and Reifsnider, K., "Stiffness-Reduction Mechanisms in Composite Laminates", *Damage in Composite Materials, ASTM STP 775*, 1982, pp. 102-117.

16. Nairn, J., "The Strain Energy Release Rate of Composite Microcracking: A Variational Approach", *Journal of Composite Materials*, Vol. 23, No. November, 1989, pp. 1106-1129.

17. Varna, J. and Berglund, L., "Multiple Transverse Cracking and Stiffness Reduction in Cross-Ply Laminates", *Journal of Composites Technology and Research*, Vol. 13, No. 2, 1991, pp. 99-106.

18. Tan, S. and Nuismer, R., "A Theory for Progressive Matrix Cracking in Composite Laminates", *Journal of Composite Materials*, Vol. 23, 1989, pp. 1029-1047.

19. Paas, M. and Van Den Eikhoff, J., "Finite Element Analysis of Degradation Processes in Laminated Composite Structures", *ICCM*, Madrid, Spain, 1993, pp. 113-120.

20. Talreja, R., Yalvac, S., Yats, L., and Wetters, D., "Transverse Cracking and Stiffness Reduction in Cross Ply Laminates of Different Matrix Toughness", *Journal of Composite Materials*, Vol. 26, No. 11, 1992, pp. 1644-1663.

21. Jamison, R., Schulte, K., Reifsnider, K., and Stinchcomb, W., "Characterization and Analysis of Damage Mechanisms in Tension-Tension Fatigue of Graphite/Epoxy Laminates", *Effectsd of Defects in Composite Materials, ASTM STP*, Vol. 836, 1984, pp. 21-55.

22. Kimpara, I., Kageyama, K., Ohsawa, I., and Suzuki, T., "Fatigue Damage Accumulation and Strength of CFRP Laminates with Different Moduli and Stacking Sequences", *ICCM*, Madrid, Spain, 1993, pp. 31-38.

23. Poursartip, A., Ashby, M., and Beaumont, P., "The Fatigue Damage Mechanics of a Carbon Fibre Composite Laminate: I-Development of the Model", *Composites Science and Technology*, Vol. 25, 1986, pp. 193-218.

24. Yang, J., "Fatigue and Residual Strength Degradation for Graphite/Epoxy Composites Under Tension-Compression Cyclic Loadings", *Journal of Composite Materials*, Vol. 12, No. January, 1978, pp. 19-39.

25. Yang, J. and Jones, D., "Statistical Fatigue of Graphite/Epoxy Angle-Ply Laminates in Shear", *Journal of Composite Materials*, Vol. 12, No. October, 1978, pp. 371-389.

26. Barnard, P., Butler, R., and Curtis, P., "The Strength-Life Equal Rank Assumption and its Application to the Fatique Life Prediction of Composite Materials", *International Journal of Fatique*, Vol. 3, No. July, 1988, pp. 171-177.

27. Chou, P. and Croman, R., "Residual Strength in Fatigue Based on the Strength-Life Equal Rank Assumption", *Journal of Composite Materials*, Vol. 12, No. April, 1978, pp. 177-194.

28. LaFarie-Frenot, M. and Henaff-Gardin, C., "Local Analysis and Modelling of Transverse Ply Cracking in Cross-Ply Carbon-Epoxy Laminates", 1992, pp. 631-642.

29. Boniface, L. and Ogin, S., "Application of the Paris Equation to the Fatigue Growth of Transverse Ply Cracks", *Journal of Composite Materials*, Vol. 23, July, 1989, pp. 735-754.

30. Petitpas, E., Renault, M., and Valentin, D., "Fatigue Behavior of Cross-Ply CFRP Laminates Made of T300 or T400 Fibers", *International Journal of Fatigue*, Vol. 4, 1990, pp. 245-251.

31. Gudmunson, P., Ostlund, S., and Zang, W., "Local Stresses and Thermoelastic Properties of Composite Laminates Containing Microcracks", *International Union of Theoretical and Applied Mechanics (IUTAM)*, Blacksburg, VA, 1991,

32. Bowles, D., Tompkins, S., and Funk, J., "Residual Thermal Stresses in Composites for Dimensionally Stable Spacecraft Applications", *SEM Seventh International Congress on Experimental Mechanics*, Las Vegas, NV, April, 1992,

33. Adams, D., Bowles, D., and Herakovich, C., "Thermally Induced Transverse Cracking in Graphite/Epoxy Cross-Ply Laminates", *Journal of Reinforced Plastics and Composites*, Vol. 5, No. 3, 1986, pp. 152-169.

34. Bowles, D., "Effect of Microcracks on the Thermal Expansion of Composite Laminates", *Journal of Composite Materials*, Vol. 18, 1984, pp. 173-187.

35. Bowles, D., "Thermal Stress Analysis of Composites in the Space Environment", *Fifth International Symposium on Materials in a Space Environment*, Cannes Mandelieu, France, 1991,

36. Bowles, D. and Griffin, O., "Micromechanics Analysis of Space Simulated Thermal Stresses in Composites. Part II: Multidirectional Laminates and Failure Predictions", *Journal of Reinforced Plastics and Composites*, Vol. 10, 1991, pp. 522-539.

37. Bowles, D. and Griffin, O., "Micromechanics Analysis of Space Simulated Thermal Stresses in Composites. Part I: Theory and Unidirectional Laminates", *Journal of Reinforced Plastics and Composites*, Vol. 10, 1991, pp. 505-521.

38. Hiemstra, D. and Sottos, N., "Thermally Induced Interfacial Microcracking in Polymer Matrix Composites", *Journal of Composite Materials*, Vol. 27, No. 10, 1993, pp. 1030-1051.

39. Bowles, D. and Shen, J., "Thermal Cycling Effects on the Dimensional Stability of P75 and P75-T300 (Fabric) Hybrid Graphite/Epoxy Laminates", *33rd International SAMPE Symposium and Exhibition*, Anaheim, CA, March, 1988,

40. Jennings, T., Elmes, D., and Hull, D., "Thermal Fatigue of Carbon Fibre/Bismaleimide Matrix Composites", *European Conference on Composite Materials (ECCM)*, Bordeaux, France, 1989, pp. 563-569.

41. Knouff, B., Tompkins, S., and Jayaraman, N., "The Effect of Graphite Fiber Properties on Microcracking Due to Thermal Cycling of Epoxy-Cynate Matrix Laminates", *ASTM Fifth Symposium on Composite Materials: Fatigue and Fracture*, Atlanta, Georgia, 1993, pp. 2-27.

42. Manders, P. and Maas, D., "Thin Carbon Fiber Prepregs for Dimensionally Critical Structures", *SPIE Advances in Optical Structure Systems*, Orlando, Florida, 1990, pp. 536-545.

43. Tompkins, S., "Thermal Expansion of Selected Graphite-Reinforced Polyimide-, Epoxy-, and Glass-Matrix Composites", *Internation Journal of Thermophysics*, pp. 119-132.

44. Tompkins, S. and Williams, S., "Effects of Thermal Cycling on Mechanical Properties of Graphite Polyimide", *Journal of Spacecraft and Rockets*, Vol. 21, No. 3, May, 1984, pp. 274-279.

45. Tompkins, S., Bowles, D., Slemp, W., and Teichman, A., "Response of Composite Materials to the Space Station Orbit Environment", *AIAA/NASA Space Station Symposium*, Williamsburg, VA, 1988,

46. Tompkins, S., "Effects of Thermal Cycling on Composite Materials for Space Structures", *NASA/SDIO Space Environmental Effects on Materials Workshop*, 1989, pp. 447-470.

47. Tompkins, S., Funk, J., Bowles, D., Towell, T., and Connell, J., "Composite Materials for Precision Space Reflector Panels", *SPIE International Symposium and Exhibition on Optical Engineering and Photonics*, Orlando, FL, 1992,

48. McManus, H., Bowles, D., and Tompkins, S., "Prediction of Thermally Induced Matrix Cracking", *Proceedings of the American Society of Composites*, Cleveland, Ohio, 1993,

49. Jones, R., *Mechanics of Composite Materials*, McGraw-Hill, 1975,

50. Bhat, N. and Lagace, P., "A Method for Evaluating Interlaminar Stresses at Material Discontinuities", *Journal of Composite Materials*, No. January, 1994,

51. Lagace, P. A., Brewer, J. C., and Varnerin, C., "TELAC Manufacturing Course Notes", TELAC Report 88-4B, Massachusetts Institute of Technology, 1990.

52. Tompkins, S., *Personal Communication*, 1993.

53. Kitano, A., Yoshioka, K., Noguchi, K., and Matsui, J., "Edge Finishing Effects on Transverse Cracking of Cross-Ply CFRP Laminates", *International Conference on Composite Materials (ICCM)*, Madrid, Spain, 1993, pp. 169-176.

APPENDIX A

COMPUTER CODE MANUAL AND DOCUMENTATION

****

USING CRACKOMATIC

CODE FOR THE PREDICTION OF
THERMALLY INDUCED MATRIX CRACKING

c 1994 Cecelia H. Park and Hugh L. McManus
Massachusetts Institute of Technology
Rm 33-311, 77 Massachusetts Ave.
Cambridge MA 02139 (617) 253-0672

****

Version 0.3 12/93
WRITTEN IN MPW FORTRAN

****

This program is a research tool in the development stage
and is supplied "as is" for the purpose of
scientific collaboration.

****

I. INTRODUCTION

CRACKOMATIC calculates matrix crack density and reduced laminate properties in every ply of any arbitrary laminate as functions of temperature or thermal cycles.

II. INPUT FILES

CRACKOMATIC requires three kinds of prepared input files: 1) A laminate file containing material and layup information, 2) A fatigue toughness file for thermal cyclic loading 3) A temperature/cycle dependent material property file (optional). These should be ASCII text files in the same folder or directory as the code. The entries should be separated by spaces and lines (including the last one) terminated with a carriage return.

IIa. LAMINATE FILE FORMAT

NPLY
NMATi ANGLEi THICKi FLAGi
repeat above line NPLY times

EXi EYi NUXYi GXYi
ALPHA1i ALPHA2i BETA1i BETA2i
repeat above 2 lines for each material

NPLY is the number of plies in the laminate
for each ply:
NMATi is the material number of that ply (number materials consecutively from 1)
ANGLEi is the ply angle in degrees
THICKi is the ply thickness
FLAGi is a ply printing option It should be set to 1 to printout the output data/results for the ply. Others should be set to 0. If the cracks are to appear in a ply group, it should be entered as one thick ply
for each material:
EXi is the longitudinal ply modulus
EYi is the transverse ply modulus
NUXYi is the major Poisson's ratio
GXYi is the shear modulus
ALPHA1i is the longitudinal ply CTE
ALPHA2i is the transverse ply CTE
BETA1i and BETA2i are currently dormant ply CMEs- use 0.0

EXAMPLE: (A P75/934 [0/45/90/-45]s laminate, English units)

```
7
1 .005  0   0
1 .005  45 1
1 .005  90 1
1 .010 -45 1
1 .005  90 0
1 .005  45 0
1 .005  0   0
34.3E6 0.9E6 .29 0.7E6
-0.6E-6 16.E-6 0 0
```

IIb. FATIGUE TOUGHNESS FILE FORMAT

NPOINTS
Ni GCi
repeat above line NPOINTS times

NPOINTS is the number of data points that defines the Gc vs N curve for each point:
Ni is the number of cycles
GCi is the measured transverse fracture toughness corresponding to that number of cycles

EXAMPLE: (P75/ERL1962, extrapolated from very limited data)

```
6
1          .59566
10         .55627
100        .51947
1000       .48512
10000      .45303
100000     .42307
```

IIc. TEMPERATURE/CYCLE DEPENDENT MATERIAL PROPERTY FILES

The temperature dependent material file is similar to the fatigue toughness file format. Instead of just listing Gc, all material constants are listed.

File format for progressive loading:

```
NPOINTS
Ti EXi EYi NUXYi GXYi ALPHA1i ALPHA2i GCi
repeat above line NPOINTS times
```

Ti is the temperature
Other variables are as previously described

EXAMPLE (P75/934)

```
3
-250  33.76E6  .9E6  .31  1.1E6  -0.43E-6  21.923E-6  .22791
75    41.97E6  .83E6 .35  .61E6  -0.584E-6 19.18E-6   .22791
250   45.36E6  .81E6 .30  .46E6  -0.365E-6 26.455E-6  .22791
```

File format for the material properties as function of cyclic loading is similar:

```
NPOINTS
Ni EXi EYi NUXYi GXYi ALPHA1i ALPHA2i GCi
repeat above line NPOINTS times
```

III. INTERACTIVE SESSION

Once you have defined some layups and material files, run CRACKOMATIC. The following capitalized text refers to the questions/options during the interactive session.

The program will first ask for the laminate input file, give it one. Then it asks:

COMPUTE MINIMUM (1), MAXIMUM (2), OR AVERAGE (3) CRACK DENSITY?
Minimum seems to work best, so always choose it unless you specifically want to check theoretical maximum or average densities.

The code then outputs a review of the laminate, and a complete set of calculated laminate properties.

ANALYSIS TYPE-
1 = CRACK DENSITY AND PROPERTIES AS FUNCTION OF DELTA-T
2 = CRACK DENSITY AND PROPERTIES AS FUNCTION OF N
3 = READ NEW LAMINATE
4 = QUIT
Choices 1and 2 have their own sections below.
Choice 3 lets you pick a new laminate and/or change your choice of crack density.
Choice 4 stops the code, leaving the session in an editable text window, where the results can be cut and pasted into other documents.

IIIa. ANALYSIS TYPE 1

This analysis calculates the progressive change in crack density and laminate properties as functions of decreasing temperature. The code asks:

GIVE G (TRANSVERSE PLY FRACTURE TOUGHNESS),
SHEAR LAG FACTOR
AND LAMINATE STRESS FREE TEMPERATURE

G is the transverse ply fracture toughness or critical energy release rate, a material property that is not generally available directly. Reasonable guesses include the delamination Gic or a scaled function of the transverse tensile strength Y, e.g. G=A*Y**2, where A is a constant. We used A=3.96E-8 in**3/lb with some success, but that may have been luck.
SHEAR LAG FACTOR is a geometric parameter which can reasonably range from around 0.5 to around 2.0. We have found 0.65 for pitch fiber composites and 0.90 for pan fibers to work well.
LAMINATE STRESS FREE TEMPERATURE is usually the laminate cure temperature. The code then asks

GIVE TEMPERATURE RANGE AND INCREMENT:
INITIAL TEMP, FINAL TEMP, AND TEMP INCREMENT
User option variables to control the printed output

WANT TO SOFTEN LAMINATE AS IT PROGRESSES?
User option to include material softening effect

WANT TO INCORPORATE TEMPERATURE DEPENDENCE OF MATERIAL CONSTANTS (REQUIRES INPUT FILE)?
User option to include temperature dependent material properties, required input file with appropriate data.

The output is a tab-separated table of temperatures, crack densities and laminate longitudinal stiffness and CTE. These can be used to generate plots of progressive cracking and changing laminate properties as the temperature is progressively decreased. At the final temperature, the program computes all the degraded laminate properties.

IIIb. ANALYSIS TYPE 2

This analysis calculates the change in crack density and laminate properties as functions of numbers of constant thermal cycles. The code asks:

INPUT G(N) FILE NAME, OR HELP IF YOU NEED IT
Give it the name of a FATIGUE TOUGHNESS FILE (see above format).

GIVE SHEAR LAG FACTOR AND GREATEST DELTA-T
Give the shear lag factor described above, and the DELTA-T at the lowest temperature in the cycle. (The highest temperature or cycle R-value are assumed to be the same as those used to generate the data in the fatigue toughness file, so you don't input either of these).

INCREASE N LINEARLY (ENTER Y) OR EXPONENTIALLY (N)?
This choice controls the output. A "Y" will give output suitable for making a linear plot, while an "N" will generate output suitable for making a semi-log plot. If you choose Y, you are asked

GIVE MAXIMUM N AND INCREMENT
which is self-explanatory; if you choose N, you are asked
GIVE MAXIMUM N AND POINTS PER DECADE
which is almost so; points per decade is the number of plot points generated for each power of ten on the plot.

WANT TO SOFTEN LAMINATE?
User option to include material softening effect

WANT TO INCORPORATE MATERIAL CONSTANTS AS FUNCTION OF THERMAL CYCLES (REQUIRES INPUT FILE)?
User option to include material properties as a function of thermal cycles, required input file with appropriate data.

The output is a tab-separated table of number of cycles, crack densities, and laminate longitudinal stiffness and CTE. These can be used to generate plots of cracking and changing laminate properties as the laminate is thermally cycled.

IV. A FEW USEFUL TRICKS

On Macintosh computers, after the program stops the output remains in an editable, saveable text window. Note the menu bar; the edit and file commands work. Usually, all work in a session can be accessed by scrolling; very long

sessions save themselves in a file and must be closed and reopened using an editor.

The outputs of analyses 1 and 2 are in tab-separated tables that can be cut and pasted directly into spreadsheets or plotting programs. The code expects all inputs in a consistent set of units. Make sure, for example, that if you are using metric units you enter ply thicknesses in METERS, not millimeters as they are usually reported.

A "hack" in the code allows you to give all properties in English units except Gc (which is usually reported in metric) by entering negative Gc values; the code converts the absolute value of Gc to English units.

V. SAMPLE SESSION

Two samples sessions are listed below. The first is an example of analysis type 1. This example includes material softening effects and temperature dependent material properties. The second session is an example of analysis type 2 using material softening effects. User input is in **bold**.

Va. SAMPLE SESSION A: ANALYSIS TYPE 1 OF P75/934 $[0/45/90/-45]_S$

```
INPUT LAYUP FILE OR HELP IF YOU NEED IT
p75934zfnf

                    LAMINATE
 PLY   MATERIAL   THICKNESS    ANGLE

  1        1         0.0050      0.00
  2        1         0.0050     45.00
  3        1         0.0050     90.00
  4        1         0.0100    -45.00
  5        1         0.0050     90.00
  6        1         0.0050     45.00
  7        1         0.0050      0.00

    MATERIAL PROPERTIES FOR MATERIAL  1-
 E11      3.4300E+07   E22      9.0000E+05
 NU12     2.9000E-01   G12      7.0000E+05
 ALPHA1   -6.0000E-07   ALPHA2    1.6000E-05
 BETA1    0.0000E+00   BETA2     0.0000E+00

ENGINEERING CONSTANTS FOR UNCRACKED LAMINATE-
 E11 =  1.2317E+07  E22 =  1.2317E+07  G  =  4.6943E+06
 V12 =  3.1191E-01  V21 =  3.1191E-01
 ALPHA1 = -6.0484E-08  ALPHA2 = -6.0484E-08  ALPHA12 = -4.8557E-19
 BETA1  =  0.0000E+00  BETA2  =  0.0000E+00  BETA12  =  0.0000E+00

HIT RETURN TO CONTINUE

COMPUTE: (1) MINIMUM, (2) MAXIMUM, (3) AVERAGE  CRACK SPACING
1
```

ANALYSIS TYPE-
1 = CRACK DENSITY AS FUNCTION OF DELTA-T
2 = CRACK DENSITY AS FUNCTION OF CYCLES (N)
3 = READ NEW LAMINATE
4 = QUIT
1

GIVE G (TRANSVERSE PLY FRACTURE TOUGHNESS)
SHEAR LAG FACTOR,
LAMINATE STRESS FREE TEMPERATURE
-40 .65 350

GIVE TEMPERATURE RANGE AND INCREMENT:
INITIAL TEMP, FINAL TEMP, AND TEMP INCREMENT
75 -250 25

WANT TO SOFTEN LAMINATE AS IT PROGRESSES?
y

WANT TO INCORPORATE TEMPERATURE DEPENDENCE OF
MATERIAL CONSTANTS (REQUIRES INPUT FILE) ?
y

PLEASE INPUT TEMPERATURE DEPENDENT MATERIAL FILE
p75934_tdep

TRANSVERSE PLY FRACTURE TOUGHNESS = 4.0000E+01 (METRIC)
TRANSVERSE PLY FRACTURE TOUGHNESS = 2.2791E-01
SHEAR LAG FACTOR = 0.65
STRESS FREE TEMPERATURE = 350.00

	* PLY 2 *	* PLY 3 *	* PLY 4 *	LAMINATE	
Temperature	Crack Density	Crack Density	Crack Density	Stiffness	CTE
75	0.0000E+00	0.0000E+00	0.0000E+00	1.4776E+07	-7.3510E-08
50	0.0000E+00	0.0000E+00	8.0141E+00	1.4571E+07	-5.7974E-08
25	0.0000E+00	0.0000E+00	1.5183E+01	1.4367E+07	-4.1396E-08
0	0.0000E+00	0.0000E+00	1.8989E+01	1.4173E+07	-1.9946E-08
-25	0.0000E+00	0.0000E+00	2.2130E+01	1.3981E+07	2.6973E-09
-50	0.0000E+00	0.0000E+00	2.4945E+01	1.3788E+07	2.6106E-08
-75	2.6459E+01	3.6858E+01	2.7567E+01	1.3517E+07	-1.3391E-08
-100	3.3482E+01	4.6949E+01	3.0048E+01	1.3300E+07	-8.4506E-09
-125	3.9021E+01	5.4842E+01	3.2430E+01	1.3086E+07	-1.4497E-10
-150	4.3892E+01	6.1767E+01	3.4737E+01	1.2872E+07	9.5830E-09
-175	4.8371E+01	6.8126E+01	3.6984E+01	1.2660E+07	2.0111E-08
-200	5.2588E+01	7.4108E+01	3.9184E+01	1.2446E+07	3.1153E-08
-225	5.6616E+01	7.9821E+01	4.1345E+01	1.2233E+07	4.2564E-08
-250	6.0469E+01	8.5284E+01	4.3457E+01	1.2027E+07	5.3318E-08

ALL LAMINATE PROPERTIES AT FINAL TEMPERATURE
E11 = 1.2027E+07 E22 = 1.2026E+07 G = 4.6281E+06
V12 = 3.0888E-01 V21 = 3.0887E-01

```
 ALPHA1 =  5.3318E-08  ALPHA2 =  5.2551E-08  ALPHA12 = -4.8800E-08
 BETA1 =  0.0000E+00  BETA2 =  0.0000E+00  BETA12 =  0.0000E+00

 ANALYSIS TYPE-
 1 = CRACK DENSITY AS FUNCTION OF DELTA-T
 2 = CRACK DENSITY AS FUNCTION OF CYCLES (N)
 3 = READ NEW LAMINATE
 4 = QUIT
4
```

Vb SAMPLE SESSION B: ANALYSIS TYPE 2 OF P75/ERL1962 [0/90/0/90]s

```
 INPUT LAYUP FILE OR HELP IF YOU NEED IT
p75znzn

                        LAMINATE
  PLY    MATERIAL       THICKNESS        ANGLE

   1          1            0.0050         0.00
   2          1            0.0050        90.00
   3          1            0.0050         0.00
   4          1            0.0100        90.00
   5          1            0.0050         0.00
   6          1            0.0050        90.00
   7          1            0.0050         0.00

     MATERIAL PROPERTIES FOR MATERIAL  1-
   E11       3.4300E+07    E22       9.0000E+05
   NU12      2.9000E-01    G12       7.0000E+05
   ALPHA1    -5.3000E-07   ALPHA2    2.2000E-05
   BETA1     0.0000E+00    BETA2     0.0000E+00

 ENGINEERING CONSTANTS FOR UNCRACKED LAMINATE-
  E11 =  1.7635E+07  E22 =  1.7635E+07  G  =  7.0000E+05
  V12 =  1.4830E-02  V21 =  1.4830E-02
  ALPHA1 =  2.0225E-07  ALPHA2 =  2.0225E-07  ALPHA12 = -6.8180E-18
  BETA1 =  0.0000E+00  BETA2 =  0.0000E+00  BETA12 =  0.0000E+00

 HIT RETURN TO CONTINUE

 COMPUTE: (1) MINIMUM, (2) MAXIMUM, (3) AVERAGE CRACK SPACING
1

 ANALYSIS TYPE-
 1 = CRACK DENSITY AS FUNCTION OF DELTA-T
 2 = CRACK DENSITY AS FUNCTION OF CYCLES (N)
 3 = READ NEW LAMINATE
 4 = QUIT
2

 INPUT G(N) FILE NAME OR HELP IF YOU NEED IT
p75gs
```

GIVE SHEAR LAG FACTOR AND GREATEST DELTA-T
.65 -600

INCREASE N LINEARLY (ENTER Y) OR EXPONENTIALLY (N)?
y

GIVE MAXIMUM N AND INCREMENT
500 25

WANT TO SOFTEN LAMINATE?
y

WANT TO INCORPORATE MATERIAL CONSTANTS
AS FUNCTION OF CYCLES?
n

FRACTURE TOUGHNESS AS A FUNCTION OF CYCLE

N	FRACTURE TOUGHNESS
1.0000E+00	5.9566E-01
1.0000E+01	5.5627E-01
1.0000E+02	5.1947E-01
1.0000E+03	4.8512E-01
1.0000E+04	4.5303E-01
1.0000E+05	4.2307E-01

SHEAR LAG FACTOR = 0.65
MAXIMUM DELTA-T = -600.00

	* PLY 1 *	* PLY 2 *	* PLY 4 *	LAMINATE	
Cycle	Crack Density	Crack Density	Crack Density	Stiffness	CTE
0	1.8201E+01	1.8037E+01	3.5615E+01	1.7558E+07	9.5881E-08
25	3.4207E+01	3.4483E+01	3.7763E+01	1.7540E+07	6.3889E-08
50	3.5999E+01	3.6245E+01	3.8244E+01	1.7538E+07	5.9886E-08
75	3.7677E+01	3.7901E+01	3.8733E+01	1.7536E+07	5.6050E-08
100	3.9273E+01	3.9480E+01	3.9231E+01	1.7533E+07	5.2329E-08
125	3.9423E+01	3.9629E+01	3.9280E+01	1.7533E+07	5.1975E-08
150	3.9568E+01	3.9773E+01	3.9326E+01	1.7533E+07	5.1633E-08
175	3.9712E+01	3.9916E+01	3.9374E+01	1.7533E+07	5.1291E-08
200	3.9856E+01	4.0059E+01	3.9421E+01	1.7533E+07	5.0950E-08
225	4.0000E+01	4.0201E+01	3.9468E+01	1.7532E+07	5.0609E-08
250	4.0143E+01	4.0343E+01	3.9516E+01	1.7532E+07	5.0269E-08
275	4.0286E+01	4.0485E+01	3.9563E+01	1.7532E+07	4.9930E-08
300	4.0429E+01	4.0626E+01	3.9610E+01	1.7532E+07	4.9591E-08
325	4.0572E+01	4.0767E+01	3.9658E+01	1.7532E+07	4.9252E-08
350	4.0713E+01	4.0907E+01	3.9706E+01	1.7531E+07	4.8915E-08
375	4.0854E+01	4.1047E+01	3.9754E+01	1.7531E+07	4.8575E-08
400	4.0995E+01	4.1187E+01	3.9802E+01	1.7531E+07	4.8239E-08
425	4.1135E+01	4.1327E+01	3.9850E+01	1.7531E+07	4.7902E-08
450	4.1275E+01	4.1465E+01	3.9898E+01	1.7531E+07	4.7566E-08
475	4.1415E+01	4.1604E+01	3.9946E+01	1.7530E+07	4.7230E-08
500	4.1555E+01	4.1742E+01	3.9995E+01	1.7530E+07	4.6894E-08

```
ALL LAMINATE PROPERTIES AT FINAL TEMPERATURE
 E11 =  1.7530E+07  E22 =  1.7564E+07  G  =  5.6136E+05
 V12 =  1.1942E-02  V21 =  1.1965E-02
 ALPHA1 =  4.6894E-08  ALPHA2 =  7.6861E-08  ALPHA12 = -7.6337E-18
 BETA1  =  0.0000E+00  BETA2  =  0.0000E+00  BETA12  =  0.0000E+00

ANALYSIS TYPE-
1 = CRACK DENSITY AS FUNCTION OF DELTA-T
2 = CRACK DENSITY AS FUNCTION OF CYCLES (N)
3 = READ NEW LAMINATE
4 = QUIT
4
```

APPENDIX B

PROGRESSIVE THERMAL LOADING ANALYTICAL AND EXPERIMENTAL RESULTS

This section presents all the results for the progressive cooling tests of the $[0/45/90/-45]_s$, $[0/90/\pm45]_s$, $[0/\pm45/90]_s$, $[0_2/45_2/90_2/-45_2]_s$ and $[0/90/0/90]_s$, and $[0_2/\pm30]_s$ specimens. Correlations of the analytical prediction to experimental data for crack density are graphed. Laminate property degradation is also shown for the temperature range tested. The analytical prediction of laminate longitudinal stiffness and CTE properties are presented.

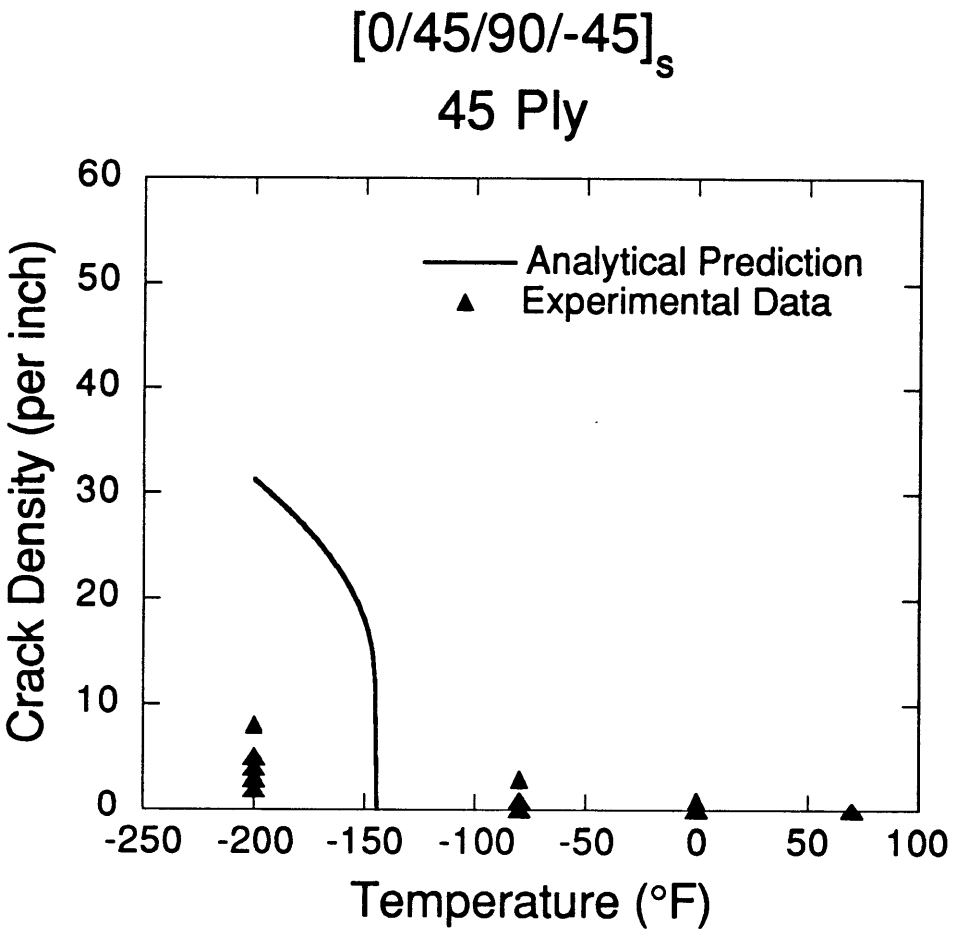

Figure B.1 Analytical and experimental correlation of crack density vs. decreasing temperature. 45 ply of $[0/45/90/-45]_s$ laminate.

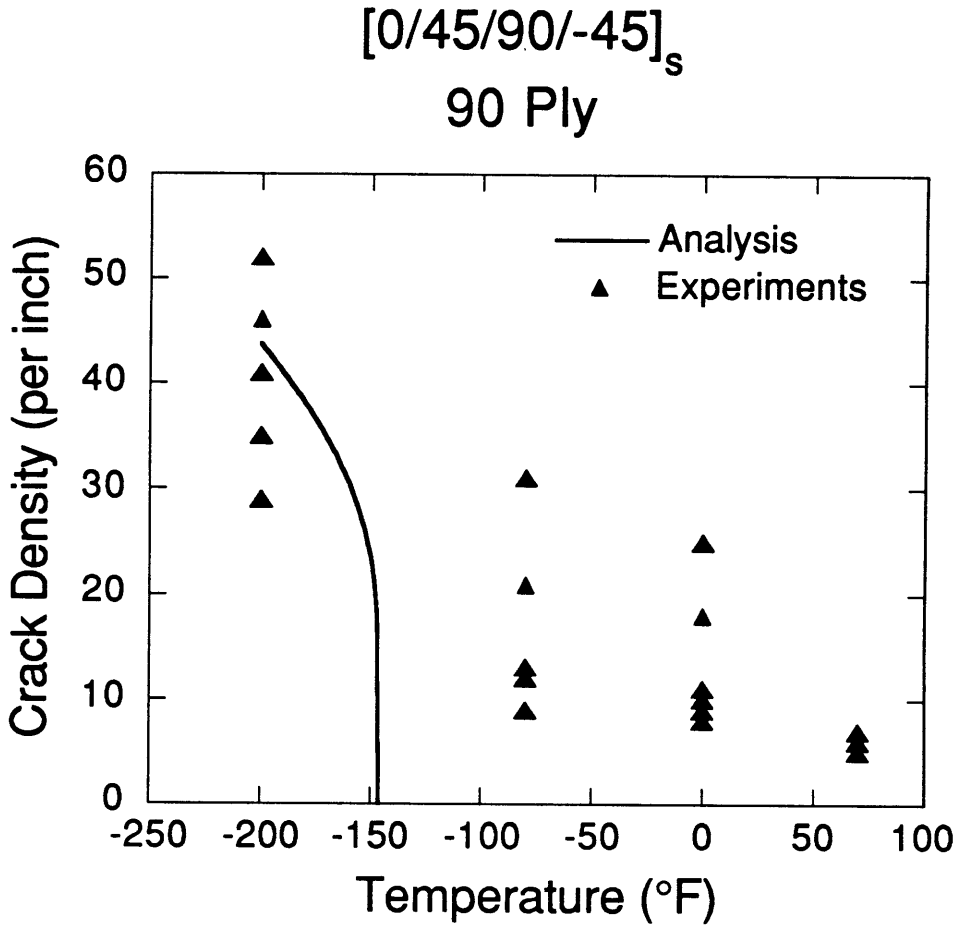

Figure B.2 Analytical and experimental correlation of crack density vs. decreasing temperature. 90 ply of $[0/45/90/-45]_s$ laminate.

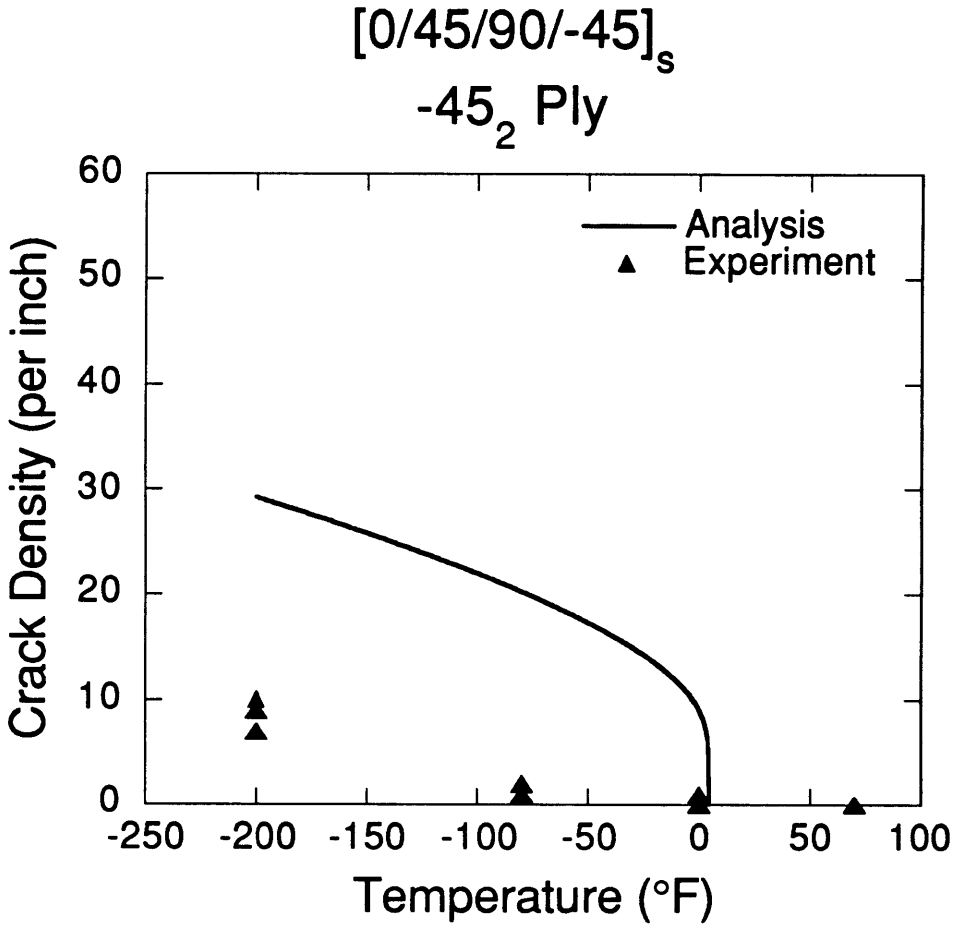

Figure B.3 Analytical and experimental correlation of crack density vs. decreasing temperature. -45_2 ply of $[0/45/90/-45]_s$ laminate.

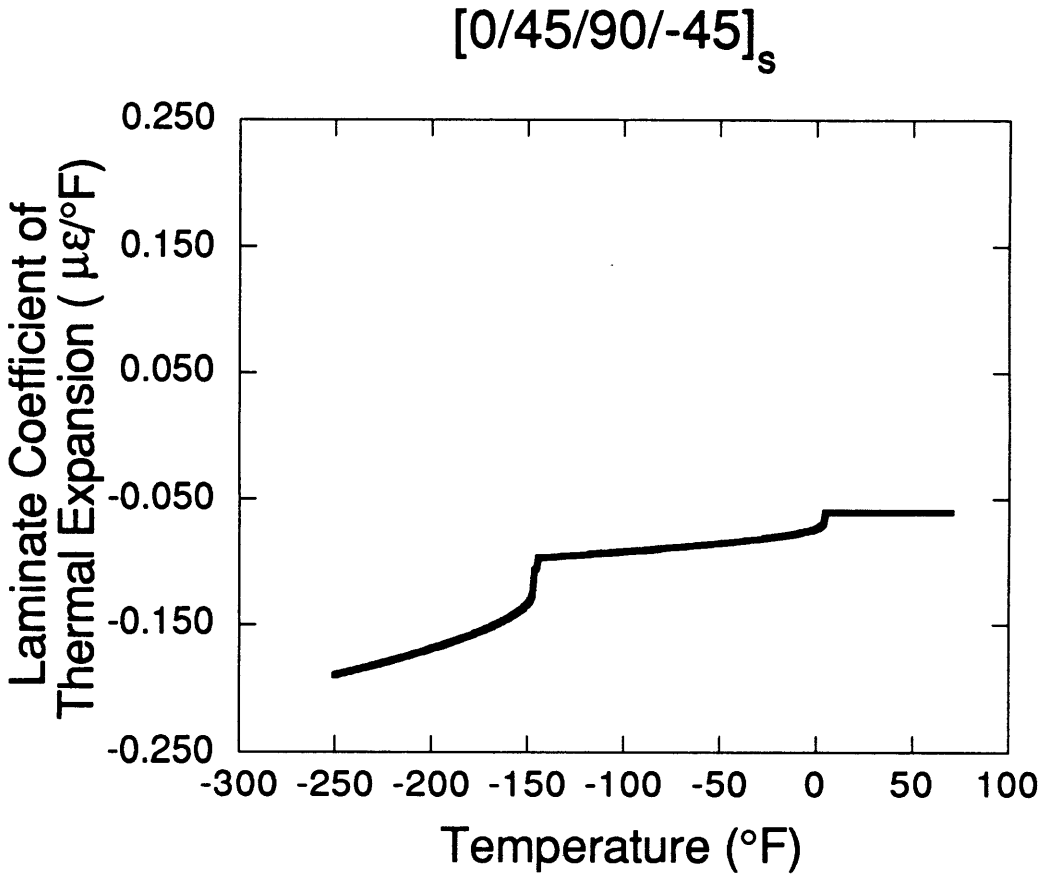

Figure B.4 Analytical CTE prediction vs. temperature for $[0/45/90/-45]_s$ laminate.

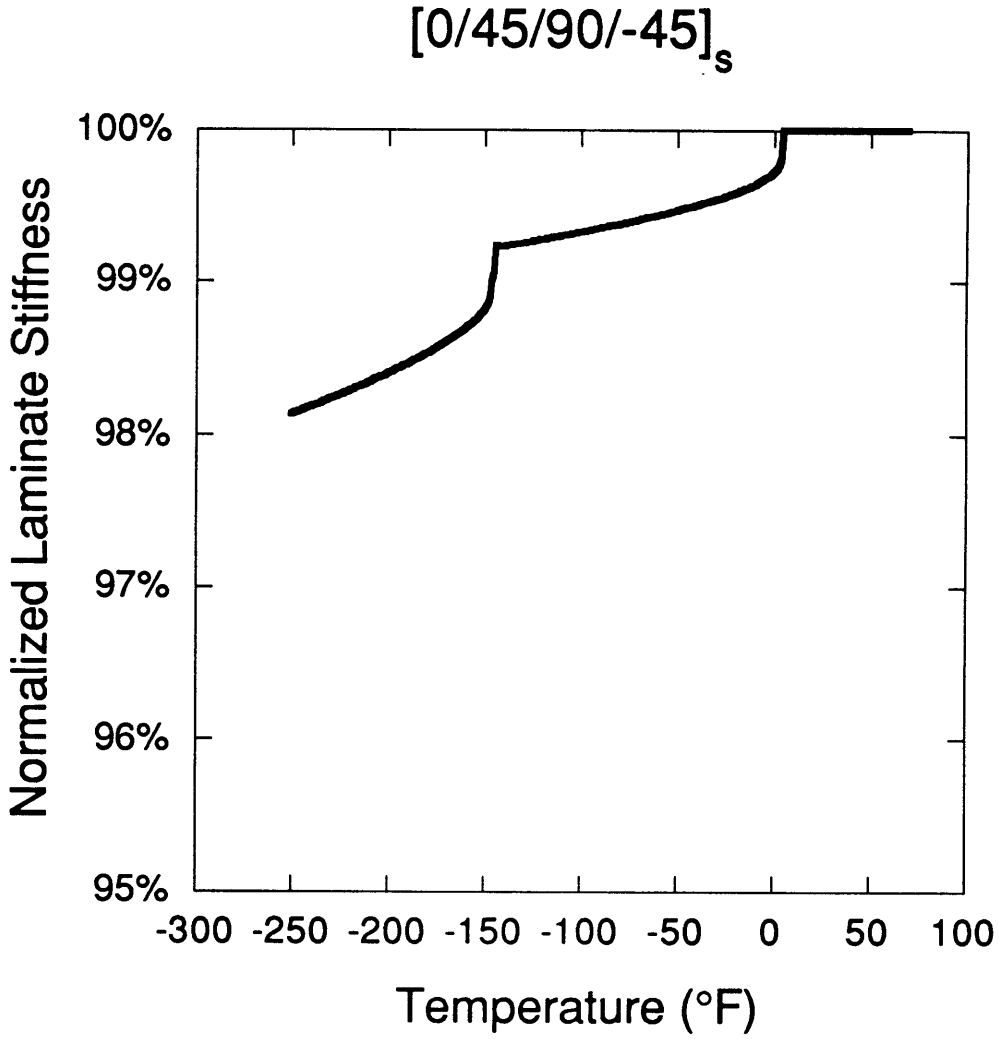

Figure B.5 Analytical stiffness prediction vs. temperature for $[0/45/90/-45]_s$ laminate. Laminate longitudinal stiffness normalized by undamaged value.

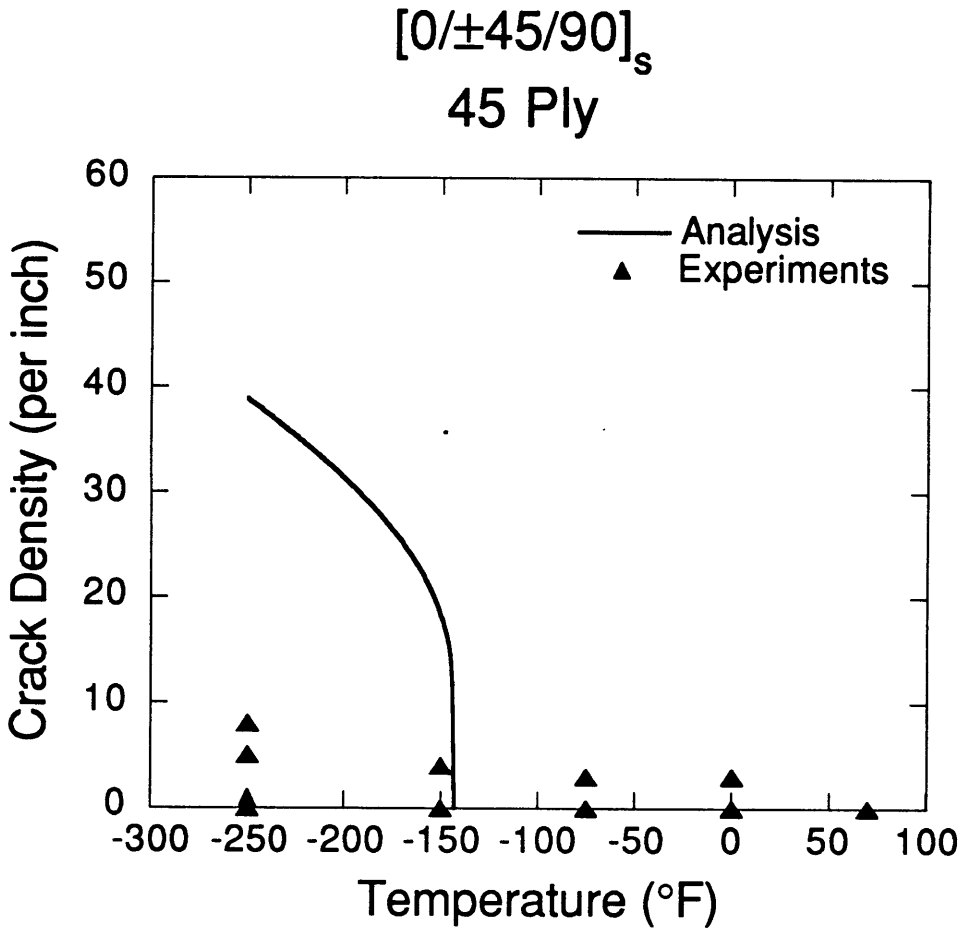

Figure B.6 Analytical and experimental correlation of crack density vs. decreasing temperature. 45 ply of $[0/\pm45/90]_s$ laminate.

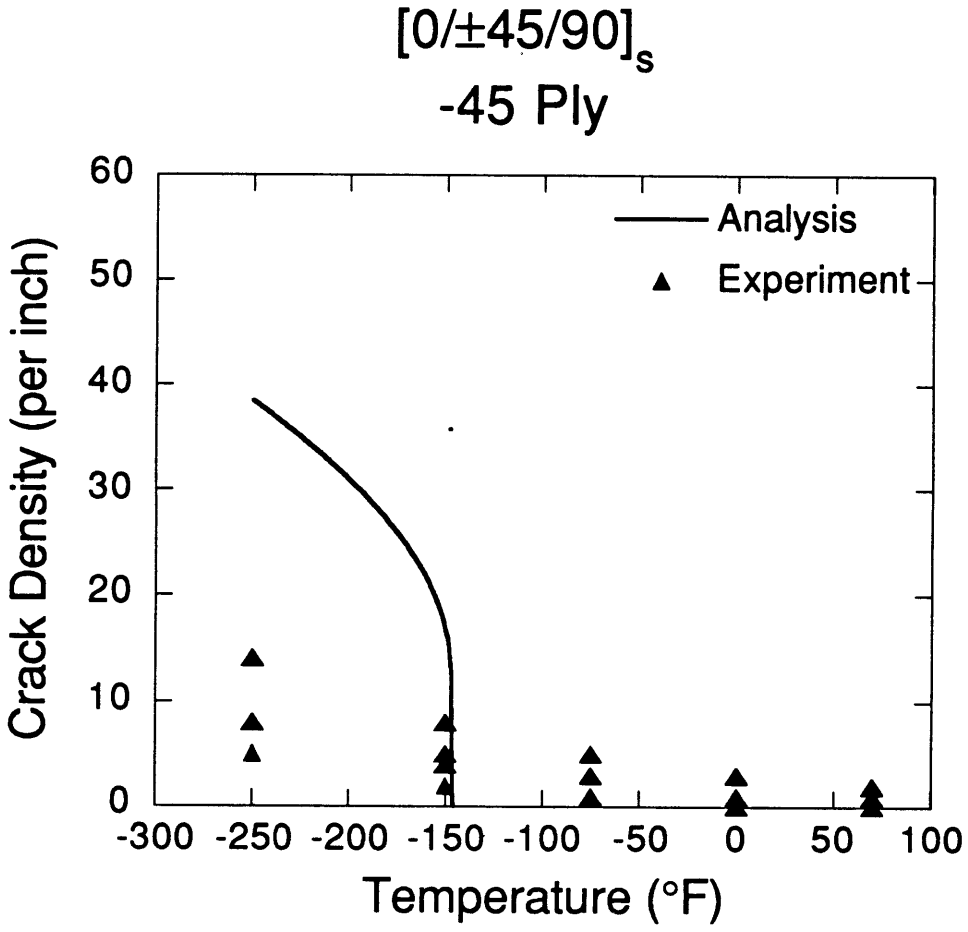

Figure B.7 Analytical and experimental correlation of crack density vs. decreasing temperature. -45 ply of $[0/\pm45/90]_s$ laminate.

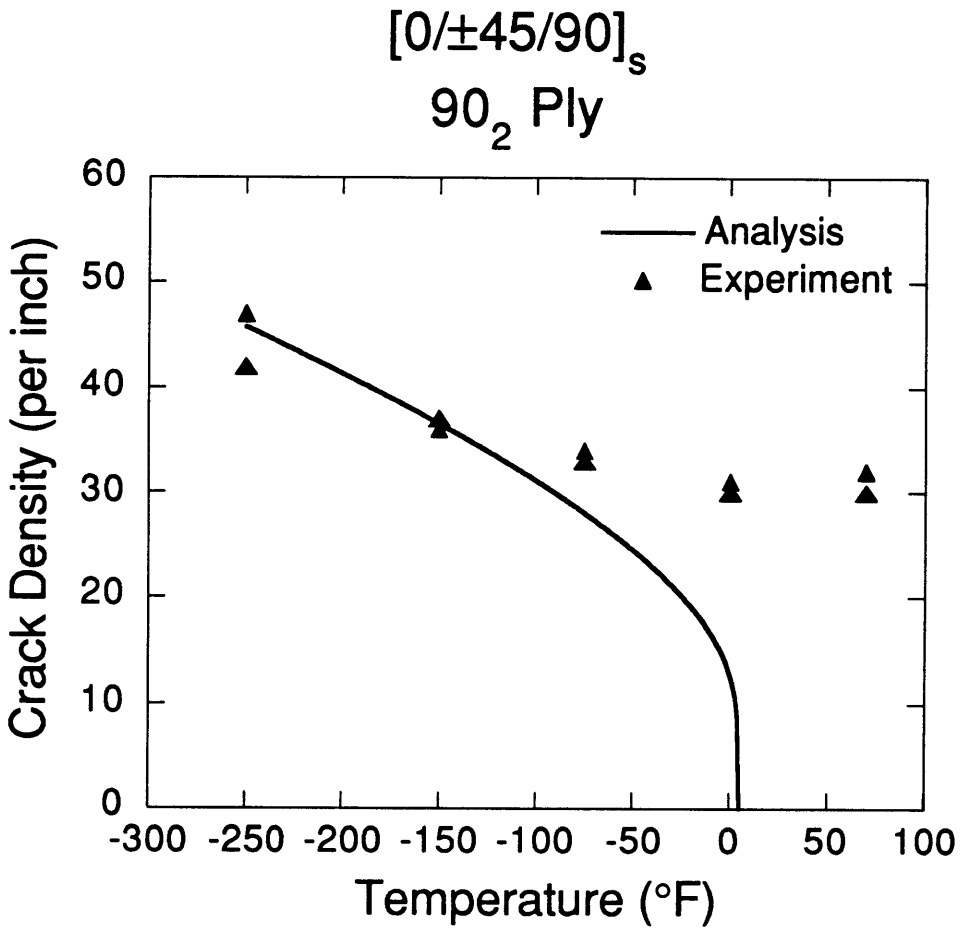

Figure B.8 Analytical and experimental correlation of crack density vs. decreasing temperature. 90_2 ply of $[0/\pm45/90]_s$ laminate.

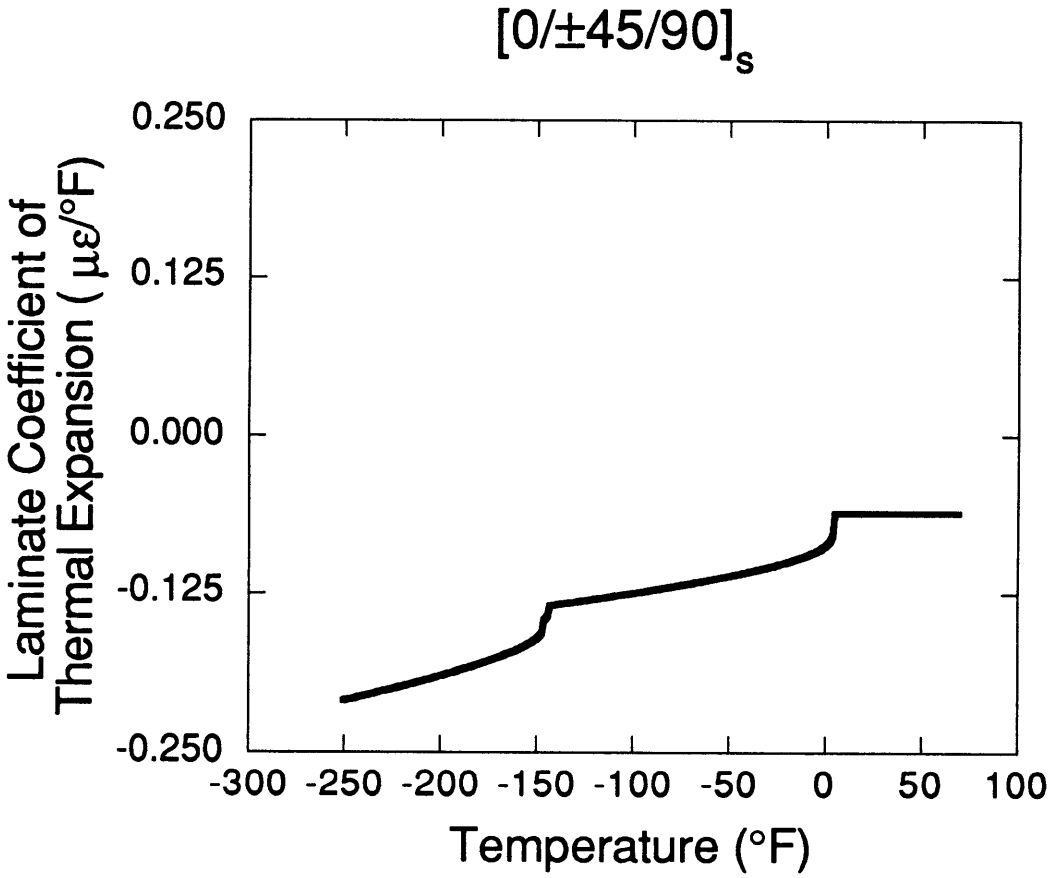

Figure B.9 Analytical CTE prediction vs. temperature for $[0/\pm45/90]_s$ laminate.

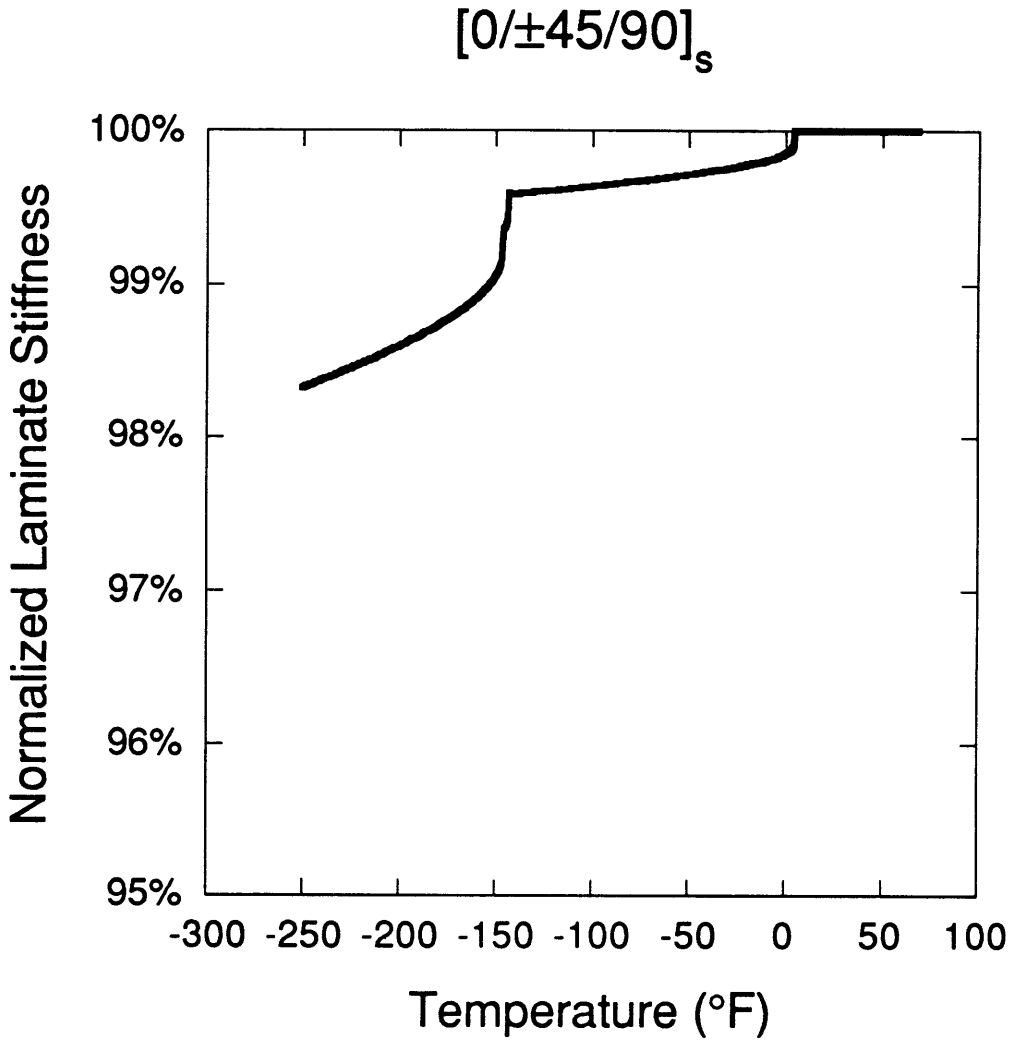

Figure B.10 Analytical stiffness prediction vs. temperature for $[0/\pm45/90]_s$ laminate. Laminate longitudinal stiffness normalized by undamaged value.

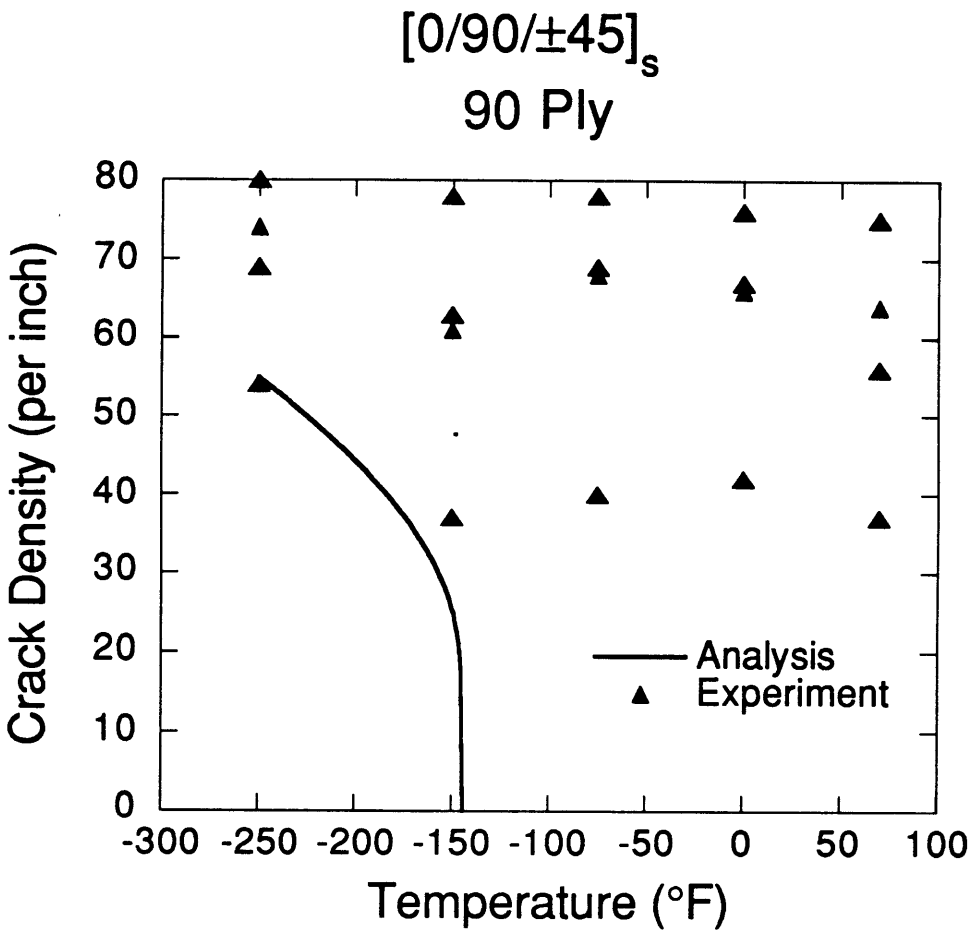

Figure B.11 Analytical and experimental correlation of crack density vs. decreasing temperature. 90 ply of $[0/90/\pm45]_s$ laminate.

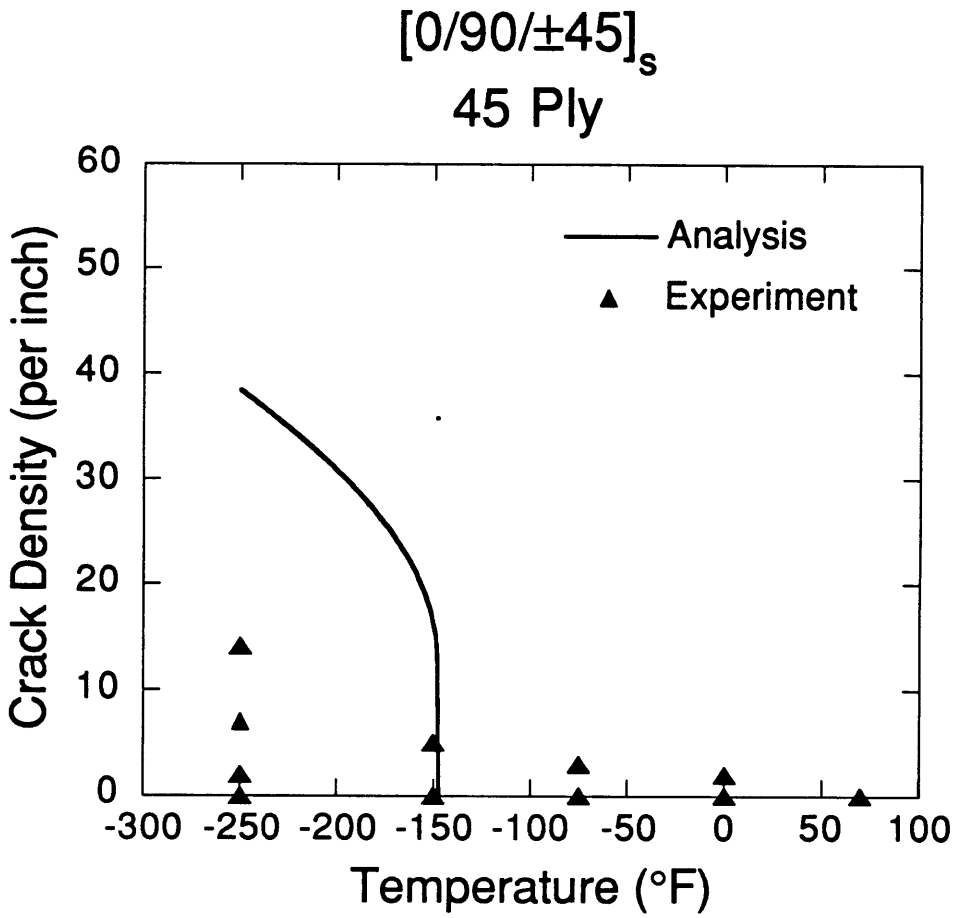

Figure B.12 Analytical and experimental correlation of crack density vs. decreasing temperature. 45 ply of $[0/90/\pm45]_s$ laminate.

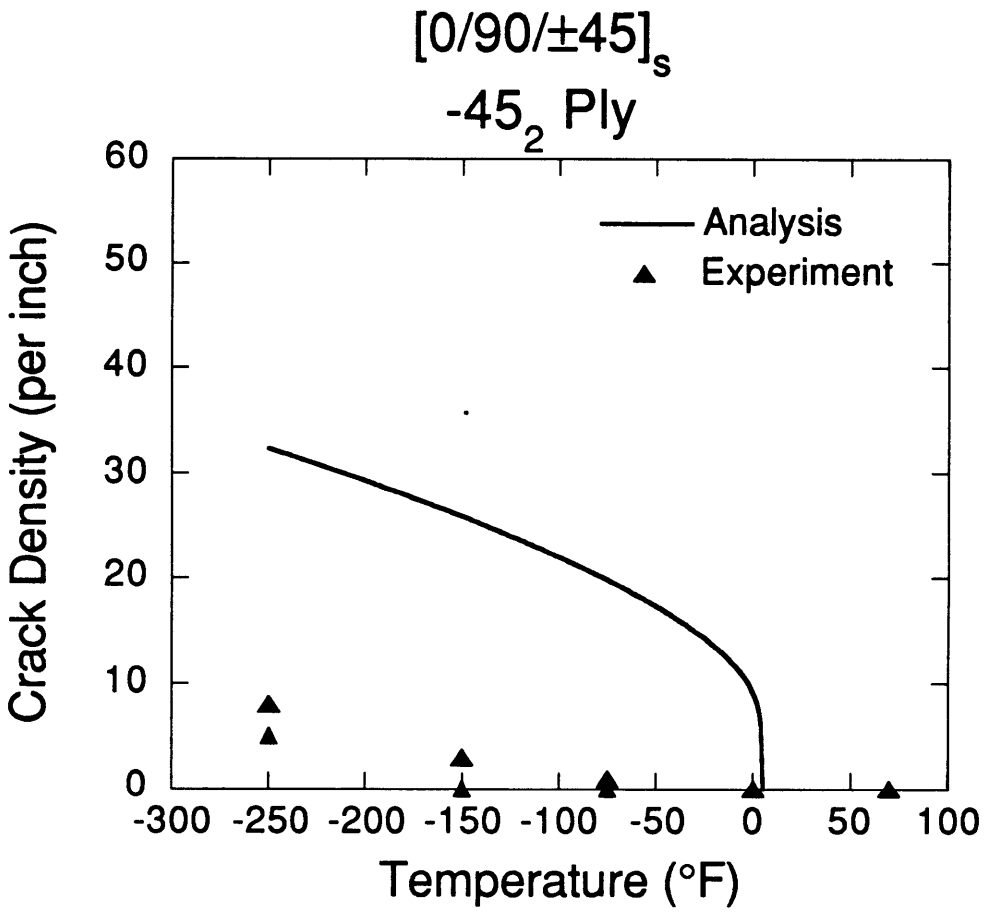

Figure B.13 Analytical and experimental correlation of crack density vs. decreasing temperature. -45_2 ply of $[0/90/\pm45]_s$ laminate.

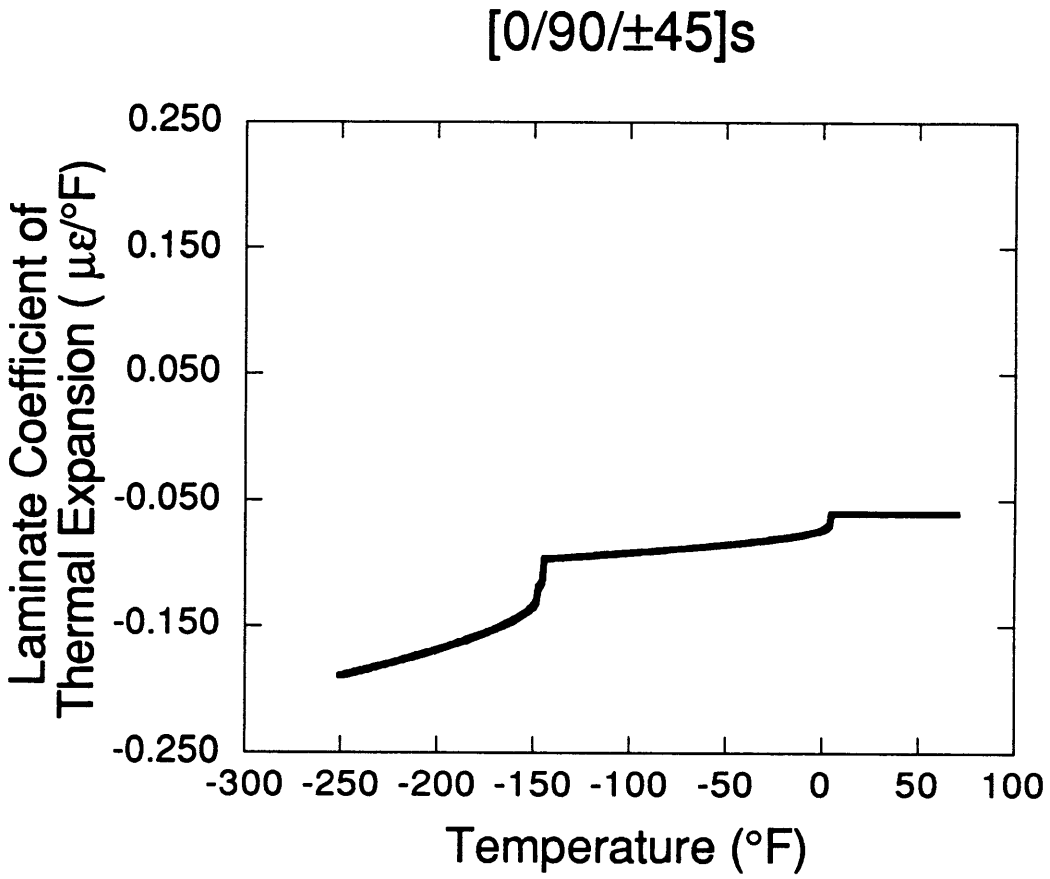

Figure B.14 Analytical CTE prediction vs. temperature for $[0/90/\pm45]_s$ laminate.

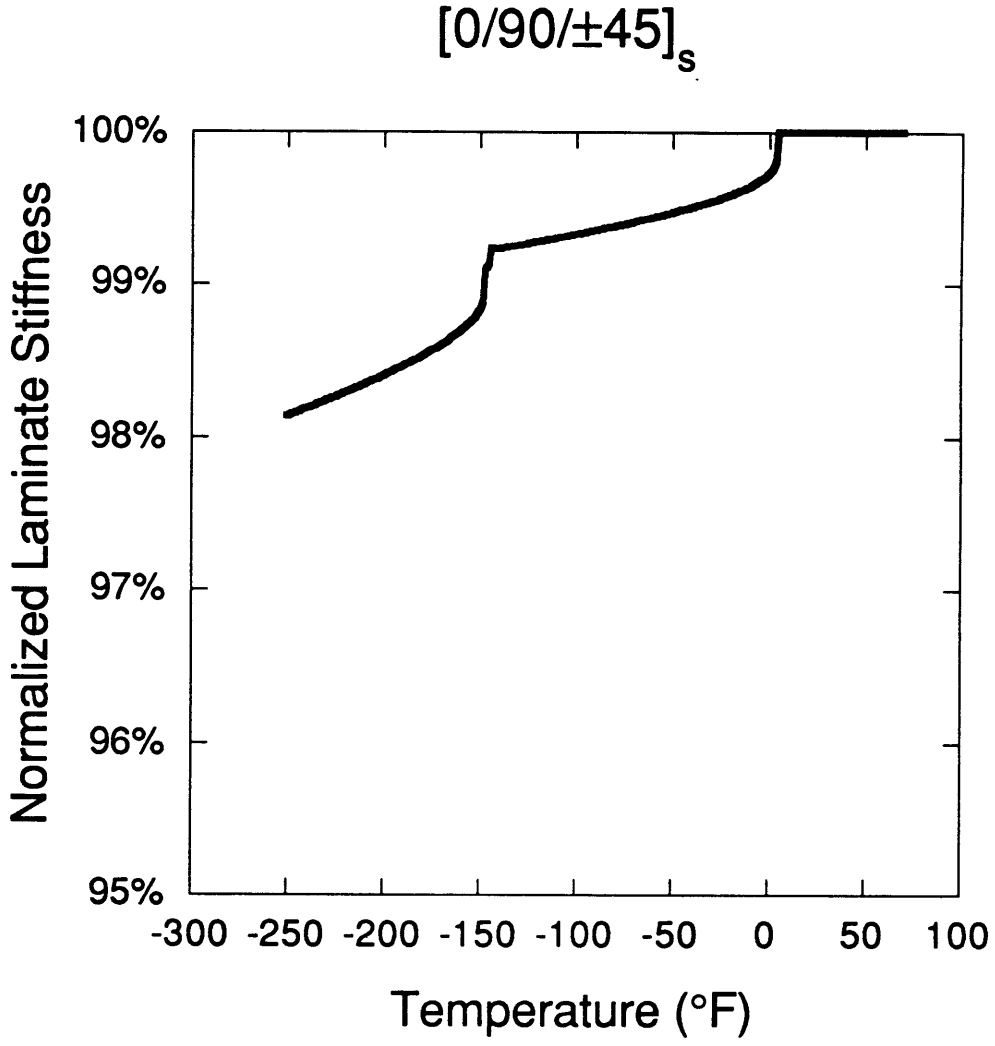

Figure B.15 Analytical stiffness prediction vs. temperature for $[0/90/\pm45]_s$ laminate. Laminate longitudinal stiffness normalized by undamaged value.

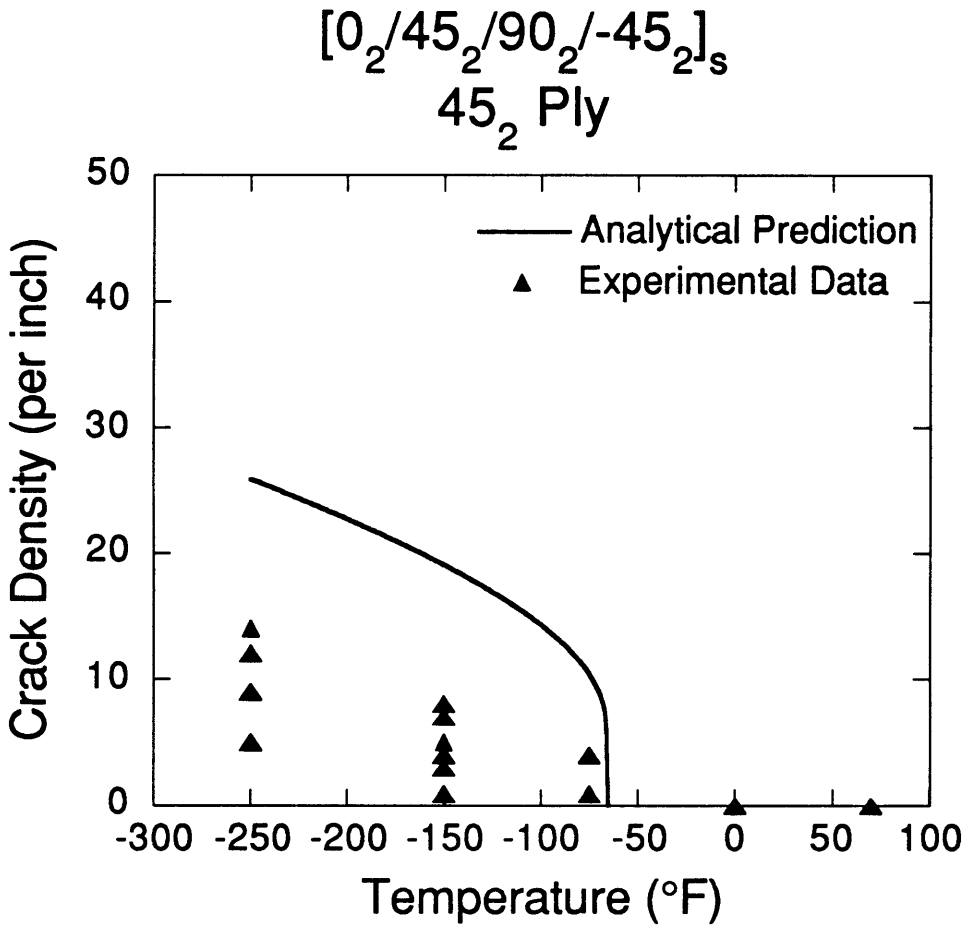

Figure B.16 Analytical and experimental correlation of crack density vs. decreasing temperature. 45_2 ply of $[0_2/45_2/90_2/-45_2]_s$ laminate.

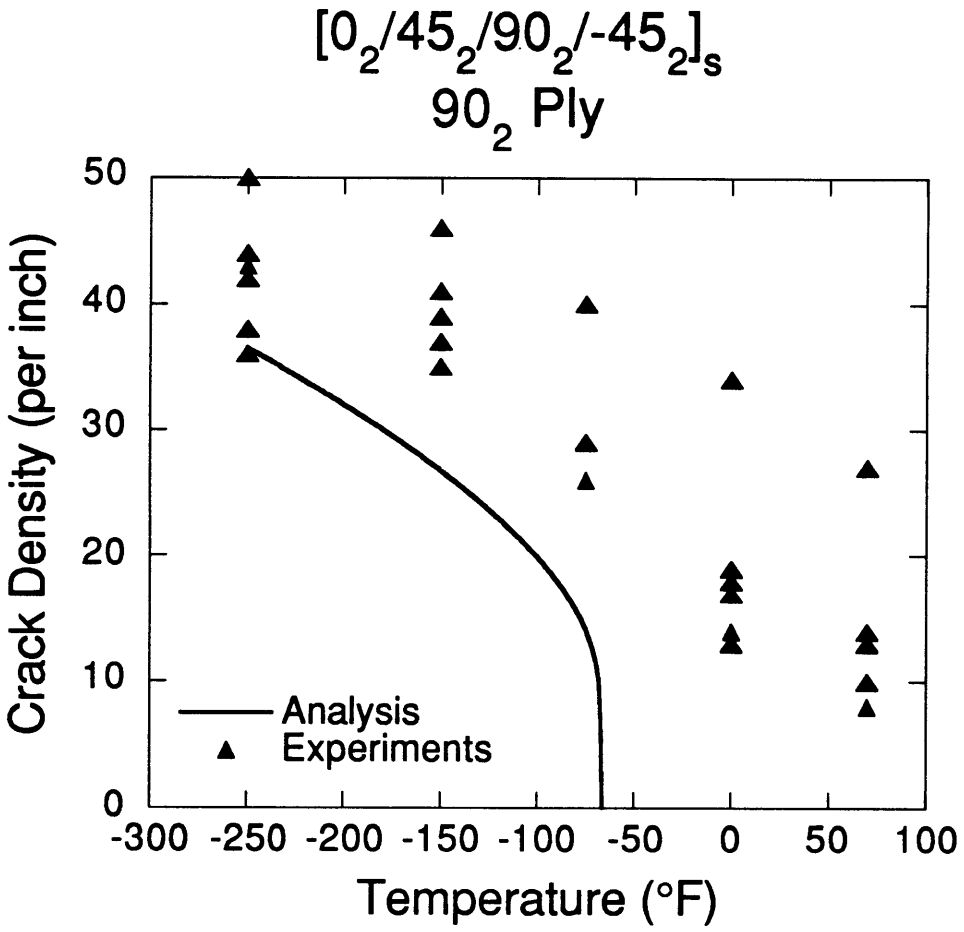

Figure B.17 Analytical and experimental correlation of crack density vs. decreasing temperature. 90_2 ply of $[0_2/45_2/90_2/-45_2]_s$ laminate.

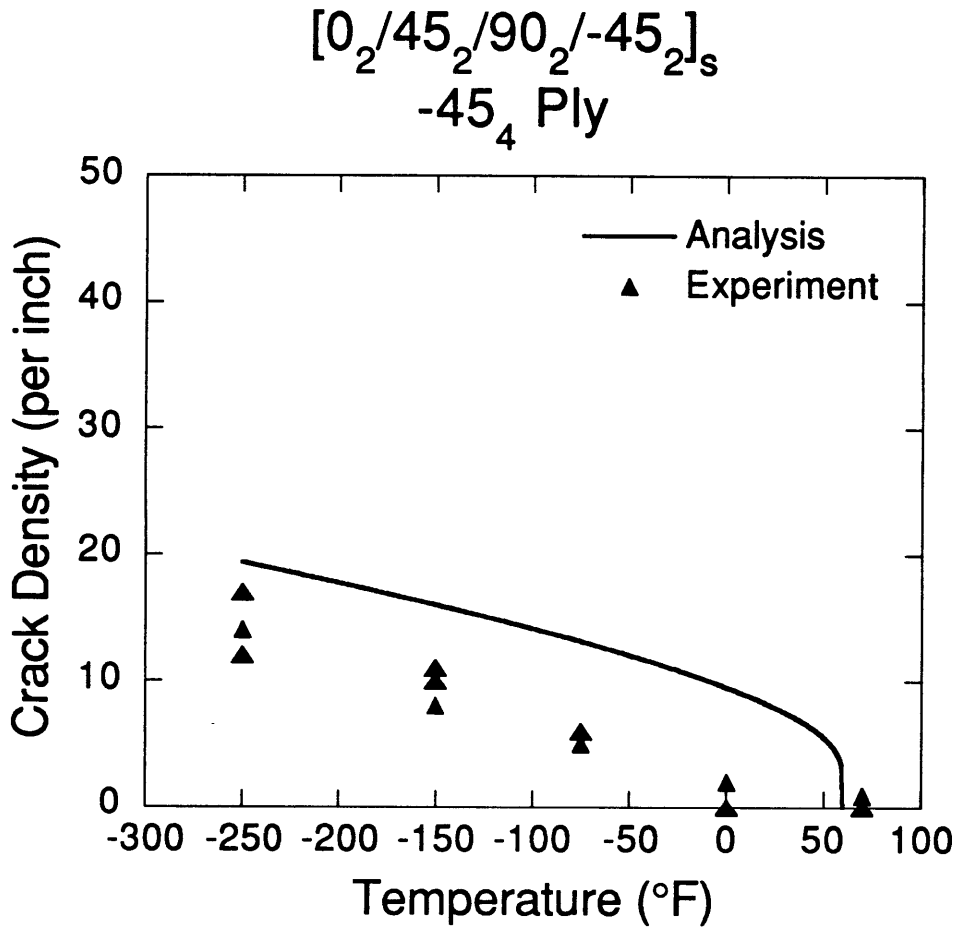

Figure B.18 Analytical and experimental correlation of crack density vs. decreasing temperature. -45_4 ply of $[0_2/45_2/90_2/-45_2]_s$ laminate.

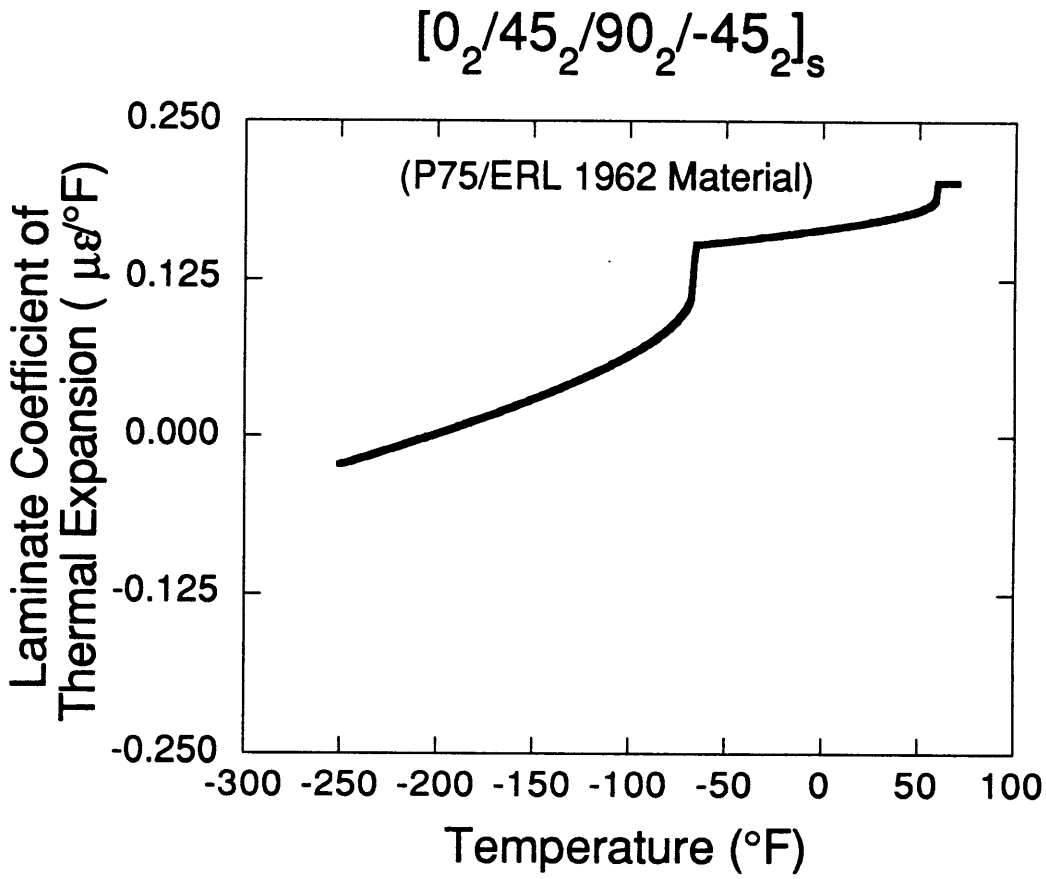

Figure B.19 Analytical CTE prediction vs. temperature for $[0_2/45_2/90_2/-45_2]_s$ laminate.

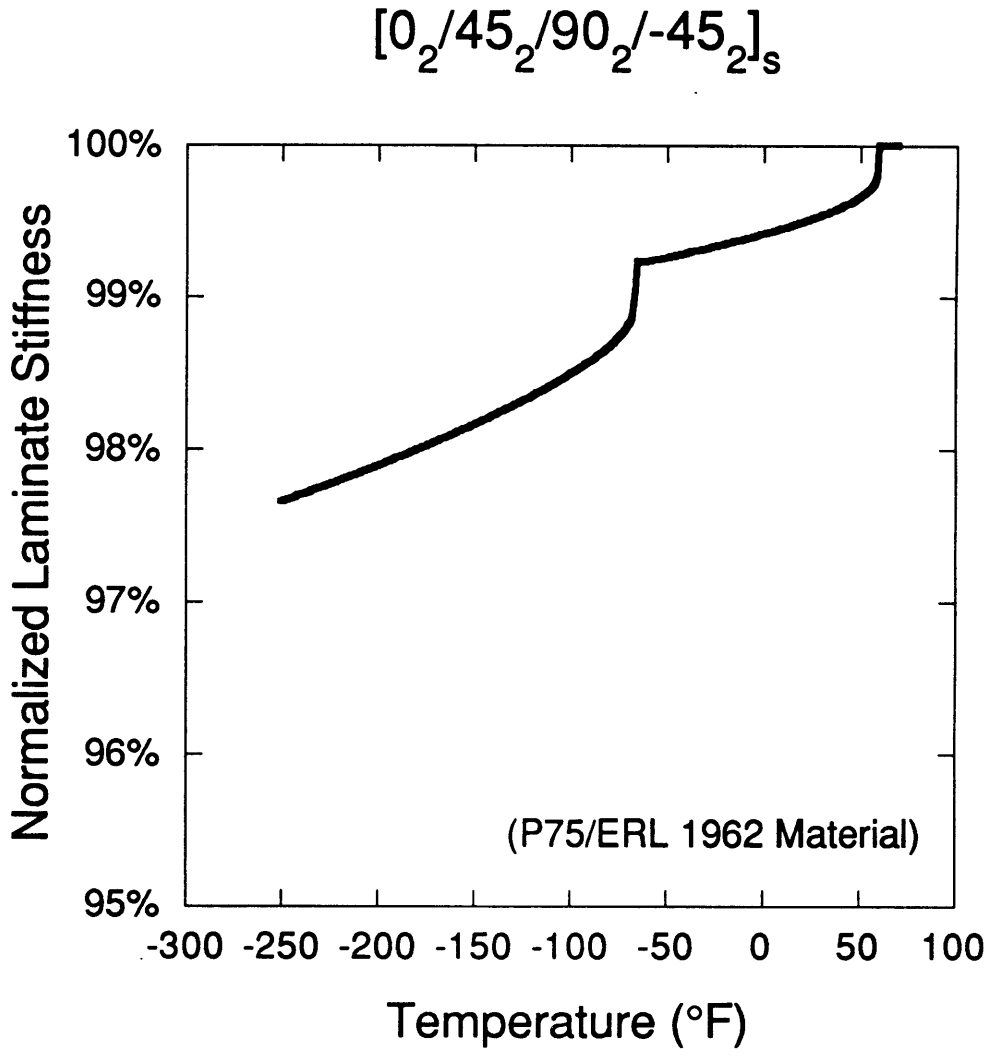

Figure B.20 Analytical stiffness prediction vs. temperature for $[0_2/45_2/90_2/-45_2]_s$ laminate. Laminate longitudinal stiffness normalized by undamaged value.

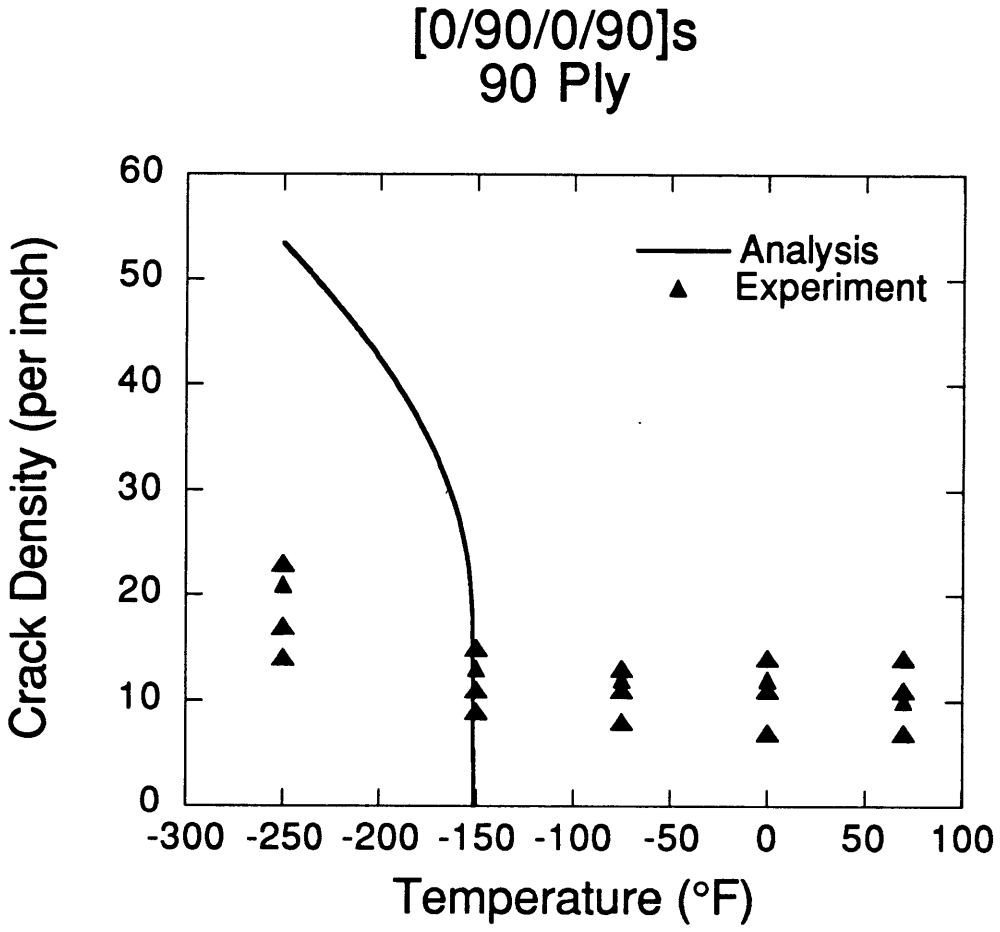

Figure B.21 Analytical and experimental correlation of crack density vs. decreasing temperature. 90 ply of $[0/90/0/90]_s$ laminate.

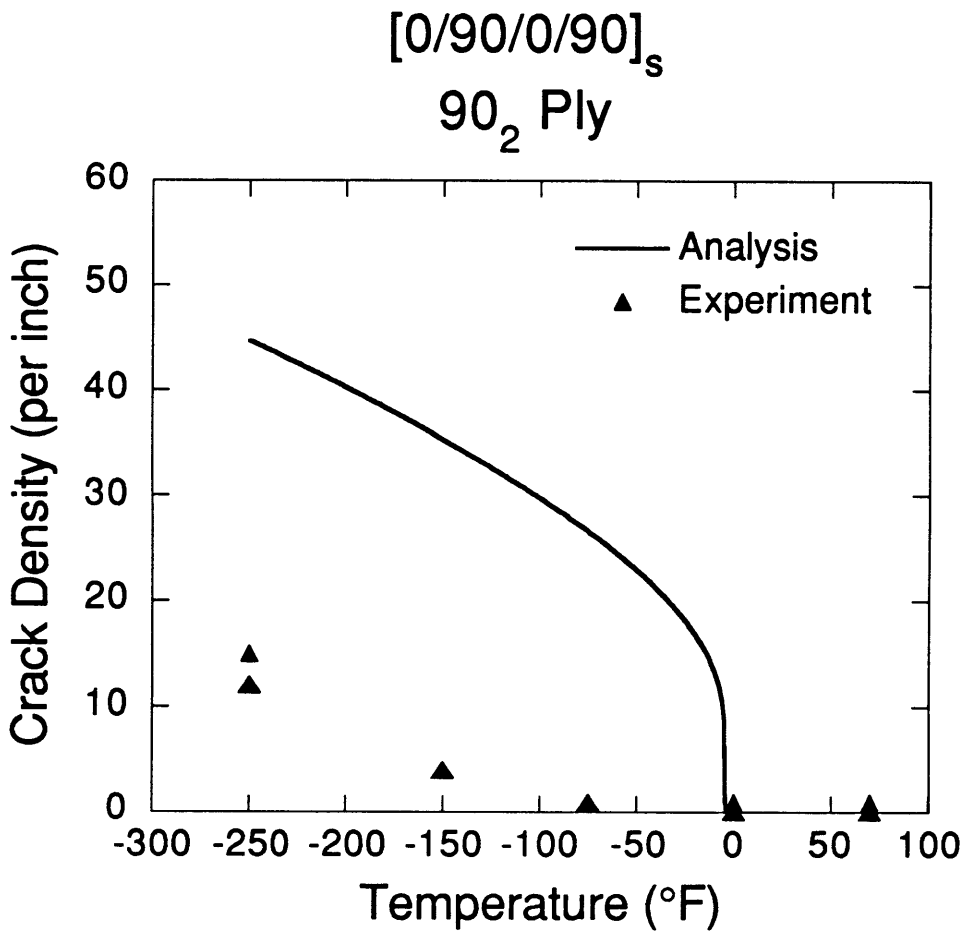

Figure B.22 Analytical and experimental correlation of crack density vs. decreasing temperature. 90_2 ply of $[0/90/0/90]_s$ laminate.

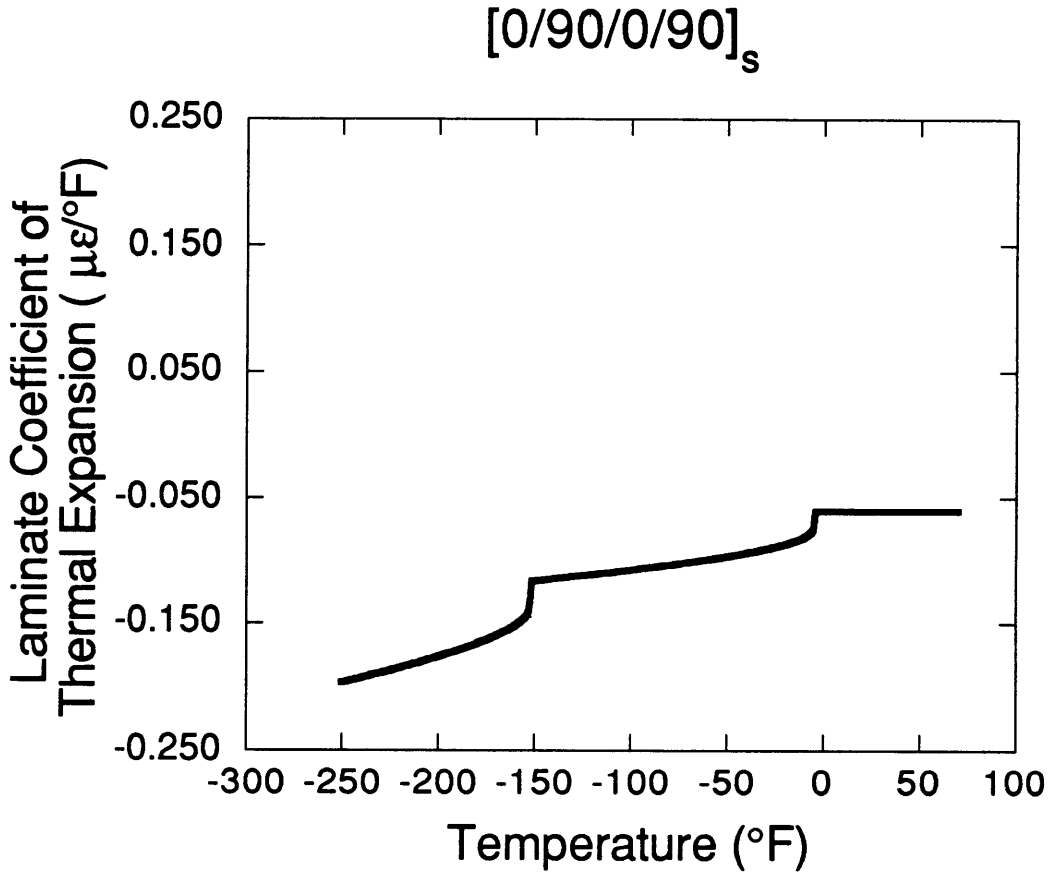

Figure B.23 Analytical CTE prediction vs. temperature for $[0/90/0/90]_s$ laminate.

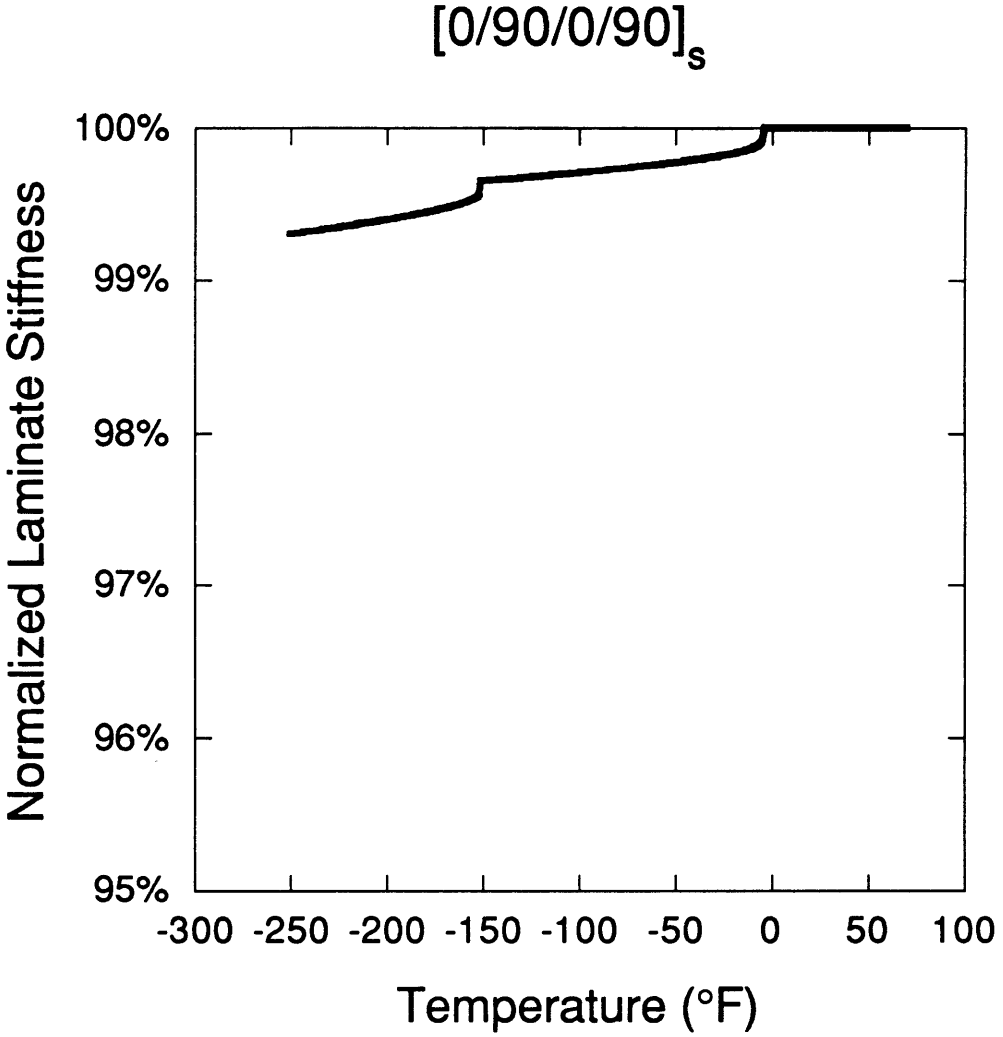

Figure B.24 Analytical stiffness prediction vs. temperature for $[0/90/0/90]_s$ laminate. Laminate longitudinal stiffness normalized by undamaged value.

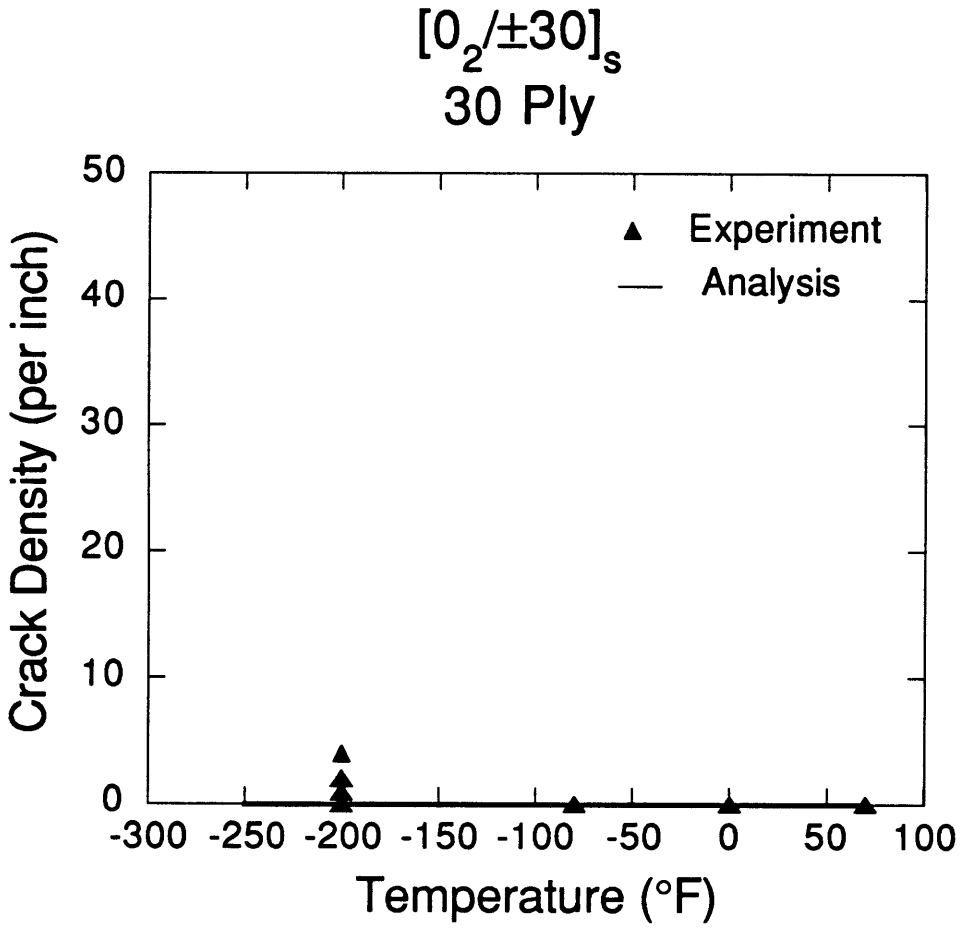

Figure B.25 Analytical and experimental correlation of crack density vs. decreasing temperature. 30 ply of $[0_2/\pm30]_s$ laminate.

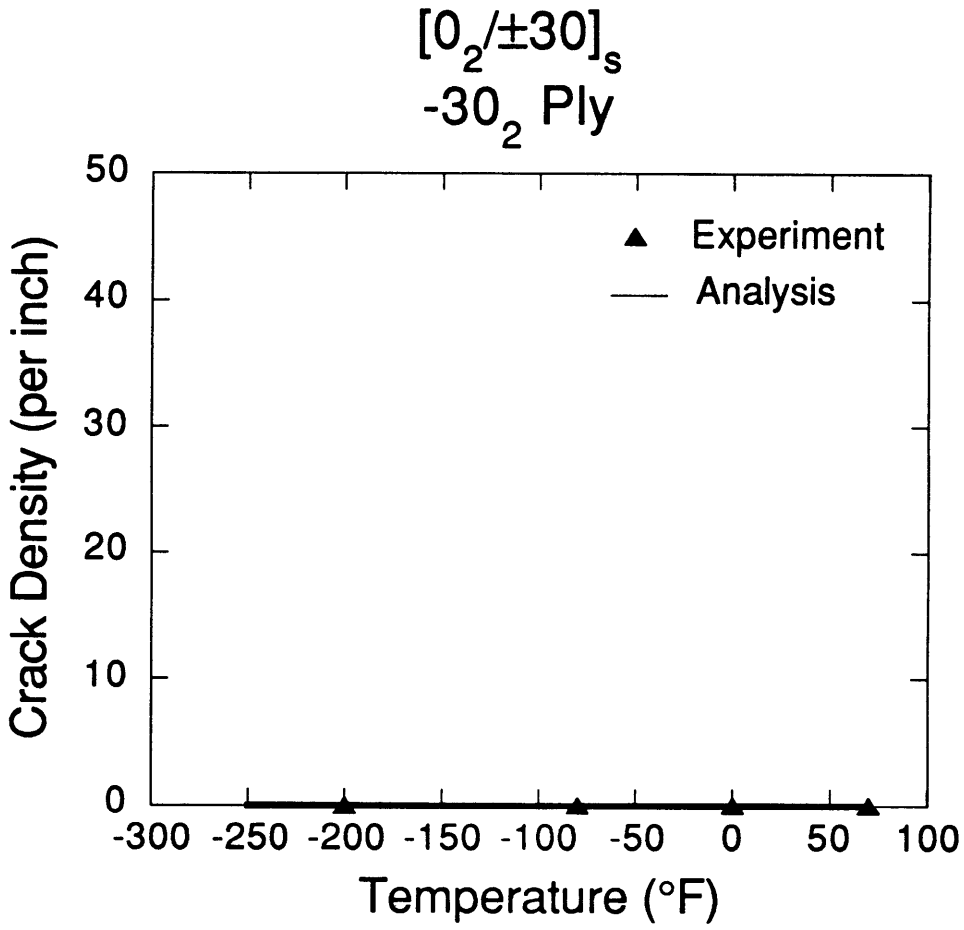

Figure B.26 Analytical and experimental correlation of crack density vs. decreasing temperature. -30_2 ply of $[0_2/\pm30]_s$ laminate.

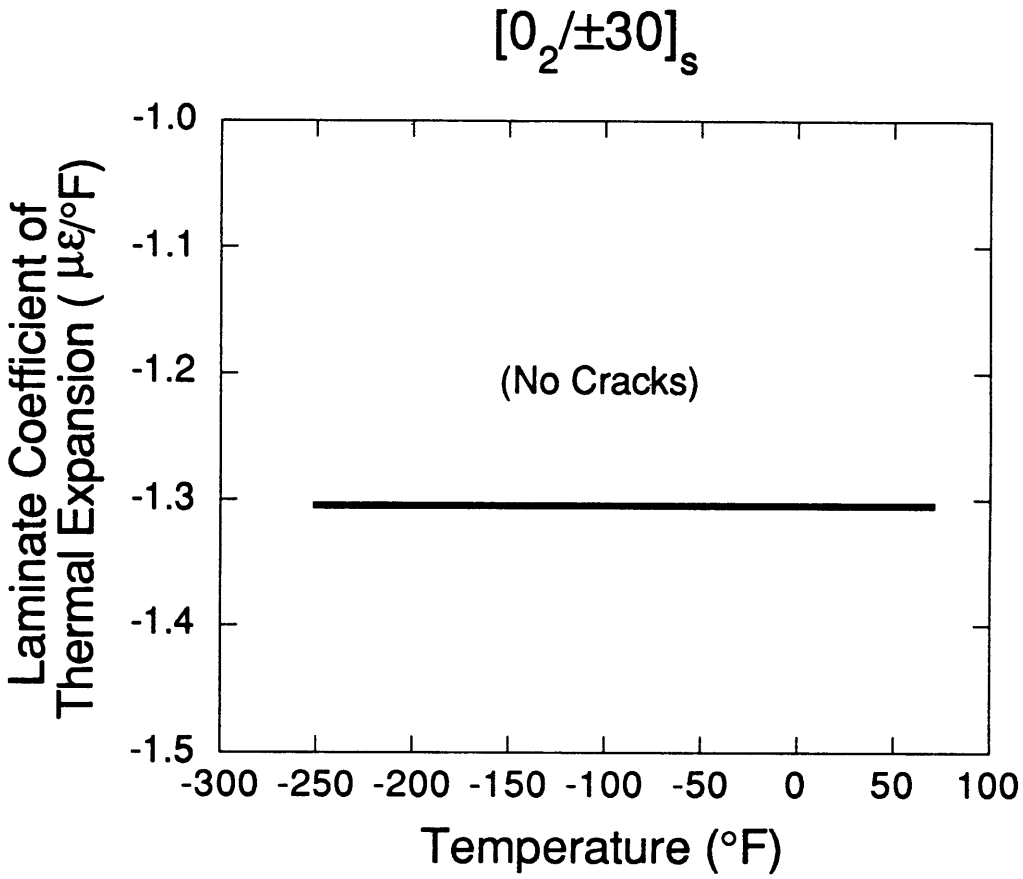

Figure B.27 Analytical CTE prediction vs. temperature for $[0_2/\pm30]_s$ laminate.

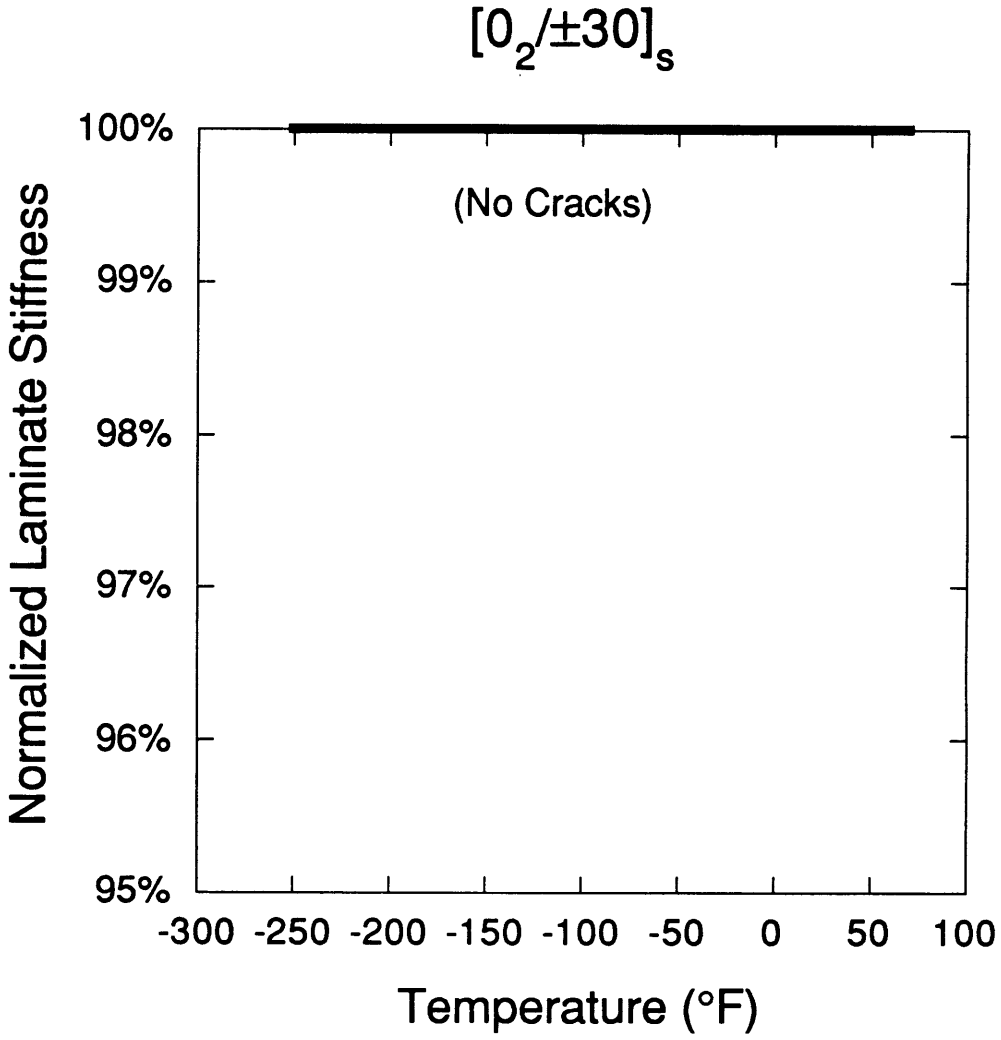

Figure B.28 Analytical stiffness prediction vs. temperature for $[0_2/\pm30]_s$ laminate. Laminate longitudinal stiffness normalized by undamaged value.

APPENDIX C

RESULTS OF FREE EDGE STRESS ANALYSIS

This section presents the analytical results of the three dimensional free edge stress calculations for $[0/45/90/-45]_s$, $[0/90/\pm45]_s$, $[0/\pm45/90]_s$, $[0_2/45_2/90_2/-45_2]_s$ and $[0/90/0/90]_s$, and $[0_2/\pm30]_s$ laminates. The graphs show the in-plane stress, transverse to the fiber direction, for each ply group of a laminate. The in-plane stress distribution is shown along the first 2mm from the free edge.

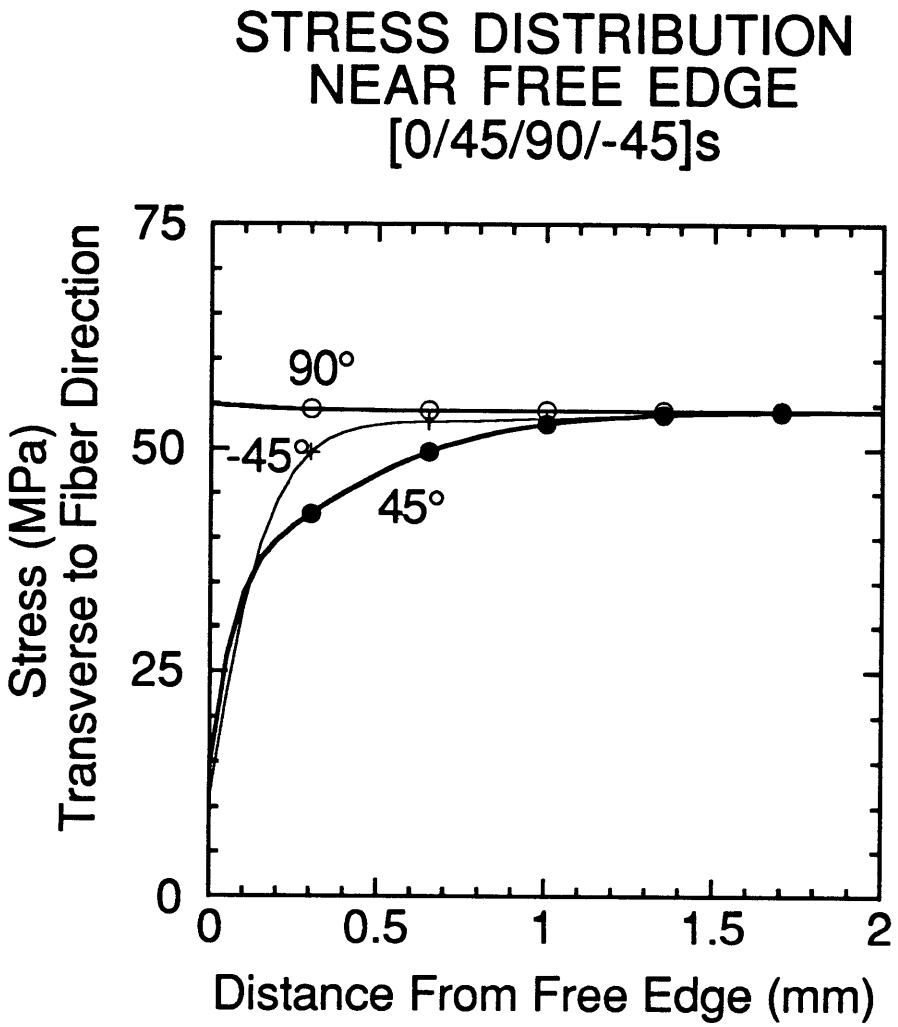

Figure C.1 Transverse in-plane stress distribution near free edge of $[0/45/90/-45]_s$ laminate.

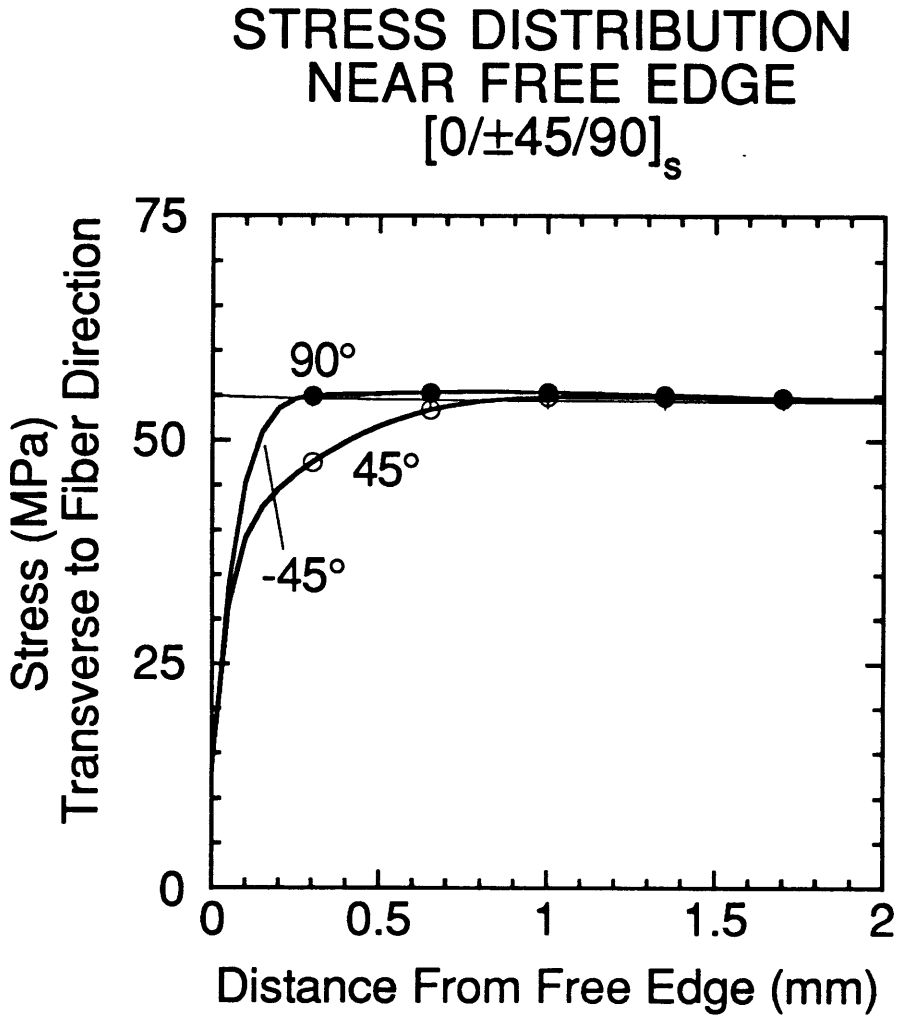

Figure C.2 Transverse in-plane stress distribution near free edge of $[0/\pm45/90]_s$ laminate.

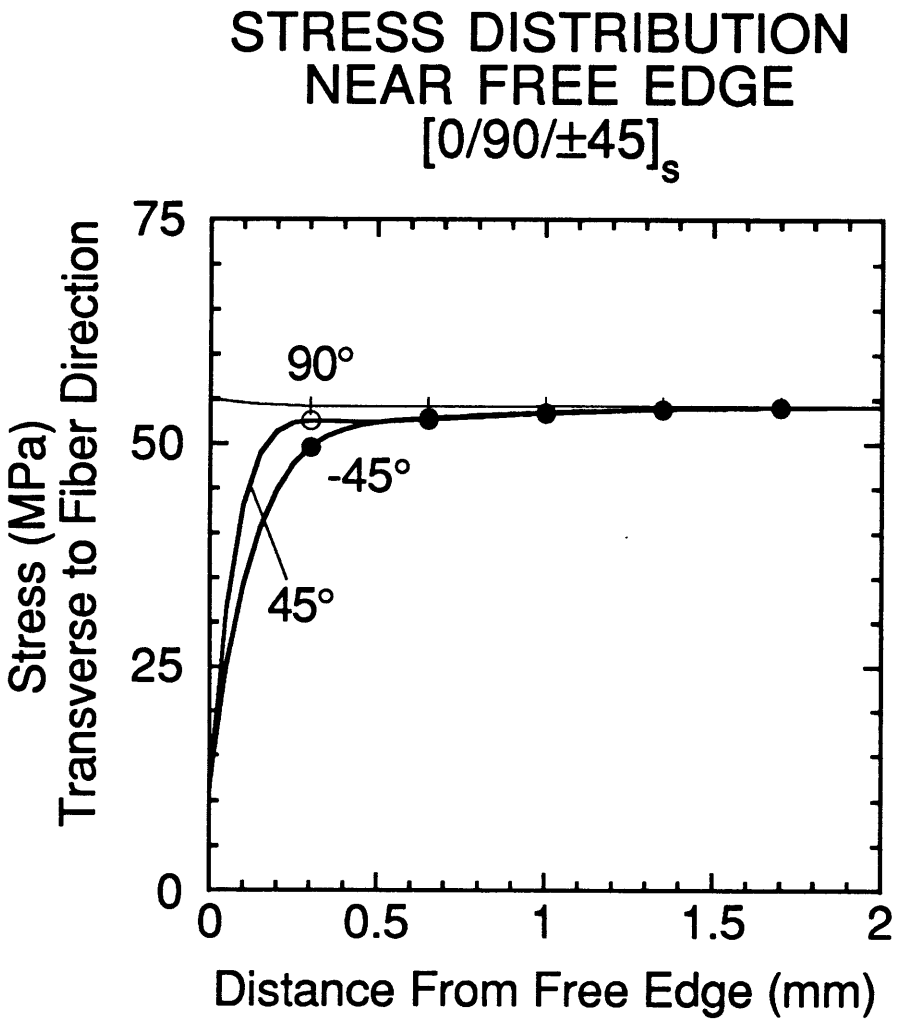

Figure C.3 Transverse in-plane stress distribution near free edge of $[0/90/\pm45]_s$ laminate.

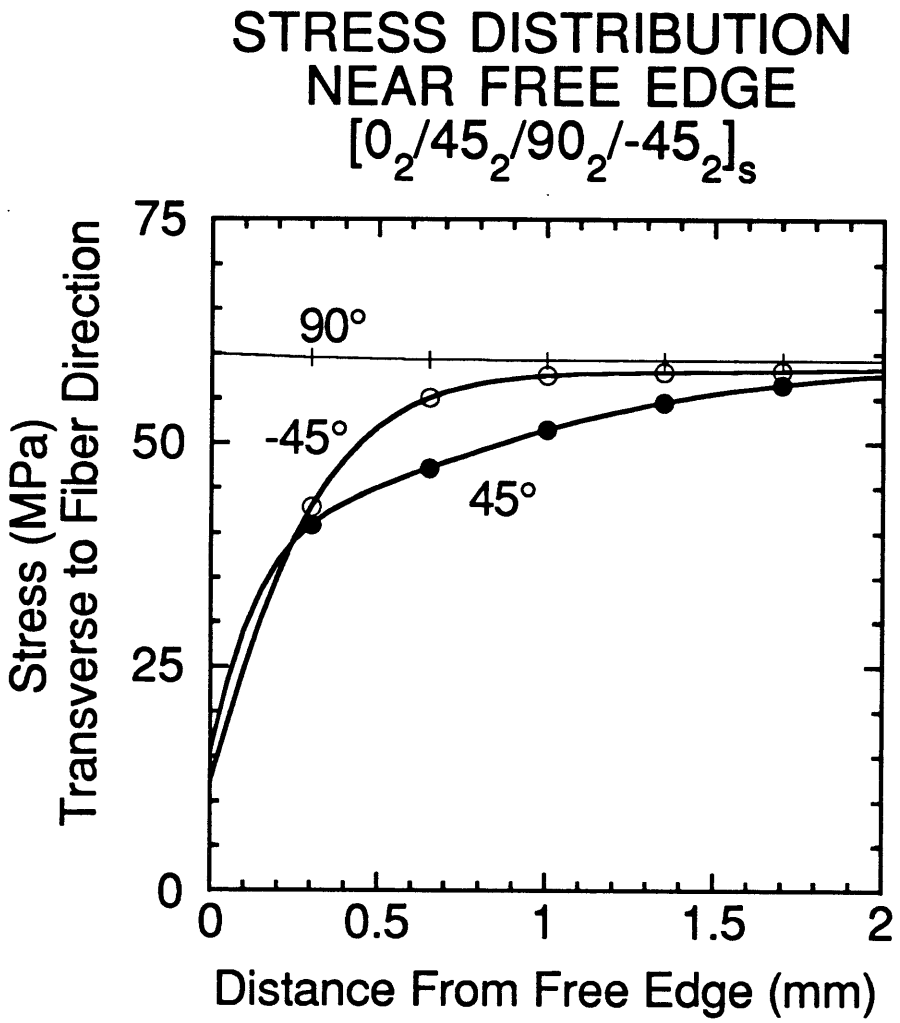

Figure C.4 Transverse in-plane stress distribution near free edge of $[0_2/45_2/90_2/-45_2]_s$ laminate.

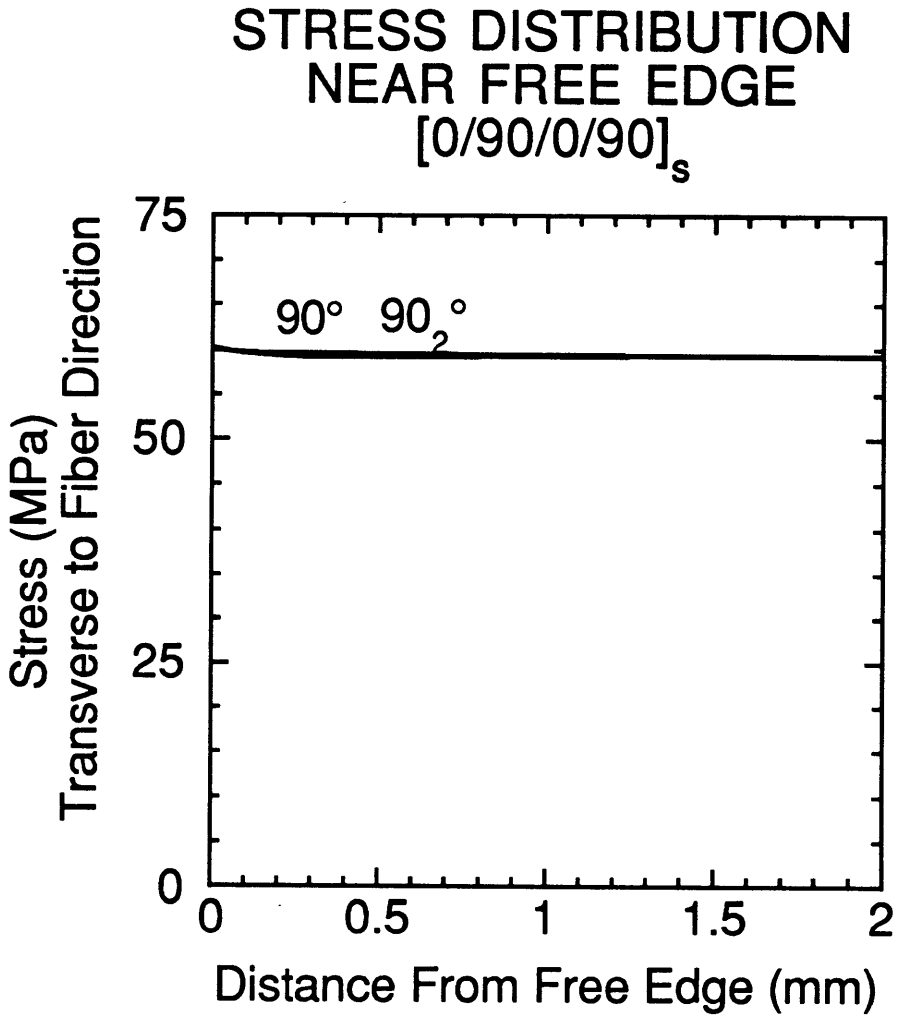

Figure C.5 Transverse in-plane stress distribution near free edge of $[0/90/0/90]_s$ laminate.

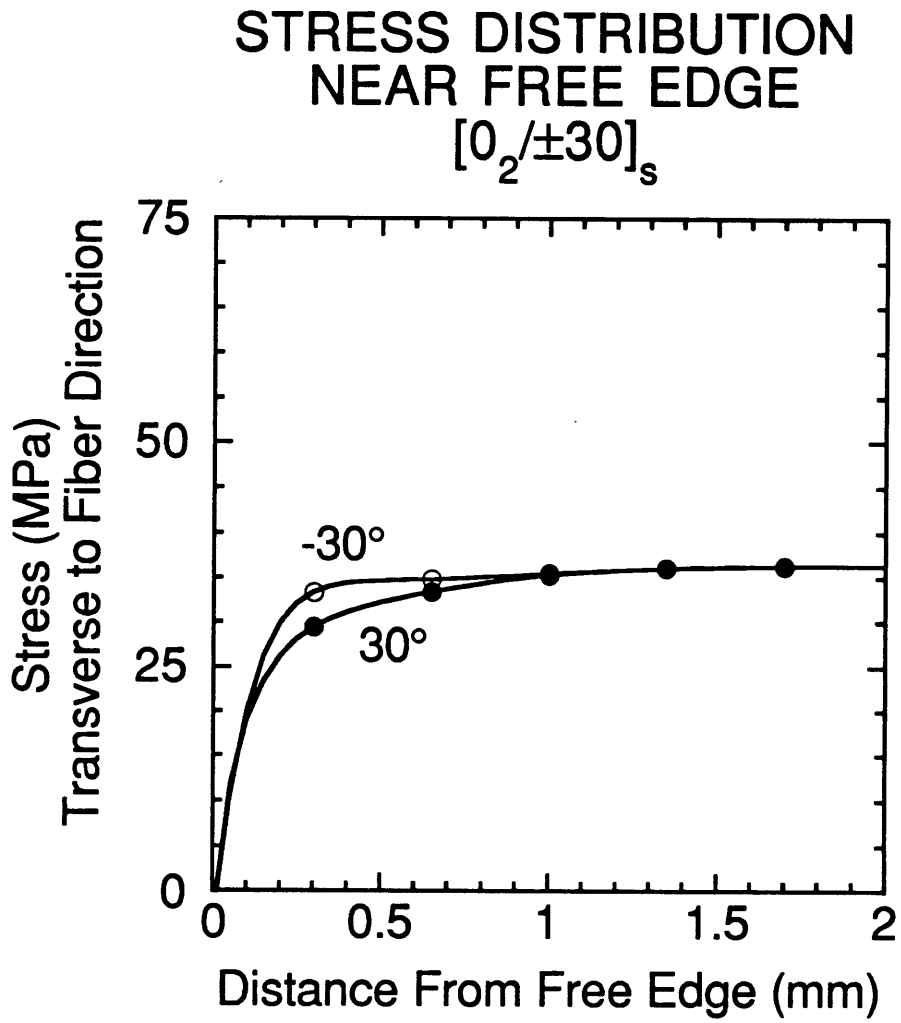

Figure C.6 Transverse in-plane stress distribution near free edge of $[0_2/\pm30]_s$ laminate.